



NAVAL POSTGRADUATE SCHOOL

MONTEREY, CALIFORNIA

THESIS

FLUIDICALLY AUGMENTED NOZZLES FOR PULSE DETONATION ENGINE APPLICATIONS

by

Larry R. Smith

December 2011

Thesis Advisor:
Second Reader:

Christopher M. Brophy
Anthony Gannon

Approved for public release; distribution is unlimited

THIS PAGE INTENTIONALLY LEFT BLANK

REPORT DOCUMENTATION PAGE			<i>Form Approved OMB No. 0704-0188</i>	
Public reporting burden for this collection of information is estimated to average 1 hour per response, including the time for reviewing instruction, searching existing data sources, gathering and maintaining the data needed, and completing and reviewing the collection of information. Send comments regarding this burden estimate or any other aspect of this collection of information, including suggestions for reducing this burden, to Washington headquarters Services, Directorate for Information Operations and Reports, 1215 Jefferson Davis Highway, Suite 1204, Arlington, VA 22202-4302, and to the Office of Management and Budget, Paperwork Reduction Project (0704-0188) Washington DC 20503.				
1. AGENCY USE ONLY (Leave blank)		2. REPORT DATE December 2011	3. REPORT TYPE AND DATES COVERED Master's Thesis	
4. TITLE AND SUBTITLE Fluidically Augmented Nozzles for Pulse Detonation Engine Applications			5. FUNDING NUMBERS N0001411WX20116	
6. AUTHOR(S) Larry R. Smith				
7. PERFORMING ORGANIZATION NAME(S) AND ADDRESS(ES) Naval Postgraduate School Monterey, CA 93943-5000			8. PERFORMING ORGANIZATION REPORT NUMBER	
9. SPONSORING /MONITORING AGENCY NAME(S) AND ADDRESS(ES) Office of Naval Research (ONR) Code 33 Ballstone Tower One 800 N. Quincy St. Arlington, VA 22203-1995			10. SPONSORING/MONITORING AGENCY REPORT NUMBER	
11. SUPPLEMENTARY NOTES The views expressed in this thesis are those of the author and do not reflect the official policy or position of the Department of Defense or the U.S. Government. IRB Protocol number _____ N/A _____.				
12a. DISTRIBUTION / AVAILABILITY STATEMENT Approved for public release; distribution is unlimited			12b. DISTRIBUTION CODE A	
13. ABSTRACT (maximum 200 words) Pulse Detonation Engines (PDE) operate in a cyclic manner resulting in large changes in the combustion chamber pressure. The widely varying pressure ratio between the chamber and nozzle exit makes it difficult to efficiently produce thrust since a fixed area ratio exhaust nozzle would operate off design nearly the entire cycle. Therefore, a nozzle with the capability to create the necessary area ratio throughout the cycle is required to produce an effective and efficient thrust profile. A dynamically varying nozzle was evaluated which investigated the possibility of using air injection into the diverging portion of the nozzle in order to effectively adjust the nozzle's exit area and provide the primary engine combustion products the most efficient area ratio throughout the combustion cycle. A two-dimensional nozzle and combustion section was created and simulated using computational fluid dynamics software to analyze the flow for various air injection pressures and velocities. A test section was designed and assembled for actual testing of the nozzle with the air injection ports and used a shadowgraph technique to observe the time-varying gas dynamics in the nozzle. The results of each were compared and analyzed to determine the validity of the CFD analysis. Subsequent computational analysis was conducted to find the most optimal injection conditions to achieve the most effective variable nozzle design for maximizing the impulse per cycle.				
14. SUBJECT TERMS Pulse Detonation Engines, PDE, Variable Nozzles, Fluidic Variable Nozzles			15. NUMBER OF PAGES 147	
			16. PRICE CODE	
17. SECURITY CLASSIFICATION OF REPORT Unclassified	18. SECURITY CLASSIFICATION OF THIS PAGE Unclassified	19. SECURITY CLASSIFICATION OF ABSTRACT Unclassified	20. LIMITATION OF ABSTRACT UU	

THIS PAGE INTENTIONALLY LEFT BLANK

Approved for public release; distribution is unlimited

**FLUIDICALLY AUGMENTED NOZZLES FOR PULSE DETONATION ENGINE
APPLICATIONS**

Larry R. Smith
Lieutenant Commander, United States Navy
B.S., United States Naval Academy, 2000

Submitted in partial fulfillment of the
requirements for the degree of

MASTER OF SCIENCE IN ASTRONAUTICAL ENGINEERING

from the

**NAVAL POSTGRADUATE SCHOOL
December 2011**

Author: Larry R. Smith

Approved by: Christopher M. Brophy
Thesis Advisor

Anthony Gannon
Second Reader

Knox T. Millsaps
Chair, Department of Mechanical and Aerospace Engineering

THIS PAGE INTENTIONALLY LEFT BLANK

ABSTRACT

Pulse Detonation Engines (PDE) operate in a cyclic manner resulting in large changes in the combustion chamber pressure. The widely varying pressure ratio between the chamber and nozzle exit makes it difficult to efficiently produce thrust since a fixed area ratio exhaust nozzle would operate off design nearly the entire cycle. Therefore, a nozzle with the capability to create the necessary area ratio throughout the cycle is required to produce an effective and efficient thrust profile. A dynamically varying nozzle was evaluated which investigated the possibility of using air injection into the diverging portion of the nozzle in order to effectively adjust the nozzle's exit area and provide the primary engine combustion products the most efficient area ratio throughout the combustion cycle. A two-dimensional nozzle and combustion section was created and simulated using computational fluid dynamics software to analyze the flow for various air injection pressures and velocities. A test section was designed and assembled for actual testing of the nozzle with the air injection ports and used a shadowgraph technique to observe the time-varying gas dynamics in the nozzle. The results of each were compared and analyzed to determine the validity of the CFD analysis. Subsequent computational analysis was conducted to find the most optimal injection conditions to achieve the most effective variable nozzle design for maximizing the impulse per cycle.

THIS PAGE INTENTIONALLY LEFT BLANK

TABLE OF CONTENTS

I.	INTRODUCTION.....	1
II	BACKGROUND	5
A.	PDE OPERATION	5
B.	NOZZLES.....	6
	1. Operation	7
	a. Underexpanded Nozzle Condition	10
	b. Overexpanded Nozzle Condition	11
	2. Variable Nozzles.....	13
III.	EXPERIMENTAL SETUP	15
A.	EXPERIMENTAL ASSEMBLY	15
	1. Initiation Section	15
	a. Air Delivery System	15
	b. Fuel Delivery System	16
	c. Ignition System.....	17
	2. Detonation Channel	17
	3. Optical Section	18
	a. Nozzle.....	19
	b. Nozzle Mounting Block.....	20
	c. Injector Air Assembly.....	20
	d. Test Section Floor	21
	4. Exhaust Section	21
B.	INSTRUMENTATION	22
	1. Kistler Probes	22
	2. Laser.....	22
	3. Mirrors.....	23
	4. Camera.....	24
C.	SHADOWGRAPH.....	24
D.	LABVIEW SOFTWARE	25
IV.	EXPERIMENTAL RESULTS.....	27
A.	PURPOSE.....	27
B.	PROCEDURE	27
C.	REFRESH EXPERIMENT	28
	1. Baseline Flow, No Injector Pressure	28
	2. One Percent Total Core Mass Flow Rate Per Injector.....	30
	3. One-Point-Four Percent Total Core Mass Flow Rate Per Injector	32
D.	DETONATION EXPERIMENT	33
V.	COMPUTER SIMULATIONS.....	41
A.	MODELING SOFTWARE	41
	1. SolidWorks 2010	42

a.	<i>Three Secondary Injectors/All Models</i>	42
b.	<i>Two Secondary Injectors Operating at a Flight Condition</i> ...	45
2.	Mime 4.1.....	45
3.	NASA CEA	46
4.	CFD++.....	46
a.	<i>Three Secondary Injectors/All Models</i>	46
b.	<i>Two Secondary Injectors Operating at a Flight Condition</i> ...	49
5.	Tecplot 360 2010.....	50
B.	SIMULATION RESULTS	50
1	Steady State/Refresh Condition.....	50
a.	<i>Three Secondary Injectors/All Models</i>	50
b.	<i>Two Secondary Injectors Operating at a Flight Condition</i> ...	59
2	Detonation Case	62
VI.	CONCLUSION AND FUTURE WORK	69
A.	CONCLUSION	69
B.	FUTURE WORK.....	69
APPENDIX A:	MANUFACTURED DRAWINGS	71
A.	TEST SECTION OVERVIEW.....	71
B.	NOZZLE WITH BLOCK AND TOP PLATE.....	72
C.	RAMP BLOCK	73
D.	TOP PLATE	76
E.	SPACER.....	78
F.	TOP SKI	80
G.	BOTTOM SKI.....	82
APPENDIX B:	NASA CEA GUI.....	85
APPENDIX C:	CFD++ DATA FILES.....	89
LIST OF REFERENCES	127
INITIAL DISTRIBUTION LIST	129

LIST OF FIGURES

Figure 1.	Comparison of Propulsion Technologies. (From [1]).....	1
Figure 2.	Variable Exhaust Nozzle of an F/A-18 Hornet.....	3
Figure 3.	Operational Cycle of a Pulse Detonation Engine. (From [2])	5
Figure 4.	Pressure Ratio vs Distance. (From [7]).....	8
Figure 5.	PDE Chamber Pressure versus Time for Hydrogen/Air Reaction at 60 Hz. (From [2]).....	9
Figure 6.	Area Ratio vs. Chamber Pressure	10
Figure 7.	Underexpanded Nozzle. (From [6]).....	11
Figure 8.	Overexpanded Nozzle. (From [6]).....	12
Figure 9.	Coefficient of Thrust vs. Area Ratio for a Fixed Exhaust Area. (From [6])...	13
Figure 10.	Coefficient of Thrust vs. Area Ratio for a Variable Exhaust Area. (From [6]).....	14
Figure 11.	SolidWorks Model of Test Section.....	15
Figure 12.	Air and Fuel Delivery System.....	16
Figure 13.	Ignition System	17
Figure 14.	Detonation Channel	18
Figure 15.	Optical Test Section.....	19
Figure 16.	Nozzle with Injectors at 45°. (From [2]).....	20
Figure 17.	Injector Air Assembly.....	21
Figure 18.	Exhaust Section.....	22
Figure 19.	Shadowgraph Mirror Arrangement.....	23
Figure 20.	Shadowgraph Setup	25
Figure 21.	Baseline Flow, No Secondary Injector Mass Flow.....	30
Figure 22.	One Percent Total Combustor Mass Flow Rate per Secondary Injector (3% Total Injected)	31
Figure 23.	1.4% Total Combustor Mass Flow Rate per Secondary Injector (4.2% Total Injected).....	33
Figure 24.	Pre-detonation Flow with Simulation for Comparison, 10% Total Combustor Mass Flow Rate.....	35
Figure 25.	Initial Detonation Wave Enters the Diverging Section of the Nozzle.....	36
Figure 26.	Detonation Products Completely Filling the Nozzle	37
Figure 27.	Secondary Injectors Rebuilding the “Pillow”	38
Figure 28.	Fully Rebuilt “Pillow”	39
Figure 29.	SolidWorks Model of 3 Injectors at a 45° Angle, Quiescent Boundary Condition (No Free Stream).....	44
Figure 30.	SolidWorks Model of 2 Injectors at a 0° and 90°, With a Free Stream Boundary Condition.....	45
Figure 31.	CFD++ Image of Initial Condition Boxes on Model of 3 Injectors at a 45° Angle, Without a Free Stream Boundary Condition.....	47
Figure 32.	CFD++ Snapshot of Initial Condition Boxes on Model of 2 Injectors at a 0° and 90°, With a Free Stream Boundary Condition.....	50

Figure 33.	Steady State Simulation, 3 Injector Nozzle at 45° Angle, No Injector Flow, Baseline.....	52
Figure 34.	Steady State Simulation, 3 Injector Nozzle at 45° Angle, Case 1, Run 1.....	52
Figure 35.	Steady State Simulation, 3 Injector Nozzle at 45° Angle, Case 1, Run2.....	52
Figure 36.	Steady State Simulation, 3 Injector Nozzle at 45° Angle, Case 2	53
Figure 37.	Steady State Simulation, 3 Injector Nozzle at 45° Angle, Case 3	53
Figure 38.	Steady State Simulation, 3 Injector Nozzle at 45° Angle, Case 4, Run 1.....	53
Figure 39.	Steady State Simulation, 3 Injector Nozzle at 45° Angle, Case 4, Run 2.....	54
Figure 40.	Steady State Simulation, 3 Injector Nozzle at 45° Angle, Case 5, Run 1.....	54
Figure 41.	Steady State Simulation, 3 Injector Nozzle at 45° Angle, Case 6, Run 1.....	55
Figure 42.	Steady State Simulation, 3 Injector Nozzle at 45° Angle, Case 6, Run 2.....	55
Figure 43.	Steady State Simulation, 3 Injector Nozzle at 45° Angle, Case 7, Max \dot{m}	56
Figure 44.	Steady State Simulation, 3 Injector Nozzle at 45° Angle, Case 8, 2 Injectors Used	56
Figure 45.	Steady State Simulation, 3 Injector Nozzle at 45° Angle, Case 9, Single Injector Used	57
Figure 46.	Thrust vs. Secondary Injector Total Combustor Mass Flow Rate Percentage (3 Injectors at a 45° Angle, Without an External Free Stream)	58
Figure 47.	Steady State Simulation, 2 Injectors , M=3.0 Free Stream at 10,000 meters, Case 10	60
Figure 48.	Steady State Simulation, 2 Injectors , M=3.0 Free Stream at 10,000 meters, Case 11	60
Figure 49.	Steady State Simulation, 2 Injectors, Free Stream at Sea Level, Case 12	61
Figure 50.	Detonation Simulation, 3 Injector Nozzle at 45° Angle, $t_{ign} + 30$ microseconds.....	62
Figure 51.	Detonation Simulation, 3 Injector Nozzle at 45° Angle, $t_{ign} + 50$ microseconds.....	62
Figure 52.	Detonation Simulation, 3 Injector Nozzle at 45° Angle, $t_{ign} + 80$ microseconds.....	63
Figure 53.	Detonation Simulation, 3 Injector Nozzle at 45° Angle, $t_{ign} + 130$ microseconds.....	63
Figure 54.	Detonation Simulation, 3 Injector Nozzle at 45° Angle, $t_{ign} + 190$ microseconds.....	64
Figure 55.	Detonation Simulation, 3 Injector Nozzle at 45° Angle, $t_{ign} + 300$ microseconds.....	64
Figure 56.	Detonation Simulation, 3 Injector Nozzle at 45° Angle, $t_{ign} + 500$ microseconds.....	65
Figure 57.	Detonation Simulation, 3 Injector Nozzle at 45° Angle, $t_{ign} + 700$ microseconds.....	65
Figure 58.	Detonation Simulation, 3 Injector Nozzle at 45° Angle, $t_{ign} + 1$ millisecond.....	65
Figure 59.	Detonation Results Overlaid on Coefficient of Thrust versus Area Ratio Curve (From [6]).....	66

LIST OF TABLES

Table 1.	Settings for Baseline Test, No Secondary Injector Flow	29
Table 2.	Settings for 1% Total Combustor Mass Flow Rate per Injector	30
Table 3.	Settings for 1.4% Total Combustor Mass Flow Rate per Injector	32
Table 4.	Settings for 3% Total Combustor Mass Flow Rate per Injector with Detonation	34
Table 5.	CFD++ Boundary Condition Boundary Settings for each Zone, Steady State Simulation	48
Table 6.	CFD++ Boundary Condition Boundary Settings for each Zone, Detonation Simulation	49
Table 7.	CFD++ Injector Boundary Conditions, Initial Conditions (3 Injectors at a 45° Angle, Without an External Free Stream)	51
Table 8.	CFD++ Injector Boundary Conditions, Same Pressure, Varying Mass Flow Rate (3 Injectors at a 45° Angle, Without an External Free Stream)	55
Table 9.	CFD++ Injector Boundary Conditions, Initial Research (2 Injectors at 0° and 90°, With an External Free Stream Flight Condition)	59

THIS PAGE INTENTIONALLY LEFT BLANK

LIST OF ACRONYMS AND ABBREVIATIONS

CEA	Chemical Equilibrium with Applications	
CFD	Computational Fluid Dynamic	
CJ	Chapman-Jouget	
DDT	Deflagration-to-Detonation Transition	
FPS	Frames per Second	
GUI	Graphical User Interface	
MSD	Multiple Spark Discharge	
NASA	National Aeronautics and Space Administration	
NI	National Instruments	
PDE	Pulse Detonation Engine	
PIV	Particle Image Velocimetry	
VEN	Variable Exhaust Nozzle	
A_1	PDE chamber area	$[m^2]$
A_e	Nozzle exit area	$[m^2]$
A^*	Nozzle throat area	$[m^2]$
c	Speed of sound	$[m \cdot s^{-1}]$
C_F	Thrust coefficient	$[-]$
ε	Nozzle area expansion ratio	$[-]$
γ	Specific heat ratio	$[-]$
F	Thrust	$[N]$
g	Acceleration of gravity	$[m \cdot s^{-2}]$
I_c	Specific impulse of combustion chamber	$[s^{-1}]$
I_n	Specific impulse of nozzle	$[s^{-1}]$
I_s	Specific impulse	$[s^{-1}]$
L	Length	$[m]$
M	Mach number	$[-]$
\dot{m}	Mass flow rate	$[kg \cdot s^{-1}]$
p_0	PDE chamber pressure	$[Pa]$
p_e	Nozzle exit pressure	$[Pa]$

p_3	Atmospheric pressure	[Pa]
p_t	Nozzle throat pressure	[Pa]
t	Time	[s]
t_{ign}	Time of Ignition	[s]
T_1	PDE chamber temperature	[K]
T_2	Nozzle exit temperature	[K]
v	Velocity	[m·s ⁻¹]
V	Volume	[m ³]

ACKNOWLEDGMENTS

I would like to thank Dr. Christopher Brophy for his tireless efforts and motivation throughout the research process. His guidance and mentorship were instrumental in my success. I also would like to thank Dave Dausen and the rest of the Rocket Lab staff for all of their help along the way. I honestly could not have completed this without their patience and professionalism. Lastly, I want to thank my fiancé, Leslie, for putting up with my complaints and whining during the last few months. It is always good to know someone will hear me moan and simply smile back.

THIS PAGE INTENTIONALLY LEFT BLANK

I. INTRODUCTION

Engine designs have been developed over many years to encompass a large range of operational speeds, but often with associated increases in technical complexity and cost. The result is a range of propulsion technologies that can deliver a desired performance in terms of specific impulse over a range of flight Mach numbers.

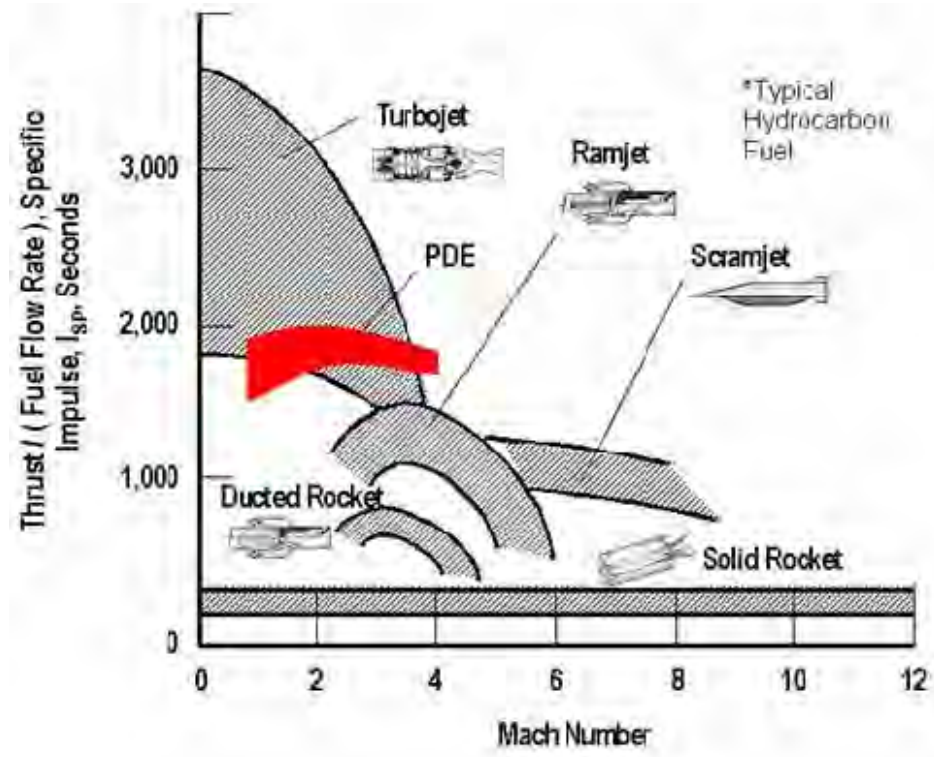


Figure 1. Comparison of Propulsion Technologies. (From [1])

Figure 1 illustrates the range of current technologies as flight Mach number versus specific impulse. The introduction of high-speed, efficient engines started with the turbojet and turbofan. These engines have the advantage of operating efficiently between static conditions and up to low Mach numbers. The disadvantage is seen when these systems reach the higher flight Mach numbers as efficiency drops off dramatically and eventually can result in insufficient thrust. This is largely due to the turbine temperature limitations. Additionally, the high number of moving parts, when compared to the other systems, also increases the complexity and cost.

At flight Mach numbers above two, the ramjet and ducted rockets become the desired engine platforms. Utilizing an optimal intake to decelerate and compress the high speed inlet air to subsonic speeds before the combustion section, it contains fewer moving parts, does not have the combustor temperature limitations, and is capable of operating at much higher velocities. However, this system is incapable of operating as a stand-alone engine at lower Mach numbers due to the inlet compression requirements. Ultimately, the ramjet reaches an operating limit near Mach 4–5 due to the high stagnation temperatures from the compression event. At these speeds, the scramjet becomes the more optimal selection since it maintains a supersonic flow through the combustor and therefore minimizes the static temperature rise before the combustion event. However, like the ramjet, the scramjet cannot operate at low Mach numbers and must be boosted to its operational speeds.

It can be seen in Figure 1 that there exists a region between high subsonic and mid supersonic velocities where an efficient technology is needed. This is where the Pulse Detonation Engine could be an effective alternative to conventional systems. Its high thermodynamic efficiency, little to no moving parts, and relative simplicity make it a very viable option for propulsion requirements. Although many of the challenges associated with these systems have been overcome, the optimization of the exhaust nozzle remains a concern for the efficient and practical application of a PDE for propulsive purposes.



Figure 2. Variable Exhaust Nozzle of an F/A-18 Hornet

As seen on most tactical fighter aircraft around the world, a Variable Exhaust Nozzle (VEN) is utilized in order to maximize the thrust for varying nozzle entrance and exit pressures. Figure 2 shows the VEN for an F/A-18C Hornet. PDE systems also operate at varying chamber pressures and are similarly plagued with lost efficiency and thrust if a conventionally fixed converging-diverging nozzle is used. The primary difference between the two is the rate at which the pressure change occurs. Where tactical fighter aircraft vary combustion conditions on a per second rate, the PDE pressure changes occur on a scale of tens of microseconds. This rapid change removes any possibility of utilizing a mechanical nozzle due to practical response times and induced fatigue. Therefore, this research investigates the possible usage of a fluidic nozzle by injecting a secondary mass flow into the exhaust section to effectively change the exhaust area “seen” by the engine combustor gases.

THIS PAGE INTENTIONALLY LEFT BLANK

II BACKGROUND

A. PDE OPERATION

A pulse detonation engine (PDE) is an engine concept that possesses and inherently high thermal efficiency and relative simplicity by design. It generates high pressure and high temperature combustion products associated with a detonation and converts the high enthalpy products to have a high exhaust velocity through a converging-diverging nozzle to produce thrust. The PDE has four distinct portions of a complete combustion cycle: the fill, the detonation, the blow-down, and the purge. This cycle is repeated at frequencies in the 40 to 100 hertz range and can be illustrated (Figure 3).

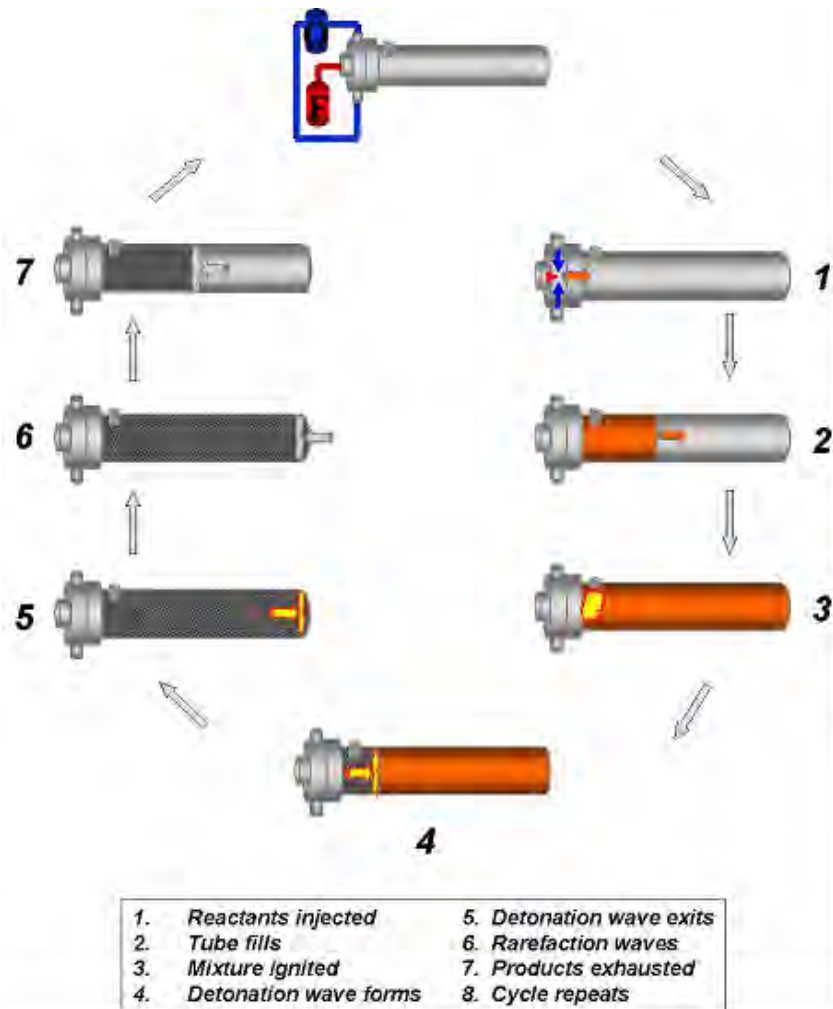


Figure 3. Operational Cycle of a Pulse Detonation Engine. (From [2])

The fill cycle, illustrated as steps 1 and 2 in Figure 3, begins the process by filling or charging the combustor with an appropriate fuel/air mixture. This mixture is then ignited, producing a flame that is initially a deflagration wave. A deflagration wave is a gaseous front that travels at a subsonic speed and has a lower pressure and density than the initial reaction flame, but an increase in temperature ([8], p. 252). As the deflagration wave continues through the combustor, it will accelerate to a finite speed unless sufficient turbulence exists to allow a substantially larger energy release rate. This process is often referred to as the deflagration-to-detonation transition (DDT) process and additional details can be found in Reference 8. Once this occurs, the wave will quickly accelerate to a supersonic velocity and transition to a detonation wave, shown as step 3 in Figure 3 ([8], pp. 15–16). The detonation wave then continues down the combustor and out the exit of the tube. The blow-down cycle, illustrated as steps 4 and 5 in Figure 3, then occurs, which reduces the chamber pressure and temperature before the next fill sequence can begin.

Although the detonation wave has exited, high temperature combustion products still exist in the combustor. In order to prevent an auto ignition of the new fuel/air mixture, the PDE must utilize a “buffer” of cooler air in order to clear these reactants. This is known as the purge phase since the products are “purged” from the combustion section shown as steps 6 and 7 in Figure 3. Once this has been completed, the cycle begins again at the fill phase and the process repeats itself.

B. NOZZLES

The use of nozzles on propulsion systems of nearly every kind serves a valuable purpose. Nozzles are responsible for taking the high pressure and temperature combustor products which have a large associated total enthalpy and converting the total enthalpy into high velocity flow with lower pressures and temperatures. The higher the velocity, the more kinetic energy. Preferably, that flow must also be in the axial direction normal to the engine or some of the axial momentum will not be utilized for a thrust force ([4], p. 244).

1. Operation

An exhaust nozzle serves two purposes. The first is to provide a back pressure to the combustor so that the combustion chamber will have sufficient pressure at high altitudes. The second is to inherently choke the flow in the throat of the nozzle. Choked flow is critical for the proper functionality any supersonic nozzle. Once the flow through the nozzle is choked, it reaches sonic velocity and then is accelerated in the diverging section of the nozzle. This divergence produces a low pressure, high speed flow that exits into the atmosphere with high kinetic energy producing thrust. However, the issues with proper nozzle design and selection are the design, shape, and most importantly area ratio between the exit plane and the throat to achieve efficient expansion and thrust.

The appropriate throat area must first be determined from the desired engine flow rates and chamber pressure. This can be accomplished by using Equation 1. Knowing that the Mach number at the throat must be 1.0, imposing a desired chamber Mach number of 0.3, and measuring the area of the existing combustion chamber, the necessary throat area can be calculated.

Equation 1:

$$\frac{A}{A^*} = \frac{1}{M} \left\{ \left(\frac{2}{\gamma + 1} \right) \left[1 + \left(\frac{\gamma - 1}{2} \right) M^2 \right] \right\}^{\frac{\gamma + 1}{2(\gamma - 1)}}$$

Solving for the appropriate exit area can be more challenging as it varies according to chamber pressure and ambient pressure. Time-varying conditions are prevalent in the PDE as the chamber pressure varies frequently based on engine cycles and the ambient pressure varies as the engine climbs and descends in altitude. Equation 2 and Figure 4 illustrate how both of these pressures contribute to creating an effective nozzle. Figure 4 also illustrates the negative effect if an inefficient nozzle is used.

Equation 2:

$$F = v_e \dot{m} + (p_e - p_3) A_e$$

The trust of an engine system can be found by using Equation 2. It illustrates that the trust is made up of two parts. The first part is the product of the mass flow rate and

the axial exit velocity, called the momentum thrust. The second is the pressure term, called the pressure thrust, which takes the produce of the exit area and the pressure difference. When the nozzle exit pressure, p_e , and the ambient pressure, p_3 , are not equal, the axial momentum thrust is reduced. Therefore, when $p_e = p_3$, the thrust is maximized and called optimally expanded. ([6], pp. 27"29, 58)

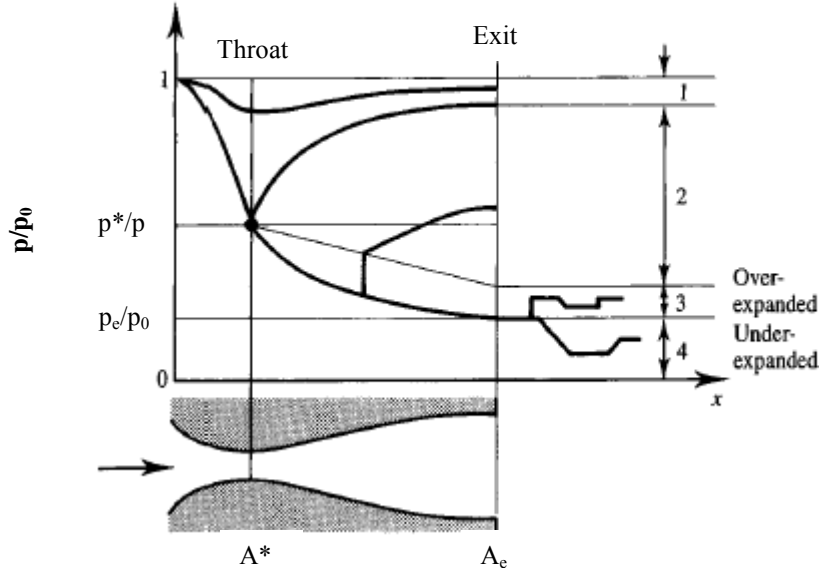


Figure 4. Pressure Ratio vs Distance. (From [7])

Equation 3 [7]:

$$\frac{A_e}{A^*} = \frac{\left(\frac{2}{\gamma+1} \right)^{\frac{\gamma+1}{2(\gamma-1)}} \left(\frac{\gamma-1}{2} \right)^{\frac{1}{2}}}{\left\{ \left(\frac{p_e}{p_0} \right)^{\frac{2}{\gamma}} + \left(\frac{p_e}{p_0} \right)^{\frac{\gamma+1}{\gamma}} \right\}^{\frac{1}{2}}}$$

There are typically four exit flow conditions that a nozzle can operate under based on the above equation: subsonic, underexpanded, full, and overexpanded. If Equation 3 is satisfied, and the pressure ratio does not change, then the flow will be considered full and the maximum nozzle performance will be realized, shown as the line between Section 3 and 4. If the throat section is not sized correctly and a Mach number of 1.0 at the throat is not achieved, then the exhaust will be subsonic, shown as Section 1 in Figure 4.

However, in the case of the PDE, the pressure ratio changes rapidly throughout the engine cycle as the chamber pressure changes throughout the cycle shown in Figure 5. As can be seen in Figure 6, as the chamber pressure increases, so does the necessary area ratio for ideal expansion of the combustion products.

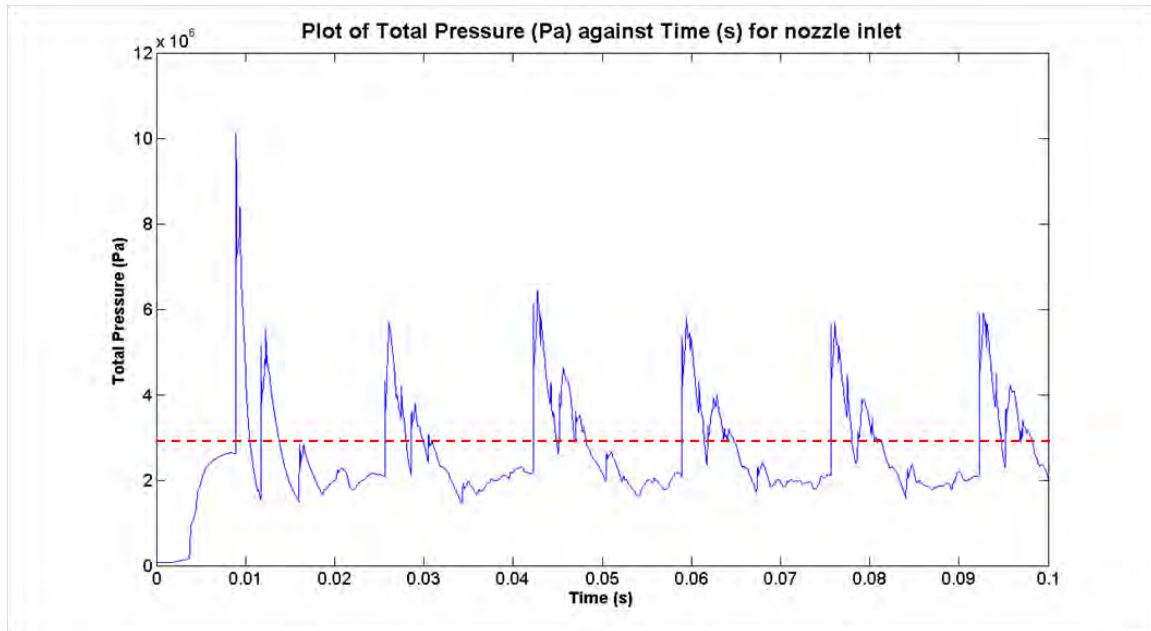


Figure 5. PDE Chamber Pressure versus Time for Hydrogen/Air Reaction at 60 Hz. (From [2])

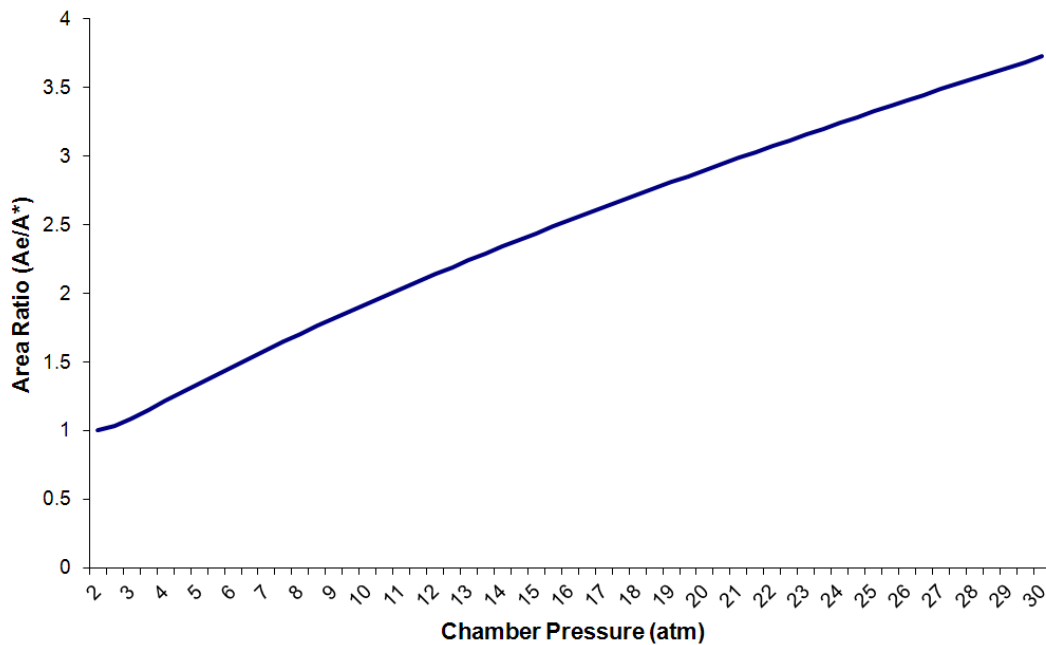


Figure 6. Area Ratio vs. Chamber Pressure

a. Underexpanded Nozzle Condition

If the nozzle were fixed and designed to flow full during the purge cycle, then an area ratio for a three atmosphere purge pressure would be around 1.09. During the combustion event, the chamber pressure would rise dramatically and the nozzle would become underexpanded at the exit plane. Figure 7 illustrates this effect. Since a full flow condition would exist during the refresh condition, the chamber pressure rise during the combustion event would cause the exit pressure to climb as well leading to an increasingly underexpanded condition since additional expansion would have resulted in increased thrust and more appropriate pressure matching. In addition, if the ambient pressure were also less than the exit pressure then the overexpansion would be magnified further. This is illustrated as Section 4 in Figure 4.

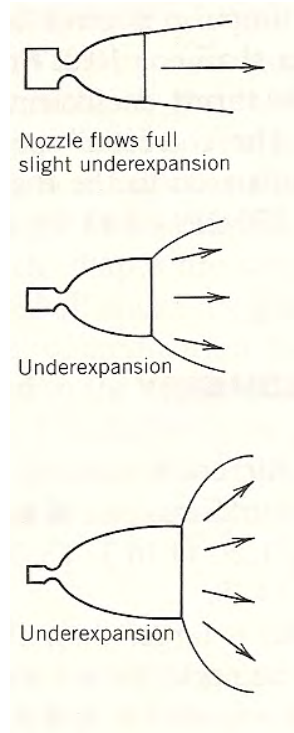


Figure 7. Underexpanded Nozzle. (From [6])

b. Overexpanded Nozzle Condition

If the nozzle area ratio was fixed and designed to flow full during the high pressure conditions immediately after the detonation event, then the flow during the purge and fill phase would be overexpanded. Figure 8 illustrates this effect. With the nozzle flowing full at the end of the combustion portion of the cycle, the chamber pressure would drop causing the exit pressure to lower as well and lead to lower thrust levels, illustrated by Section 3 in Figure 4. If the overexpansion were to continue further, a flow separation would occur inside the nozzle shown as Section 2 in Figure 4. This separation creates a very undesirable condition not only due to the severe loss in thrust and efficiency but also due to additionally imposed strains on the nozzle structure.

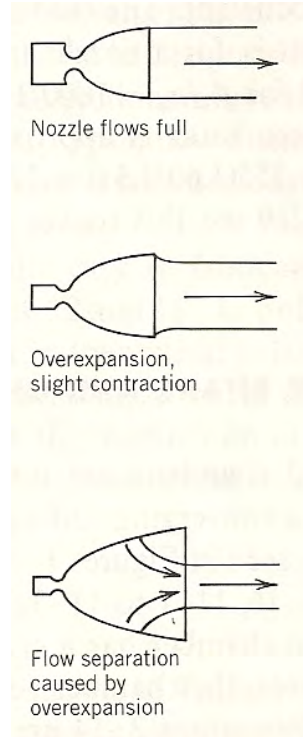


Figure 8. Overexpanded Nozzle. (From [6])

In both cases of a fixed converging-diverging nozzle, the inherent changes in chamber pressure for a PDE results in a varying exit pressure. Therefore, no fixed nozzle will ever produce consistently efficient thrust for a PDE since it would rarely be “on-design” throughout the cycle. Figure 9 illustrates the changing coefficient of thrust based on varying area and pressure ratios. For a given pressure ratio, there exists a maximum coefficient of thrust and therefore, a desired area ratio [2]. However, in the case of a PDE where a constant pressure ratio is not achieved, there exists a constantly varying area ratio required for a maximum thrust term. The red line shown depicts the range for a fixed nozzle with varying pressure ratios if designed for the condition immediately following the detonation event. The top of the line represents the pressure ratio associated with the condition immediately following the detonation event, which intersects the maximum thrust coefficient arc. The bottom of the red line illustrates the result in a lower pressure ratio at the same area ratio found during the purge phase of the

cycle. Most importantly, it illustrates that for a fixed nozzle designed to operate at the blow down phase, the flow will separate within the nozzle and produce a very undesirable condition.

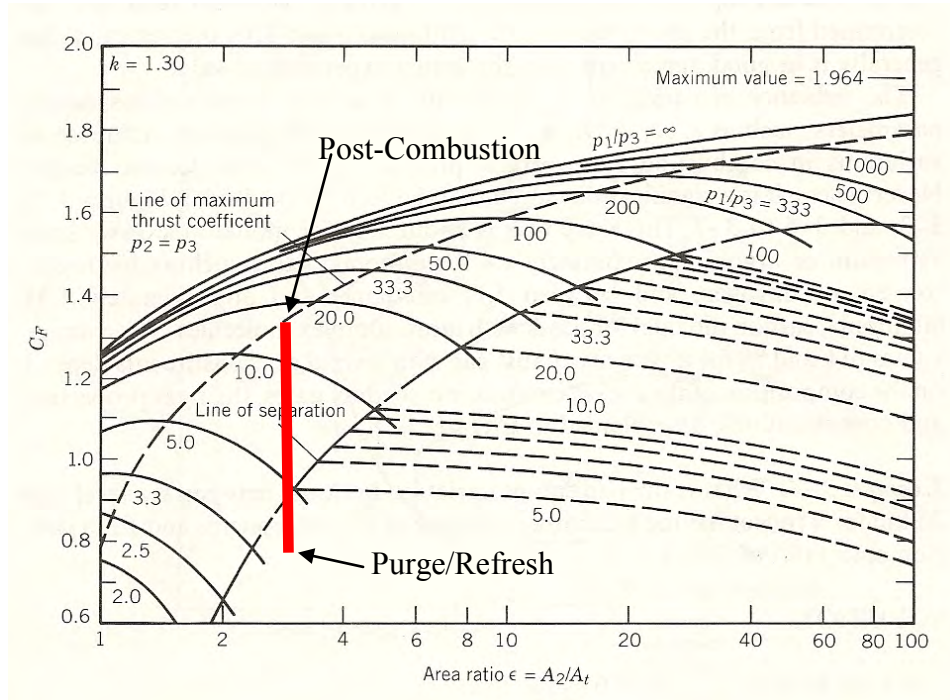


Figure 9. Coefficient of Thrust vs. Area Ratio for a Fixed Exhaust Area.
(From [6])

2. Variable Nozzles

A variable nozzle can be found on some upper-stage rocket engines and on almost every fighter aircraft around the world. As a fighter aircraft operates on widely varying operating conditions for tactical maneuvers, a fixed nozzle would produce losses due to reasons described earlier. Therefore, engineers have long utilized a mechanical nozzle that expands and contracts seeking the optimal area ratio based on chamber pressure and ambient pressure. Figure 10 illustrates the same thrust coefficient versus area ratio graph. Here, the red line depicts the capability of a variable nozzle to alter the exit area, thus vary the area ratio in order to maintain on or near the maximum thrust coefficient curve. As the pressure ratio across the nozzle decreases, the exhaust area also decreases

maintaining the desired efficient area ratio. Likewise, as the pressure climbs, the exhaust area climbs and again maintains the desired efficient area ratio.

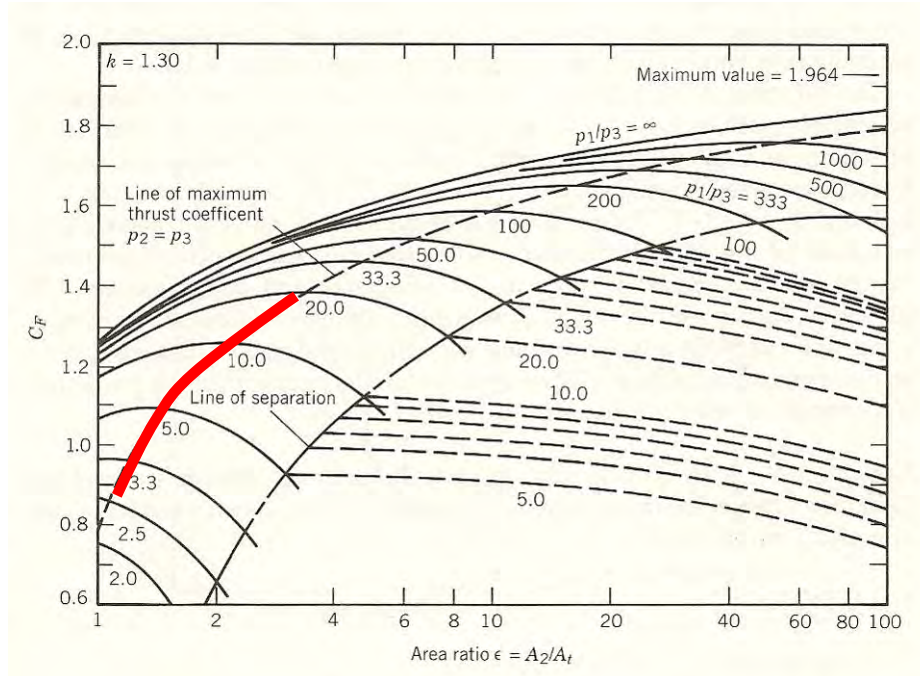


Figure 10. Coefficient of Thrust vs. Area Ratio for a Variable Exhaust Area.
(From [6])

Therefore, for a PDE, this illustrates the necessity for a variable nozzle. However, for an engine that operates up to 100 hertz and with extremely rapid pressure changes, a mechanical system is not feasible primarily due to fatigue and mechanical requirements. Therefore, this research was dedicated to developing a fluidic nozzle to function as a variable area ratio nozzle in order to achieve the most advantageous thrust characteristics for a pulse detonation engine.

III. EXPERIMENTAL SETUP

A. EXPERIMENTAL ASSEMBLY

This research was performed at the Naval Postgraduate School utilizing Test Cell 3 located at the Rocket Propulsion Laboratory. The test setup can be broken up into four categories: the initiation section, the detonation channel, the optical section, and the exhaust section. The test utilized hydrogen (H_2), oxygen (O_2) and compressed air ($O_2 + 3.76N_2$) for the reactants, mixing them at the head of the combustion section. A hydrogen and oxygen torch was used as the ignition source.

1. Initiation Section

The initiation section of the test rig is comprised of the air delivery system, fuel delivery system, and ignition system. The section is a 36-inch (914.4 mm) long machined flange of three-inch (76.2 mm) schedule 80 stainless steel tubing. Five boss connectors are welded to this three-inch (76.2 mm) diameter tube that serve as the attachment points for the fuel and igniter. Air is delivered to the initiation section through a two-inch (50.8 mm) diameter supply line as seen in Figure 11.

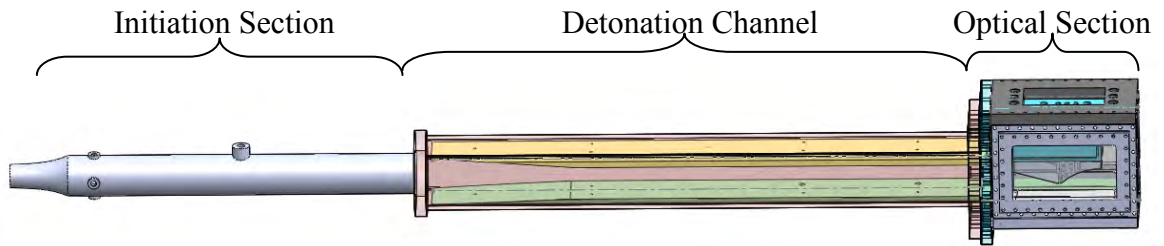


Figure 11. SolidWorks Model of Test Section

a. Air Delivery System

The propulsion lab has an air supply system with a capacity to store 65,000 SCF of air at 2500 psi. The high pressure air is regulated and supplied to every test cell throughout the lab and locally metered by an instrumented choked orifice. Once

the mass flow rate is known, air is then fed directly to the test rig through the two-inch stainless steel union and into the initiation section.

b. Fuel Delivery System

The hydrogen (H_2) fuel is delivered to the test cell through $\frac{1}{2}$ -inch (12.7 mm) diameter supply lines. A series of control valves and mounted solenoid valve eventually deliver the gas to the combustor. Choked flow and check valves are used to prevent back flow. The supply lines are split into three separate flows for the hydrogen, and one for the oxygen. Hydrogen is injected into the combustor through two Swagelock pressure fittings shown in Figure 12. The oxygen and remaining hydrogen line are connected to a Multiple Spark Discharge (MSD) system and attached to the combustor to serve as the ignition source.

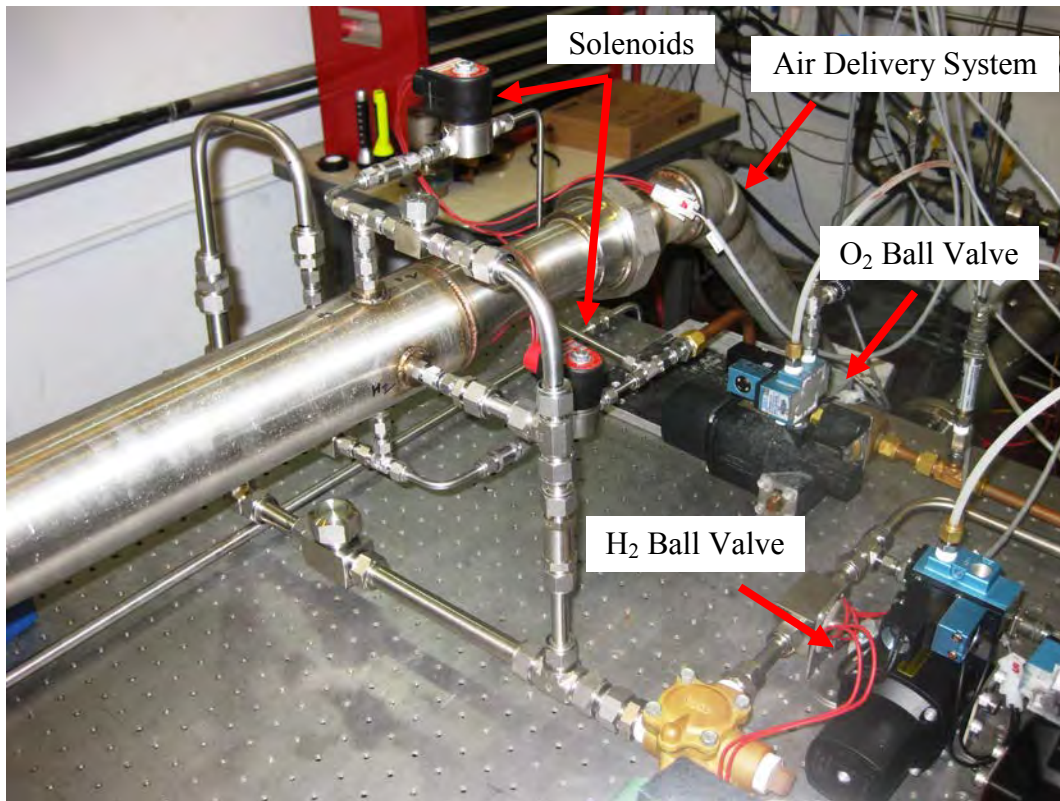


Figure 12. Air and Fuel Delivery System

c. Ignition System

A Multiple Spark Discharge (MSD) system shown in Figure 13 was used to ignite the fuel/air mixture in the initiation section. Oxygen and hydrogen supply lines were connected to a mixing chamber with a standard spark plug attached to the top. The hydrogen and oxygen were mixed in the chamber and lit, causing a high temperature torch to be injected into the fuel/air mixture in the combustor, initiating the detonation.



Figure 13. Ignition System

2. Detonation Channel

The detonation channel was a rectangular, stainless steel channel running 48 inches (1,219.2 mm) in length. Stiffener brackets were placed roughly every four inches (101.6 mm) for support. Within the channel, two “skies” were placed in order to achieve a gradual ramp up to the test section to control the cross sectional area and to ensure a detonation occurred. These skies are illustrated in Appendix A. Two Kistler pressure transducers were placed at the bottom of the detonation channel and exposed to the flow. The primary purpose of the detonation channel was to carry the detonation wave produced in the combustion section to the test section and nozzle. The detonation channel can be seen in Figure 14.

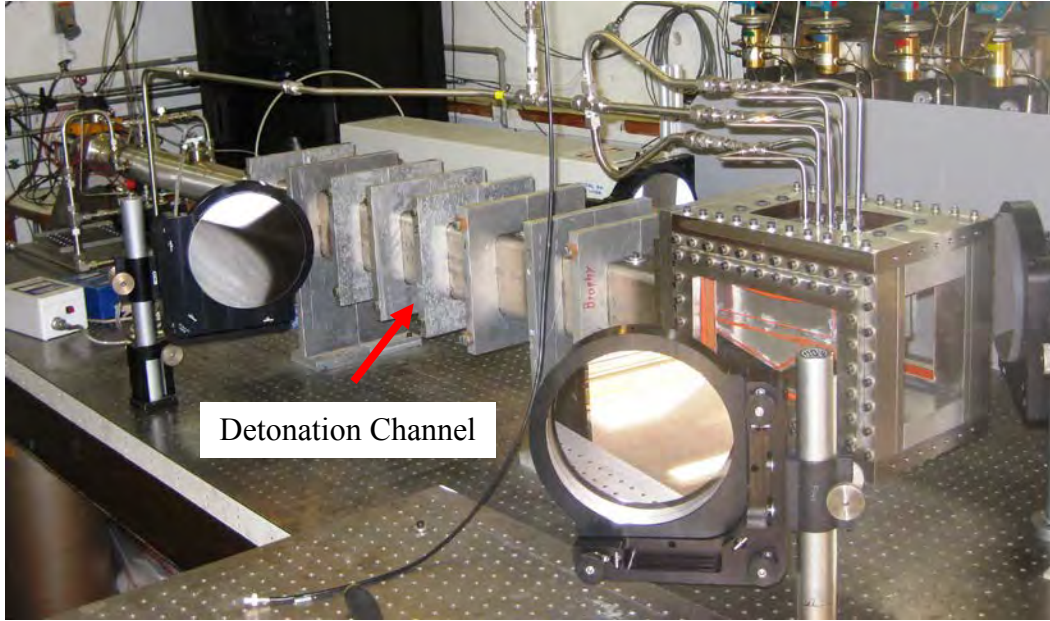


Figure 14. Detonation Channel

3. Optical Section

An optical test section from previous research was utilized, but modified and adapted for this research. It consisted of a solid stainless steel bottom section and two stainless steel side plates which allowed for glass inserts. The top plate was a stainless steel plate with a large rectangle cut out of the center section for the injector air supply to be connected to the mounting block. The nozzle was then attached to the mounting block. On the bottom of the optics section was an attached aluminum plate with a 12 x 0.125 inch (304.78 x 3.175 mm) slit. This floor section allowed for laser sheet lighting to be passed into the section for future research. The optical section can be broken up into these four major sections: the nozzle, the mounting block, the injector air assembly, and the floor section. A photograph of the optical test section is shown in Figure 15.

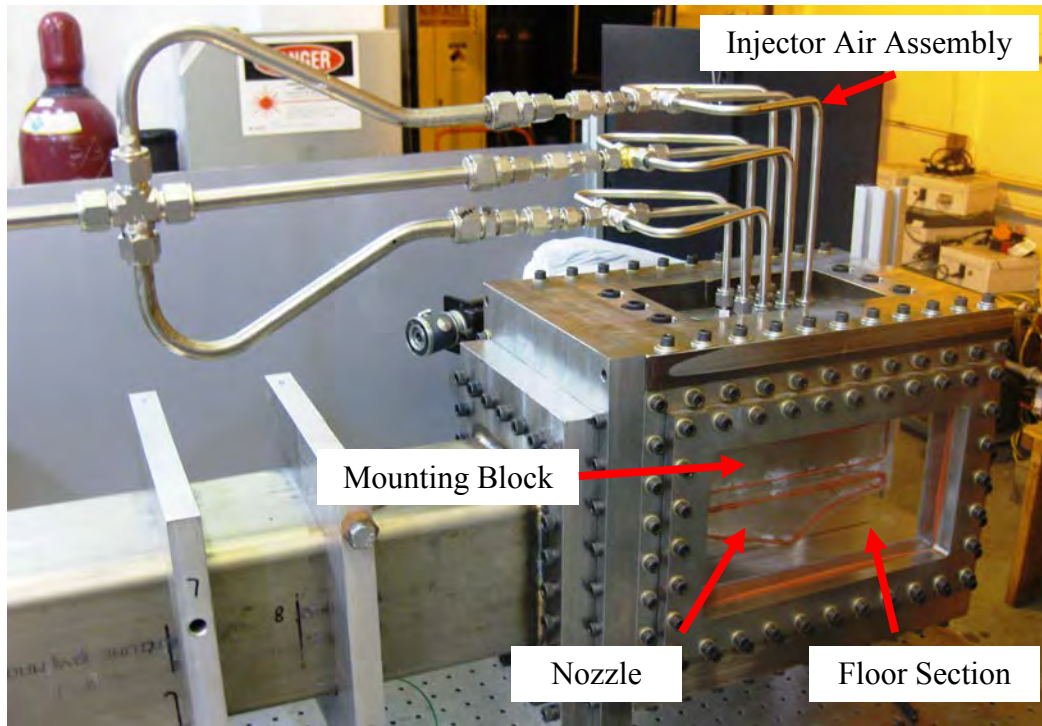


Figure 15. Optical Test Section

a. Nozzle

Three identical nozzles were originally designed, each with a different injector angle [2]. A nozzle that produced a 45 degree air injection angle was utilized throughout this effort based on previous research recommendations. Each nozzle contained three rows of 21 holes, each .125 inches (3.175 mm) in diameter. The back side of each row of holes ended in an opening that runs the entire span of the row. This opening, once married to the mounting block, created an air tight fitting for the injector air pressure to be inserted into the nozzle. The top of the nozzle also had 6 tapped holes to allow for 3/8 inch (9.52 mm) bolts to attach it to the mounting block. Once installed, the subsonic area ratio within the test section was 2.1. The nozzle is shown in Figure 16.

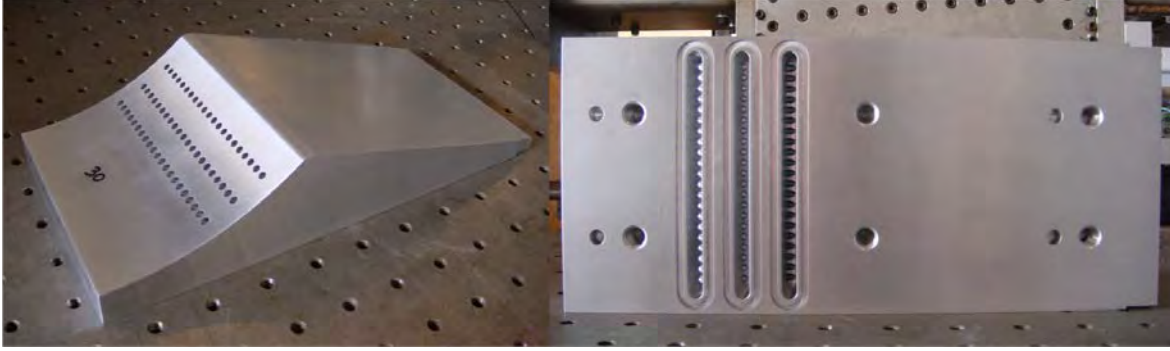


Figure 16. Nozzle with Injectors at 45°. (From [2])

b. Nozzle Mounting Block

The nozzle mounting block was similar to the one previously used but had to be redesigned to conform to the new optical section, as well as improve upon discovered imperfections in the previous design. The mounting block was designed to fit precisely within the optical section so to prevent any flow that may pass between the test section walls and the block. It was fitted with nine tapped holes running through the block where the desired secondary air could pass through to the diverging portion of the nozzle. These nine holes married up with the openings on the top of the nozzle, distributing the secondary air from three of the injector air ports into each of the three rows on the nozzle. Details of the nozzle mounting block can be seen in Appendix A.

c. Injector Air Assembly

The injector air assembly utilized a separate regulated high pressure air line and a number of splitter joints to divide the single air supply port into the required nine ports that connect to the mounting block and lead into the nozzle injector rows. The injector air was taken through a splitter and then a choke for each of the three separate rows as shown in Figure 17. This delivery approach allowed for flexibility and control over each row of injector rows independently. It also allowed for better mass flow rate control into the nozzle. Swagelock fittings connected the injector air assembly into the mounting block which delivered the air to the nozzle.

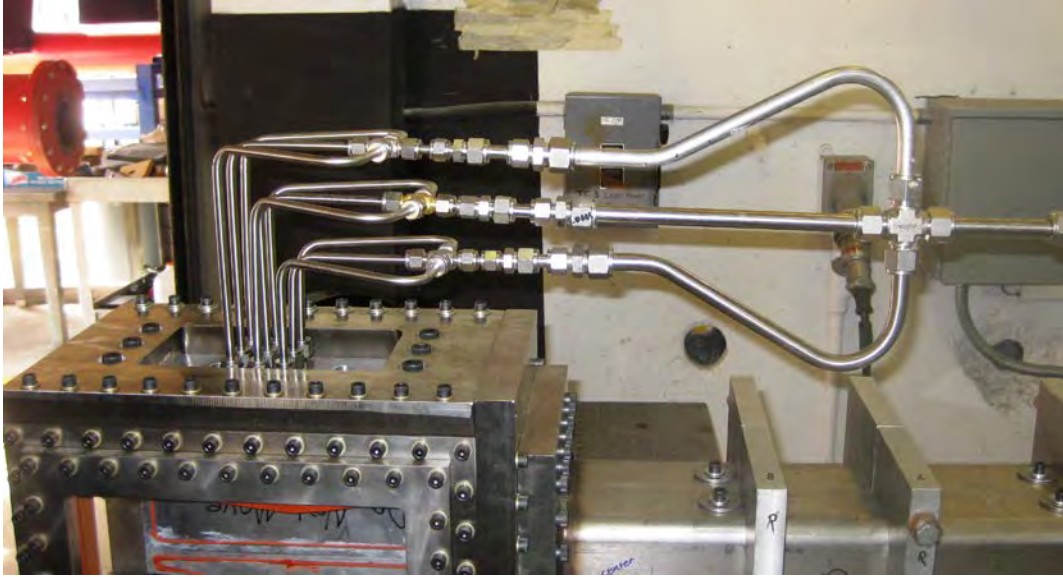


Figure 17. Injector Air Assembly

d. Test Section Floor

The floor of the optical section was an aluminum block that fitted snugly in the test section and attached to the stainless steel base plate with four 3/8 inch (9.52 mm) bolts. The floor section was roughly 1.25 inches (31.75 mm) high in order to set the desired nozzle area ratio. The floor section was also adapted to have a 1/8 inch (3.175 mm) slit cut in the middle running the length of the plate. This allowed a gap for a future laser sheet lighting. Drawings for the Floor Section can be found in Appendix A.

4. Exhaust Section

The exhaust section was completed but utilizing a 1/4 inch (6.35 mm) aluminum box beam with a 6 x 6 inch (152.4 x 152.4 mm) internal cross section. This tube was welded to a one-inch (25.4 mm) thick flange plate that was mounted on the end of the test section. It allowed the exhaust products to vent into a large exhaust flute that vented away from the lab. The exhaust section can be seen in Figure 18.



Figure 18. Exhaust Section

B. INSTRUMENTATION

1. Kistler Probes

Placed in the bottom of the detonation channel were two Kistler 603B1 piezoelectric pressure transducers to capture shock passage and time-varying pressure at the nozzle entrance. The transducers were connected and monitored by the same data acquisition system as the combustor section fuel/air lines and control valves. They were connected to the camera and data acquisition system so that the Kistler transducers would activate and begin data collection at the same moment as the fuel/air mixture ignited. The primary Kistler transducers were used to ensure a detonation wave was formed prior to the nozzle and test section and to record the time-varying pressure ratios during the combustion event and blow-down process.

2. Laser

A Lexel Model 95 Argon Ion Laser was used as the light source. The Model 95 is a water cooled argon laser operated at a 514 nm wavelength. This produces a horizontally polarized beam diameter $\leq 1.5\text{mm}$ and a beam divergence of ≤ 0.6 mrad. This particular laser was utilized due to the ability to spectrally separate the shadowgraph

image from broadband luminosity generated by the combustor products. The laser was fixed to the optical table through a shop-built aluminum mount that raised the laser to match the centerline of the test section and was directed at the first of five mirrors.

3. Mirrors

Five mirrors and a spatial filter were utilized in this research. The setup can be seen in Figure 19 and 20. The first mirror was a small two-inch (50.8 mm) diameter mirror used to reflect the initial laser beam through the 7 μm spatial filter and eventually to a second mirror. The spatial filter created a more effective point source for the second mirror which was an eight-inch (203.2 mm) diameter spherical mirror. This mirror reflected and collimated the laser light back toward a flat eight-inch (203.2 mm) diameter flat mirror next to the test section. This mirror sent the laser energy through the test section another flat eight-inch (203.2 mm) diameter mirror on the other side. The light was then reflected toward a second eight-inch (203.2 mm) diameter spherical mirror. This mirror collected the transmitted image and projected it onto a screen which was then recorded by a high speed camera.

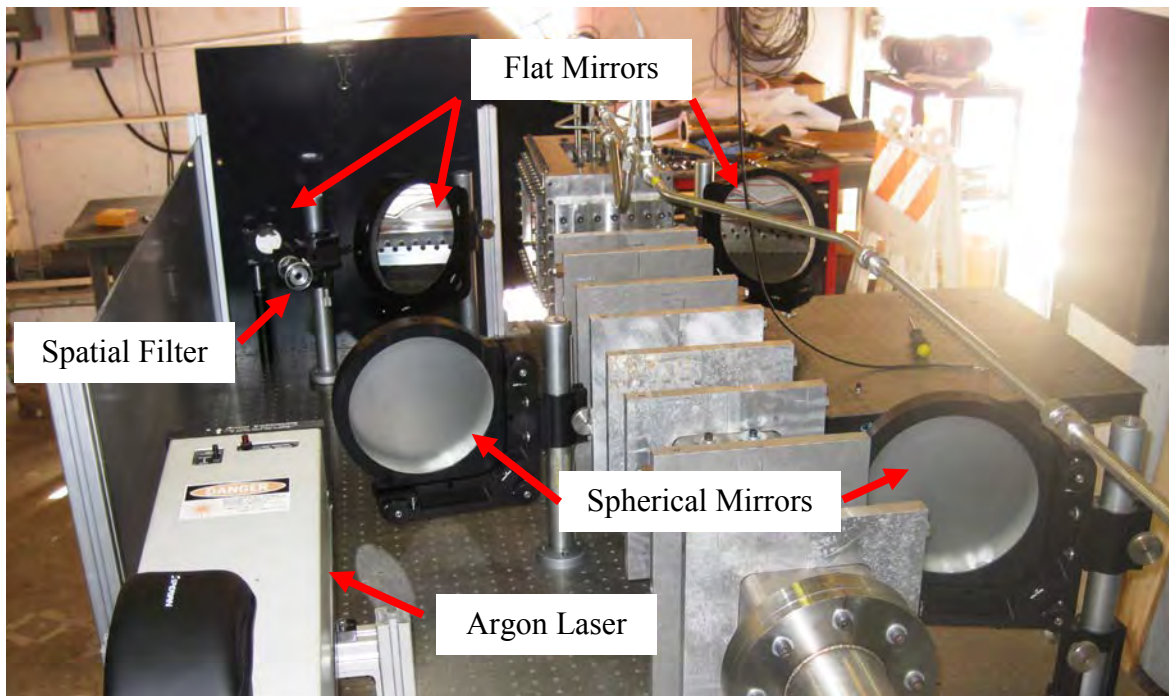


Figure 19. Shadowgraph Mirror Arrangement

4. Camera

The camera used was a Photron Fastcam SA5 high speed camera. The Photron's SA5 camera is capable of taking images at a rate up to 1.4 million frames per second on a reduced resolution setting. For mega pixel resolution, the rate is roughly 7,500 frames per second. The high frame rate of the Photron Fastcam SA5 made this camera the perfect fit for the high speed fluidic transitions occurring in the nozzle during a full detonation and blowdown event. The camera could be located at various distances from the screen to collect the projected image.

C. SHADOWGRAPH

A technique frequently used to visualize the time-varying gas dynamic processes in a compressible fluid is known as Shadowgraph. The shadowgraph is a method for which the density gradients caused by varying temperatures and pressures of transparent fluids, like air, can be seen. The shadowgraph was exceptionally useful for this research due to its simplicity and the 2-D nature of the test section. Within the nozzle test section, variations in temperature and pressure were present due to combustion section gases mixing with the injected medium and the presence of shock waves. Operating a shadowgraph system allows a picture to be taken that clearly illustrates the separation between these regions and how the nozzle shock structure is distributed. This provides a very clear means of comparison between the computer-aided models and the actual test section for analysis. The shadowgraph setup used for this analysis can be seen in Figure 20 and additional details on shadowgraph techniques can be found in Reference 10.

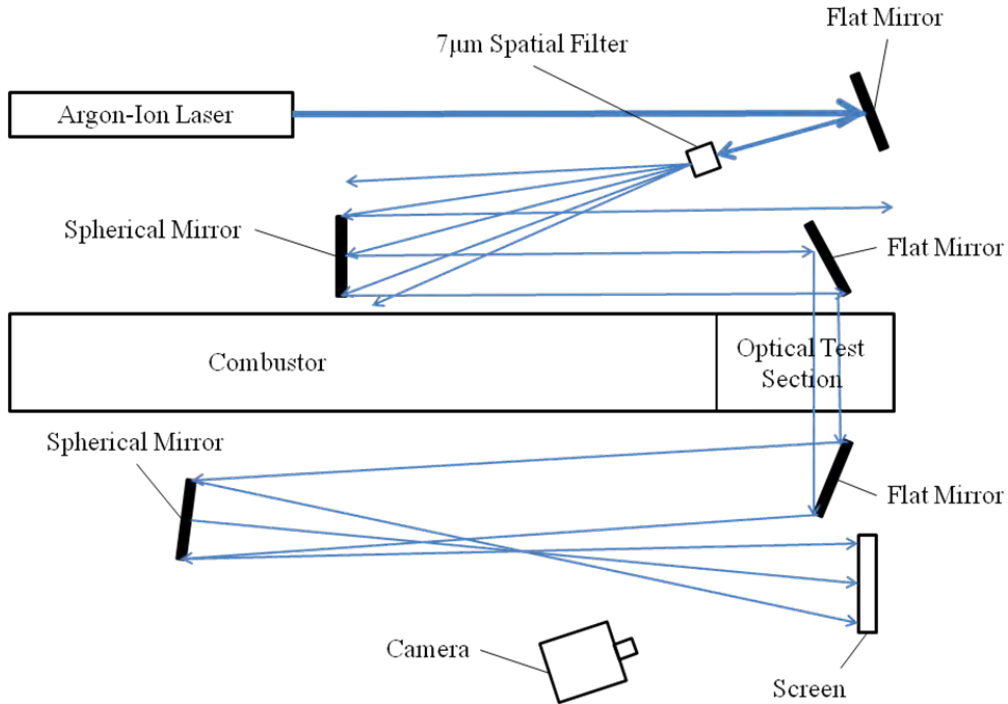


Figure 20. Shadowgraph Setup

D. LABVIEW SOFTWARE

The testing sequence was controlled via a remotely situated control room inside the propulsion laboratory employing LabVIEW Professional Development System Version 10. In conjunction with LabVIEW, a graphical Virtual Interface was uniquely designed specifically for this research to control air/fuel injections, ignition, injector air flow, camera activation, and data collection. It was also designed with an abort mechanism in case fluid pressures went outside of the expected envelope.

THIS PAGE INTENTIONALLY LEFT BLANK

IV. EXPERIMENTAL RESULTS

A. PURPOSE

The experimental testing was performed to image the actual flow field conditions in the diverging section of the nozzle under various secondary air injections settings. These shadowgraph images helped to validate the computer simulations by directly comparing the observed images with the simulation results.

The experimental evaluations were broken into two efforts. The first series of tests did not introduce a detonation in the combustor in order to visualize the refresh condition. The baseline case was for only the combustor mass flow rate proceeding through the nozzle. Secondary injector air was then introduced in varying amounts to image the effect of different mass flow ratios through the injectors on the nozzle exit area. The second test series evaluated performance for an actual detonation in the engine. The detonation was imaged in order to determine if the “pillow” would rebuild in a timely manner.

The experiments were conducted using the previously fabricated nozzle with the injectors at a 45° angle [2], which determined the computer simulation geometry requirements discussed later in Chapter IV.

B. PROCEDURE

The first step in the operating procedure was to introduce the main air flow into the engine as well as the secondary injector air into the nozzle. Once the main air and secondary injector air was stabilized, fuel was introduced upstream of the igniter. Approximately 0.5 seconds later, the ignition system was filled with the needed fuel/oxygen mixture and the torch was sparked. When the fuel/main air mixture interacted with the torch, ignition occurs and a detonation wave was eventually produced that progressed through the detonation channel and into the optical test section. The detonation product gases were then sent through the exhaust tube and out of the test cell completing the cycle. The high speed camera was triggered at the same time as the ignition system and captured the shadowgraph images from across the optical section.

All pressure data was sent into the control room via a National Instruments Graphical User Interface except for the camera where the images were self-contained.

C. REFRESH EXPERIMENT

The first test conducted was a non-detonation case, simulating the refresh segment of the PDE cycle, in order to visualize the subsonic “pillow” development. As discussed earlier, the lower combustor pressures typically found during the refresh or fill cycle forced the nozzle to an overexpanded flow condition. It is during this overexpansion that the “pillow” builds to form a larger subsonic zone and maintain a near-ideal flow for the core flow gases. The refresh condition tests began by filling the combustor with sufficient mass flow to create a chamber pressure of three atmospheres. After the flow was steady and choked flow achieved, the secondary injectors were activated and the desired secondary mass flow rate sent through the injectors. After the core combustor flow and secondary injectors were stabilized, the SA5 high speed camera was operated at 6000 frames per second to capture the shadowgraph image. Since no detonations were used, there was little difference in temperature between the main air feeding the combustor and the secondary air supply. The result was a poor shadowgraph image. Therefore, each non-detonation test used ethylene (C_2H_4) in the secondary injectors as a simulation for the air so to better separate the core combustor flow from the injector flow.

1. Baseline Flow, No Injector Pressure

The baseline flow condition was performed to visualize the flow through the diverging section of the nozzle without any secondary injector mass flow. This was necessary to not only compare later test results to but also to understand how the flow reacts in the fixed, non-augmented nozzle. The supersonic area ratio for the test section fixed nozzle was 2.14. The settings for this test are found in Table 1.

	Node 1	Node 3	Node 4
Gas Controlled	Air	Ethylene	Secondary Air
Back Pressure	4 238 179 Pa	0	N/A
Choke Size	18.39 mm	1.69 mm	1.69 mm
Mass Flow Rate	1.14 kg/sec	0	N/A

Table 1. Settings for Baseline Test, No Secondary Injector Flow

Once the desired combustor pressure of three atmospheres was achieved, the flow within the nozzle became highly overexpanded and the core flow separated from the nozzle wall. The flow separation line can be seen in Figure 21. As the flow separation line continues aft toward the nozzle exit plane, the ambient pressure outside the nozzle exerts a pressure force within the recirculation zone and pushes the interface between the core flow and the secondary flow upward.

Although the secondary injectors are turned off, the residual pressure in the lines was effectively evacuated by the lower pressure of the supersonic core flow as it passed through the diverging section of the nozzle. The trace amounts of ethylene can be seen in the baseline shadowgraph image, but they had little to no effect on the flow formation or separation.

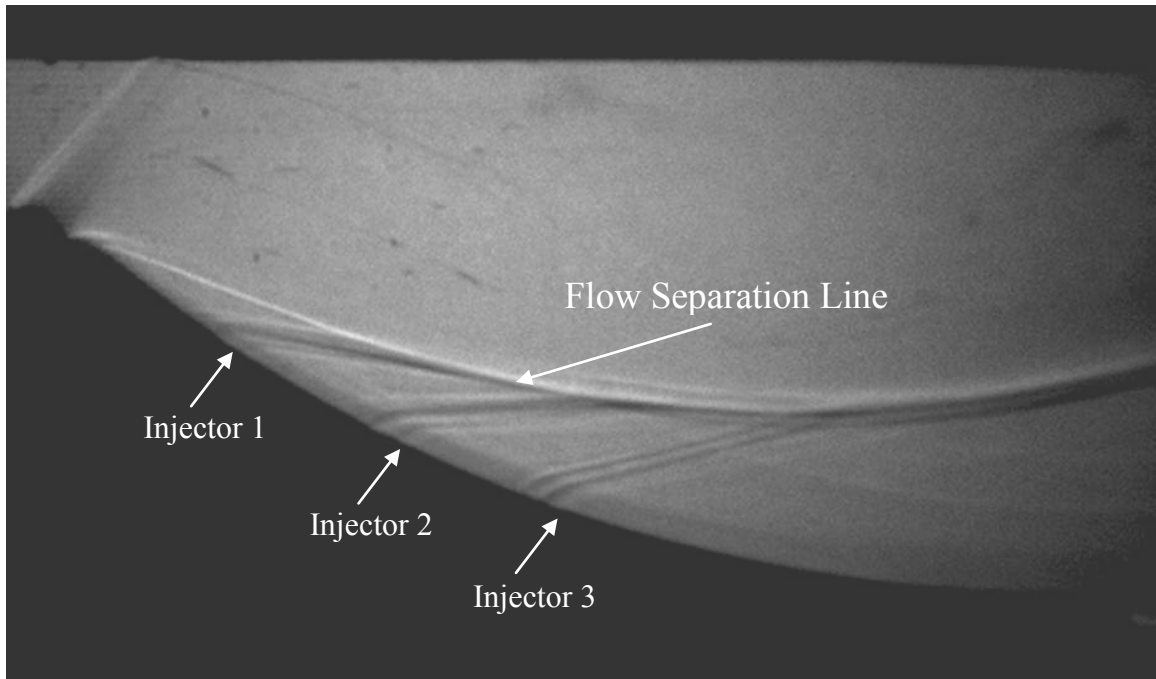


Figure 21. Baseline Flow, No Secondary Injector Mass Flow

2. One Percent Total Core Mass Flow Rate Per Injector

After achieving a baseline flow image, the ethylene was brought up to the necessary pressure in order to deliver one percent of the total combustor mass flow rate into each secondary injector. These settings can be found in Table 2.

	Node 1	Node 3	Node 4
Gas Controlled	Air	Ethylene	Secondary Air
Back Pressure	4 238 179 Pa	3 893 442 Pa	N/A
Choke Size	18.39 mm	1.69 mm	1.69 mm
Mass Flow Rate	1.14 kg/sec	0.0342 kg/sec	N/A

Table 2. Settings for 1% Total Combustor Mass Flow Rate per Injector

With one percent of the total combustor mass flow rate introduced per injector into the diverging section of the nozzle, the interface between the two flow regimes moves upward and the core flow effectively senses a smaller nozzle as seen in Figure 22. The ethylene can also be seen as it exits the injector ports. The stream from the injector ports redirects the core flow, forming a slipline between the injector mass flow and the core mass flow. As each injector stream impacts the core flow, a small deflection is produced creating a weak oblique shock rising from the slipline back into the combustor core flow. The pressure differential between the injector mass flow and the core mass flow is such that the core mass flow is lifted and the separation seen in the baseline test above is removed. Following the slipline down toward the nozzle exit, the effective height of the core flow was measured. The effective nozzle area ratio due to injecting one percent total core mass flow rate per injector was 1.9, substantially lower than the physical 2.14:1 nozzle.

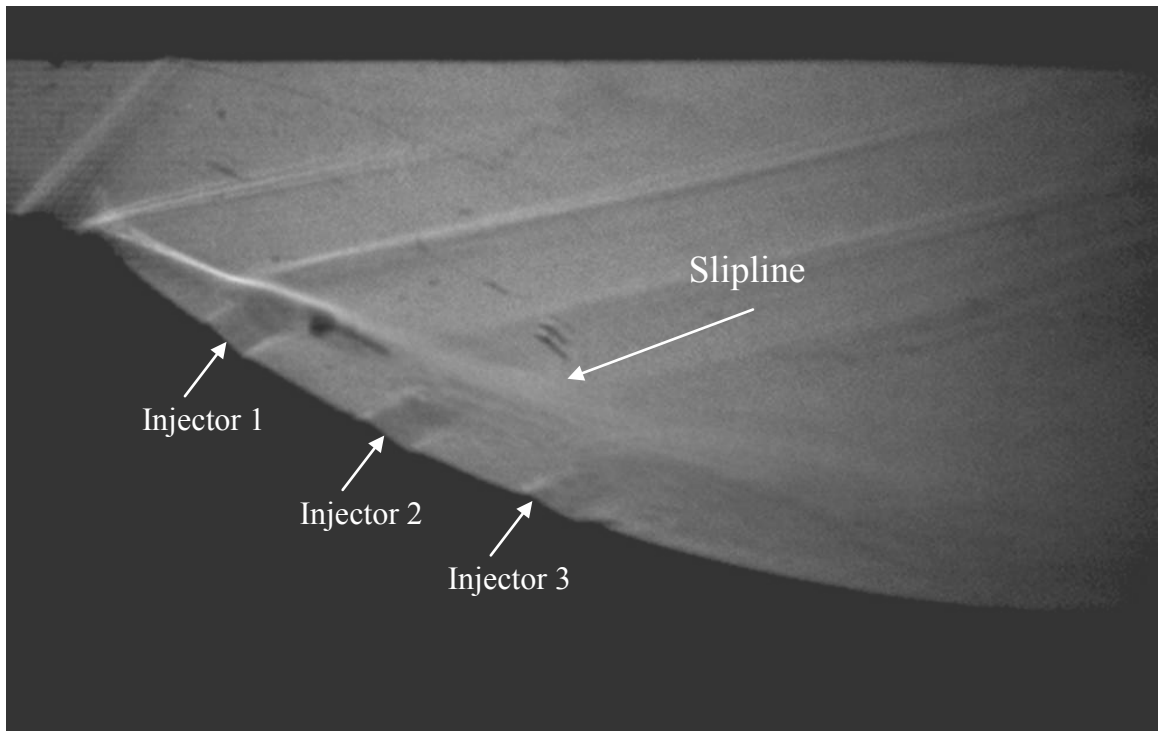


Figure 22. One Percent Total Combustor Mass Flow Rate per Secondary Injector (3% Total Injected)

3. One-Point-Four Percent Total Core Mass Flow Rate Per Injector

As previously discussed, the desired area ratio for the given test pressure ratio is estimated to be 1.3. Therefore, the total mass flow rate percentage was increased in order to amplify the “pillow” seen with only one percent total mass flow rate. The settings for 1.4 percent total combustor mass flow rate per injector can be seen in Table 3.

	Node 1	Node 3	Node 4
Gas Controlled	Air	Ethylene	Secondary Air
Back Pressure	4 238 179 Pa	4 927 655 Pa	N/A
Choke Size	18.39 mm	1.69 mm	1.69 mm
Mass Flow Rate	1.14 kg/sec	0.0479 kg/sec	N/A

Table 3. Settings for 1.4% Total Combustor Mass Flow Rate per Injector

With the increased secondary injector mass flow, the effects within the diverging portion of the nozzle can be more clearly imaged as seen in Figure 23. Similar to the test with only one percent per injector, the injector stream lifts the core flow and reduces the effective nozzle exit area. The estimated effective nozzle area ratio for injector pressures of 1.4 percent total combustor mass flow rate is 1.5. This shows that with a minor increase in injector pressure, the nozzle can be more efficient and the core flow can be nearly ideally expanded for the refresh portion of the PDE cycle.

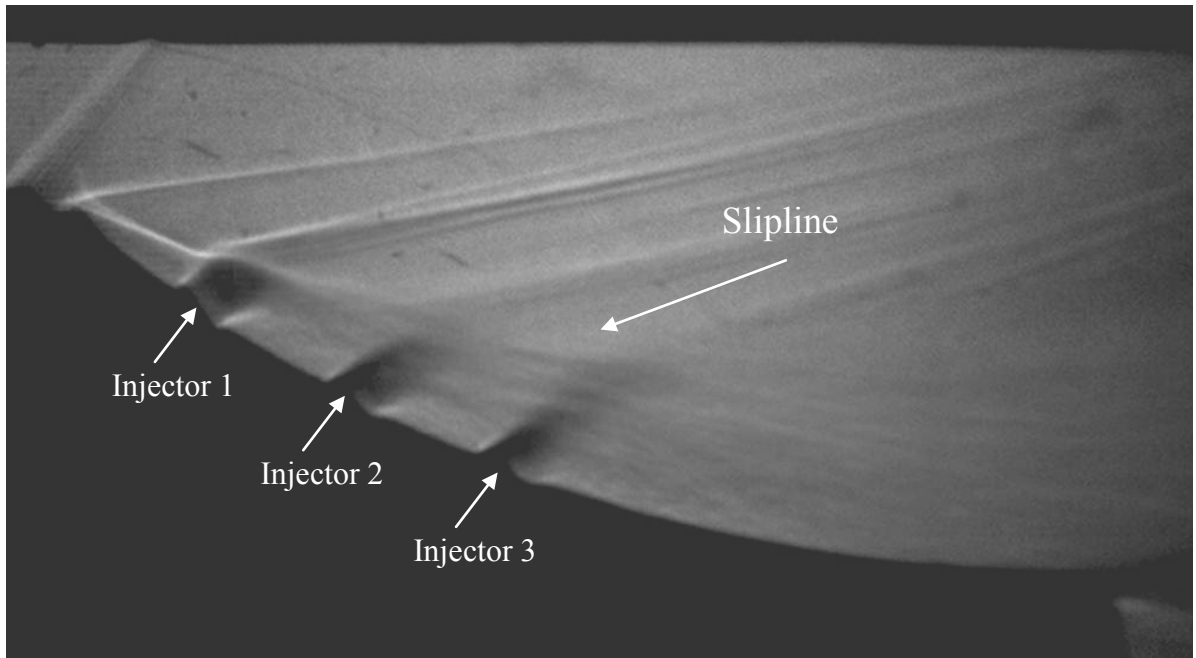


Figure 23. 1.4% Total Combustor Mass Flow Rate per Secondary Injector (4.2% Total Injected)

D. DETONATION EXPERIMENT

The second experimental test run was the detonation case in order to determine if the “pillow” rebuilds efficiently after the high pressures of the detonation and blow down have occurred. As discussed earlier, the high pressures of the detonation and the blow down portion of the PDE cycle will fill the diverging section of the nozzle completely and seek near-ideally expanded flow if the nozzle were designed for this condition. For this section of the experimental test, the combustor section was filled to the three atmosphere operating condition. Once the flow was steady, the secondary injector air was injected, the fuel (H_2) was then introduced for 0.5 seconds, and the ignition sequence was activated as described in Chapter III. In order to assist in the development of the detonation, a shchelkin spiral was inserted into the initiation section and the area ratio was increased to 2.89. The LabView software activated the SA5 high speed camera when the ignition source was triggered and the shadowgraph image was captured at a rate of 15000 frames per second. Ethylene was no longer used in order to prevent combustion in the nozzle due to the high temperatures associated with the detonation. The initial conditions for the detonation test can be seen in Table 4.

	Node 1	Node 2	Node 4
Gas Controlled	Air	Hydrogen	Secondary Air
Back Pressure	2 275 270 Pa	4 171 328 Pa	3 447 379 Pa
Choke Size	18.39 mm	0.190 mm	1.69 mm
Mass Flow Rate	1.09 kg/sec	0.048 kg/sec	0.112 kg/sec

Table 4. Settings for 3% Total Combustor Mass Flow Rate per Injector with Detonation

The detonation case began as the steady state condition similar to that shown previously. Figure 24 shows how the “pillow” is formed and flow is pressed upward toward a near-ideally expanded condition. For comparison purposes, the CFD++ simulation in Chapter V is shown beneath the image. As previously mentioned, the secondary injectors are filled with air; therefore, they are not as noticeable as heretofore shown. Based on Table 4, the secondary injector mass flow rate is roughly ten percent of the total combustor mass flow rate. This allows for a direct comparison the simulations found later in Chapter V.

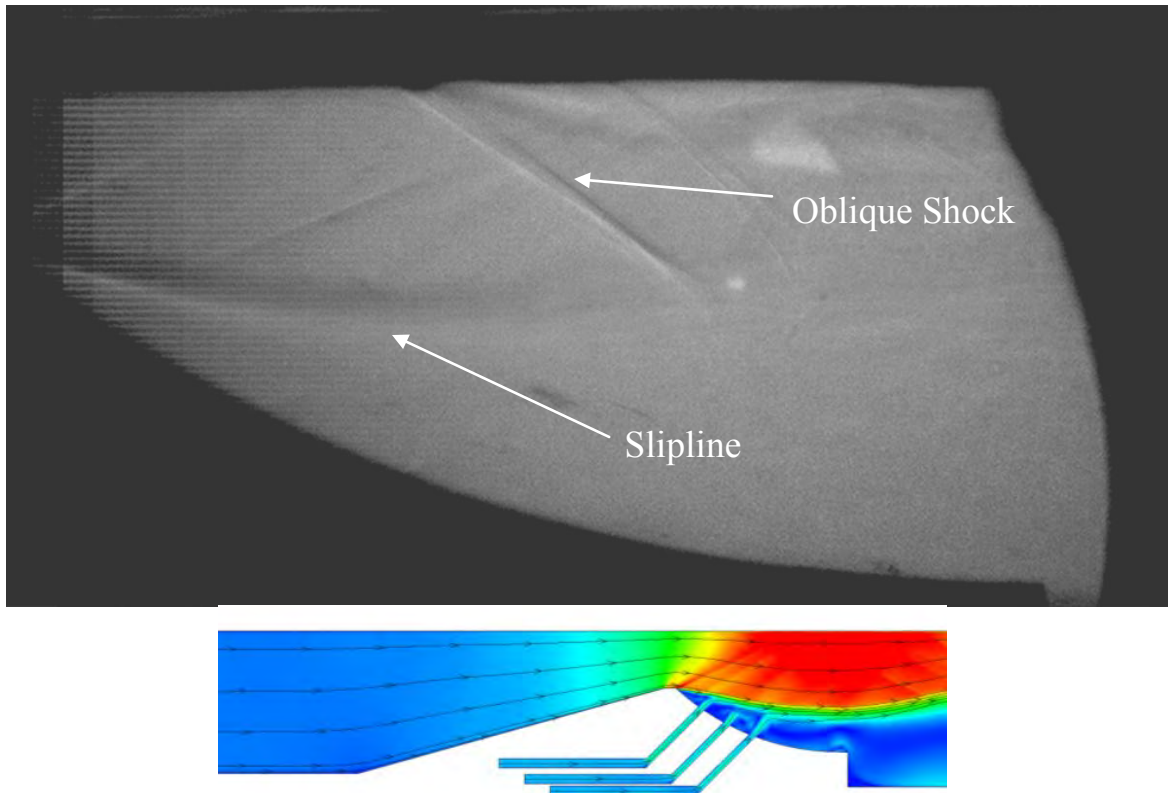


Figure 24. Pre-detonation Flow with Simulation for Comparison,
10% Total Combustor Mass Flow Rate

Once the flow was stabilized, the detonation sequence was started and the initiation section was filled with fuel. The fuel/air mixture was ignited and the combustion wave ultimately transitioned into a detonation after the initiation section. The combustion products eventually travelled through the combustion channel and nozzle. Figure 25 captured the flow soon after the leading shock wave passed through the diverging section of the nozzle. As can be seen, the “pillow” has begun to be suppressed and the combustor flow began to fill the nozzle.

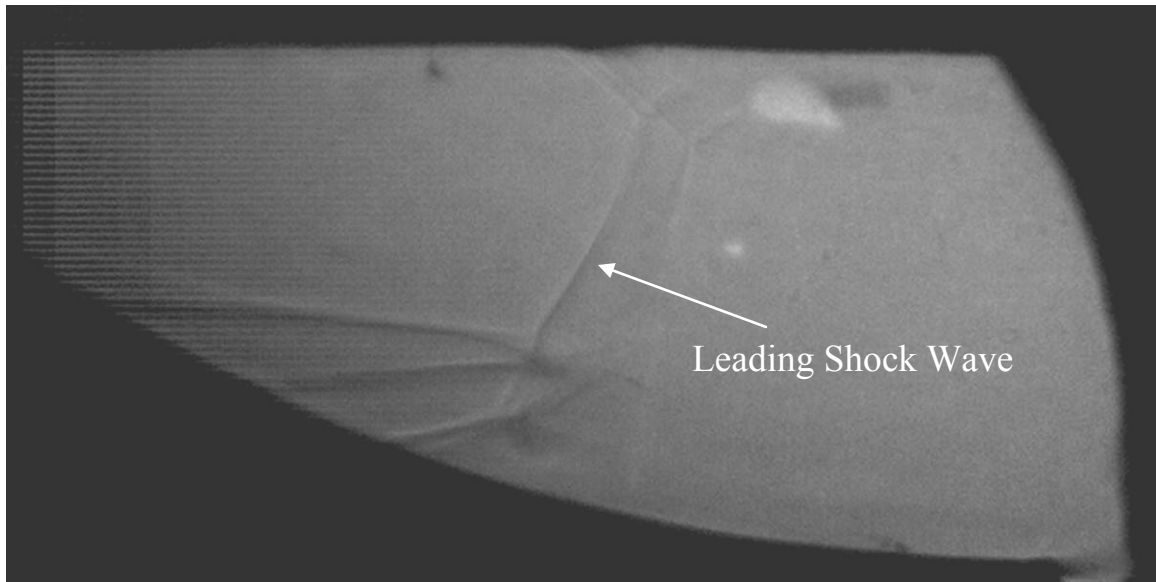


Figure 25. Initial Detonation Wave Enters the Diverging Section of the Nozzle

Due to the large vibrations and shock waves associated with a detonation, the shadowgraph mirrors and laser began to vibrate during the test which eventually caused the picture quality to degrade as the vibrations from the detonation travel throughout the test section. This can be seen in Figure 26 where the combustor flow can be seen fully encompassing the nozzle. The secondary injectors have been completely suppressed. Also seen in the image is a gasket that has been blown out due to the pressures and temperatures associated with the detonation. Although more images were taken, again due to the dynamic situation found during the detonation, very few clear images were actually captured during the detonation passage and initial blowdown.

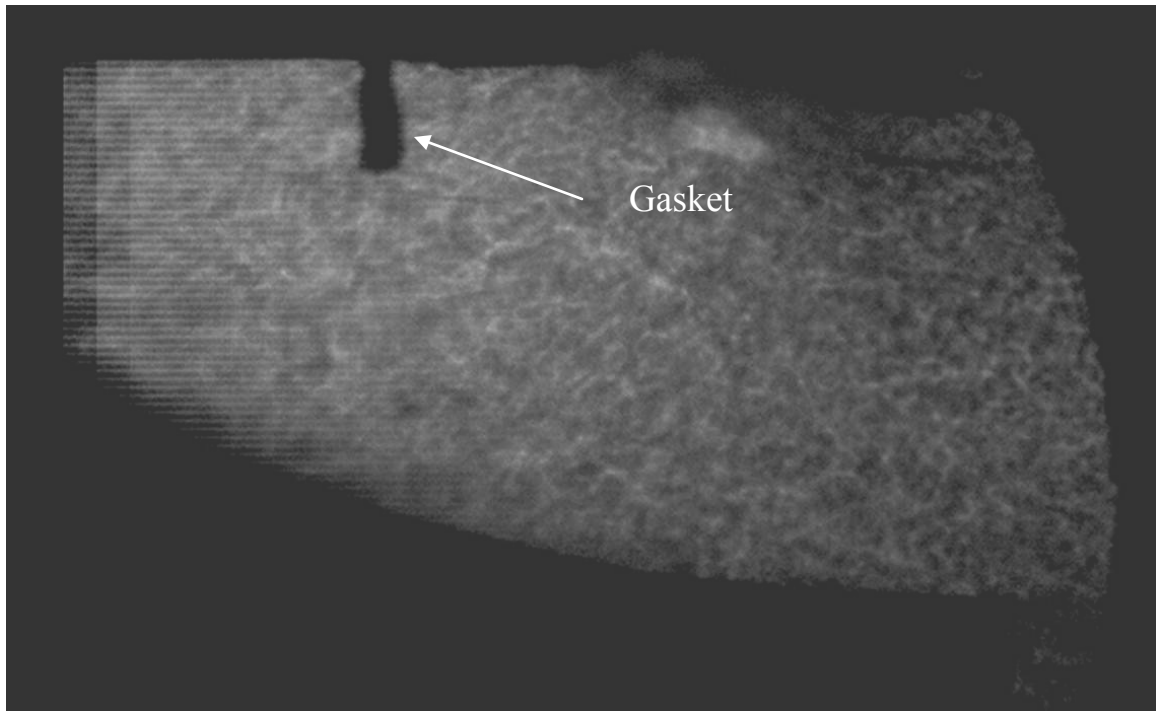


Figure 26. Detonation Products Completely Filling the Nozzle

As the blow down phase travels through the combustion channel, the chamber pressure begins to reduce. As this occurs, the secondary injectors are reestablished and begin to build pressure in the diverging section of the nozzle. Figure 27 illustrates the rebuild of the “pillow” seen in Figure 24. As can be seen, the slipline begins to reform and an oblique shock from the top of the test section can be seen developing midway down the nozzle as seen prior to the detonation.

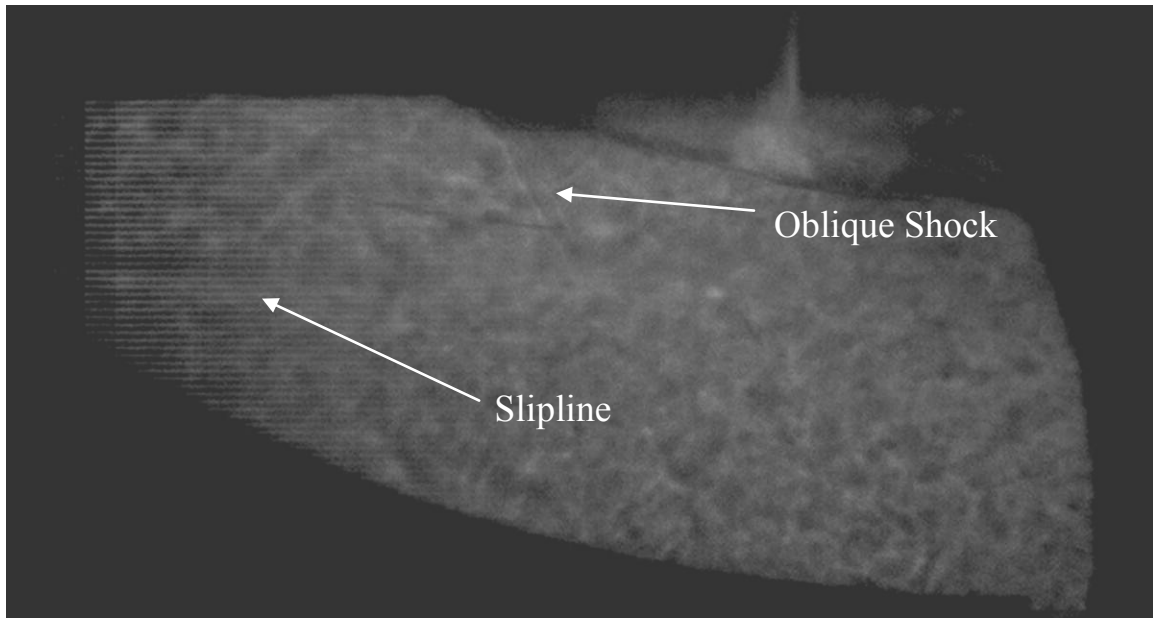


Figure 27. Secondary Injectors Rebuilding the “Pillow”

Finally, as the pressures in the combustor began to stabilize and return to the initial conditions, set for refresh pressures, the secondary injectors are fully formed and have completely rebuilt the “pillow” This can be seen in Figure 28. Again, although the dynamic nature of the test altered the image, the slipline and oblique shocks can be seen in the core flow.

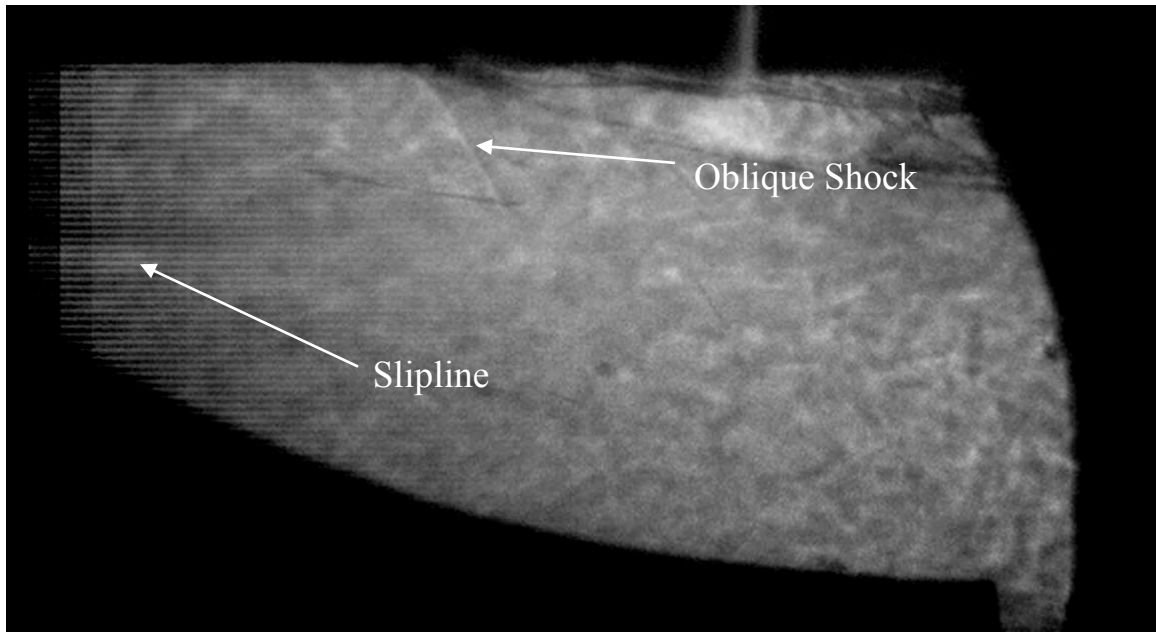


Figure 28. Fully Rebuilt “Pillow”

After the test was concluded and the images analyzed, it became clear after viewing many frames that the secondary injectors were successful. They were able to set the desired effective exit area for the core flow as well as rebuild the “pillow” after a detonation wave and blow down passed through the nozzle.

THIS PAGE INTENTIONALLY LEFT BLANK

V. COMPUTER SIMULATIONS

A number of computer software packages were utilized to generate models of the experimental set-up and simulate the complete combustion cycle for the experiment. The purpose of the experimental effort was to validate the use and fidelity of the computer simulations in order to explore a wider design space and minimize manufacturing costs and time. By confirming an accurate comparison between actual test results and computer simulations, a multitude of varying injector nozzle numbers, angles, and mass flow rates can be tested without the cost of manufacturing and testing each configuration.

The detonation simulations were run with a stoichiometric hydrogen and air mixture while the steady state was simple flow simulation without combustor chemistry. The steady state simulations described how the nozzle would operate at the refresh condition where a nearly constant pressure differential across the nozzle would be present. Once the proper refresh conditions were generated, a detonation was simulated and ran through the combustor and nozzle until the refresh condition was again realized. Since the actual test section was square and a Shadowgraph technique used, the simulations needed to be two-dimensional. Therefore, the three-dimensional model was reduced to a two-dimensional frame before fluid dynamics analysis could be run.

A computational mesh was created from solid model geometries for each two-dimensional nozzle of just under one million elements. Simulated flight condition models for the nozzles were closer to 1.2 million elements. After the models and fluid dynamics software was configured, the simulation was sent to a cluster of 64 processors for analysis. Computational times were normally two days for a steady state simulation and six days for a detonation simulation.

A. MODELING SOFTWARE

SolidWorks 2010 was used to create the geometry for each simulated nozzle and flight condition. The model was created as a three-dimensional model that was then reduced to a two-dimensional model before being meshed. The model was then saved as a parasolid so it would be compatible with subsequent software packages. Mime 4.1 was

used to mesh the geometric models and then the result was imported into CFD++. CFD++ was used to solve the fluid dynamics simulation for both the steady state and the detonation cases. Before a detonation case could be run, the chemistry had to be determined and set into the CFD++ conditions. This was accomplished by using the NASA CEA website. After the CFD++ analysis was completed, the data was transferred to Tecplot 360 2010 for visual analysis and data interpretation.

1. SolidWorks 2010

SolidWorks 2010 is a CAD modeling software package that is with the other utilized software. SolidWorks was used in two phases of this research. The first was to create the actual test section pieces needed to complete the research. These pieces can be found in Appendix A and discussed in Chapter III. Secondly, SolidWorks was used to create the CFD++ two-dimensional models.

As previously discussed, the initial geometries were created as three-dimensional models. However, after completion, the 'Surface' and 'Body Delete' functions were used to reduce the model into a two-dimensional model. This was necessary to precisely mimic the two-dimensional photos being taken through the Shadowgraph technique. It was also important that the 'Surface' function be taken on the $Z=0$ axis. For a two-dimensional model, if any value in the Z axis was present, the CFD++ model would not process.

One specific model was created that was an exact simulation replica of the nozzle to be tested. Using this model, variations in injector mass flow, pressure, and velocities were analyzed to determine the optimal condition.

a. Three Secondary Injectors/All Models

This model was an accurate representation of the actual test section run at the Rocket Lab and discussed in Chapter IV. The initial SolidWorks model was taken from previous work (See [2]) and then altered to support this research. Most of the changes occurred in the area ratio by altering the distance between the top symmetry wall

and the nozzle throat. Figure 29 shows the final model with a plane taken and the body removed so that it could be compatible with CFD++ and Mime 4.1.

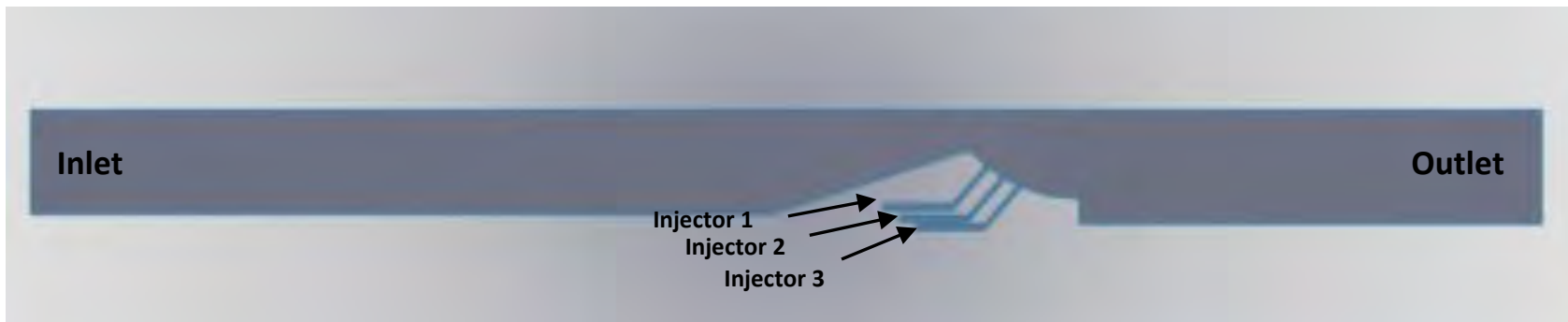


Figure 29. SolidWorks Model of 3 Injectors at a 45° Angle, Quiescent Boundary Condition (No Free Stream)

b. Two Secondary Injectors Operating at a Flight Condition

After the initial simulations were analyzed, a new SolidWorks model was created to determine the effect that a free stream velocity, simulating flight conditions, would have on the nozzle performance. In order to minimize future fabrication time, the injectors were also changed to a more fabrication friendly design to determine if a better injector approach could be used. Figure 30 shows the SolidWorks design of this model. It was started by modifying the model in Figure 29 and then altered. The free stream boundary, still called Injector 3, was started at the exit plane of the nozzle and the parameters were set to a flight condition found in Appendix C.

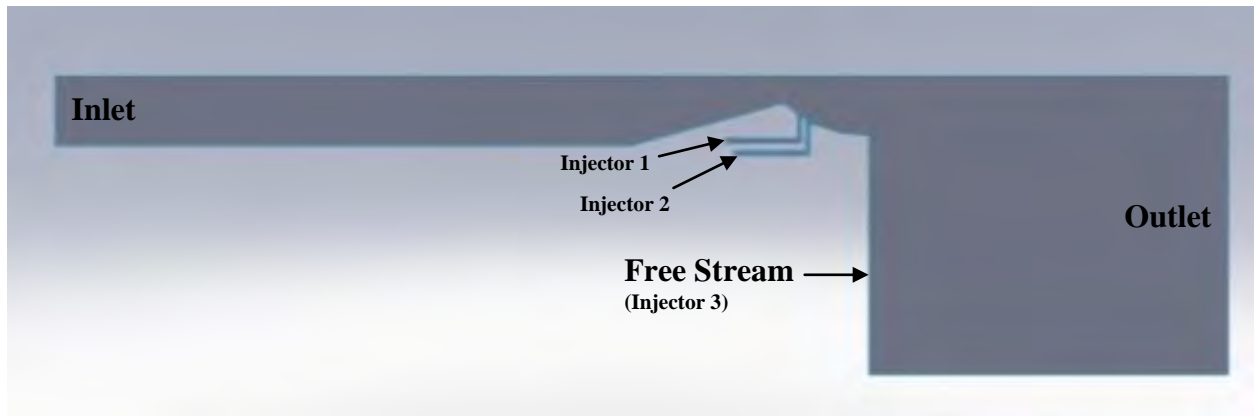


Figure 30. SolidWorks Model of 2 Injectors at a 0° and 90° , With a Free Stream Boundary Condition

2. Mime 4.1

Mime 4.1 is a mesh generation software created by Metacomp Technologies, Inc. Although the current version does not have a direct interface with SolidWorks, it is compatible if the model created is saved as a parasolid. The software was used to produce a computational model that was easily integrated into CFD++. The mesh created for each model was roughly 1 million elements, although the software was capable of creating much finer meshes. This value was set in order to minimize the computational time requirements without sacrificing the result quality. The model was broken up into eight different zones/interfaces: face, inlet, outlet, injector1, injector2, injector3,

symmetry, and walls. These eight regions were used with every model so that new models could utilize the same initial and boundary conditions saving set-up time when using the CFD++ program.

3. NASA CEA

The NASA CEA (Chemical Equilibrium with Applications) software is a computer program that calculates chemical equilibrium between given chemical mixtures and produces the thermodynamic and transport properties for the reaction of those mixtures [11]. For this research, it was applicable to use this program for the detonation case in order to determine the pressure, temperature, and other combustion properties at the Chapman-Jouguet detonation condition for the hydrogen/air mixture used. These values were directly inserted into the CFD++ detonation simulation as input parameters, but the pressure was magnified by three times in order to ensure a comparable pressure rise was simulated. The NASA CEA output used for the model shown above in Figure 29 can be found in Appendix B.

4. CFD++

CFD++ created by Metacomp Technologies, Inc was used on a Linux operating system to perform the fluid dynamic simulations for every run and condition. By importing the Mime 4.1 meshed SolidWorks model into the program, the boundary conditions and chemical reaction rate set-up was designed for two conditions. First was the steady state condition that was to represent the refresh condition of the PDE cycle. The second was the detonation condition which took the final steady state condition output file and set it as the starting point for the detonation simulation.

a. Three Secondary Injectors/All Models

The first step in setting up the CFD++ models was to calculate the properties for each section of the engine. In this case, to closely simulate the actual test conditions, the refresh pressure used in the combustion section was three atmospheres and a temperature of 450 K. Using the known geometry within the combustion section, nozzle throat, and nozzle exit plane, the mass flow rate in the combustion section was

calculated to be 1.94 kg/sec. This value was the foundation of the varying conditions set in the injectors for this research. The initial approach was to utilize a standard bleed percentage of combustor mass flow rate to feed the injectors.

The next step was to set-up the three secondary injector model seen in Figure 29. The CFD++ software allowed for the creation of boxes to set initial conditions. These boxes were created around the families produced in the meshing process. From Figure 31, Box 1 was created around the inlet and set for the expected refresh condition of three atmospheres for the steady state simulation. Box 2 was set around the remaining portion of the combustion section before the nozzle. This value was also set to the refresh condition. Box 3 was formed around all three injectors. Since the initial condition in CFD++ was only a starting point, it was acceptable to set all three injectors as the same since the individual boundary conditions would ultimately define the actual simulation. Box 4 was set at the beginning of the nozzle's converging section and a lower refresh pressure and higher velocity was utilized. Box 5 was the final portion of the nozzle's converging section and applied a slightly lower pressure. And finally, Box 6 housed the exhaust and was set for ambient conditions of one atmosphere.

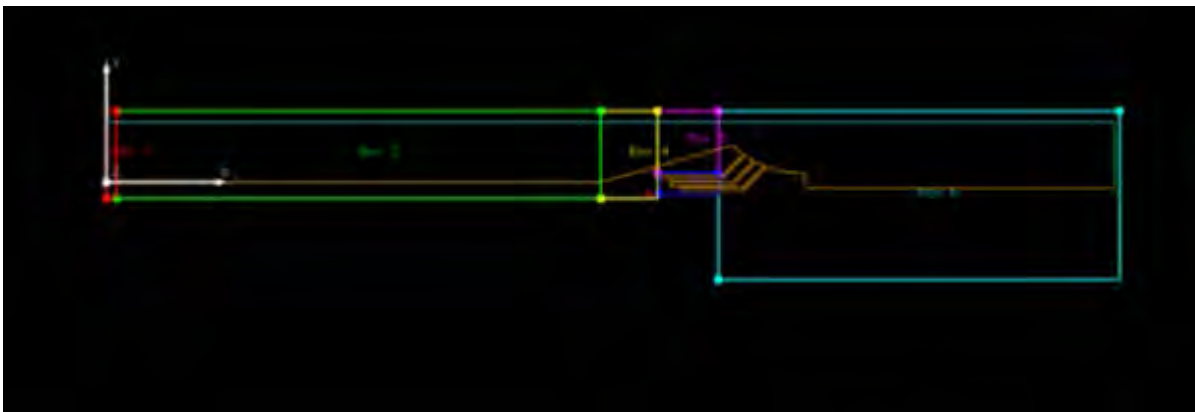


Figure 31. CFD++ Image of Initial Condition Boxes on Model of 3 Injectors at a 45° Angle, Without a Free Stream Boundary Condition

The final step was to produce the boundary conditions for both the refresh and the detonation cases. These can be found below in Appendix C and Tables 5 and 6. These boundary conditions varied based on the simulation performed. The first

simulation continued from previous work [2] and utilized the existing nozzle with three injectors at a 45 degree angle. A number of simulations were then performed varying the mass flow rate from three percent to ten percent of the total combustion section mass flow across all three injectors. Those same mass flow rates were also simulated under two separate pressure conditions, thus separate velocities, to produce the same mass flow rate.

<u>Name</u>	<u>Boundary Condition</u>
Inlet	Multi-species Pressure/Velocity Based Inflow/Outflow
Outlet	Simple Back Pressure
Injector 1, Injector 2, and Injector 3	Pressure, Temperature, and Normal Velocity Inflow
Symmetry and Walls	Multi-species Adiabatic Wall

Table 5. CFD++ Boundary Condition Boundary Settings for each Zone, Steady State Simulation

The detonation simulation was produced by taking the final output file from the steady state simulation and placing it as the starting input file in the detonation condition. However, the initial conditions for Box 1 were overridden from this steady state output file using the post detonation products found from the NASA CEA code. The introduction of the detonation pressure, temperature, combustion species, and CJ parameters, created the simulated detonation that was able to travel down the model and set up the flow conditions across the nozzle. As can be seen in Table 6, in order to closely simulate the actual test and the normal operation of a PDE, the Inlet was set to a multi-species adiabatic wall.

<u>Name</u>	<u>Boundary Condition</u>
Inlet	Multi-species Adiabatic Wall
Outlet	Simple Back Pressure
Injector 1, Injector 2, and Injector 3	Pressure, Temperature, and Normal Velocity Inflow
Symmetry and Walls	Multi-species Adiabatic Wall

Table 6. CFD++ Boundary Condition Boundary Settings for each Zone, Detonation Simulation

b. Two Secondary Injectors Operating at a Flight Condition

The second nozzle simulation was to create a nozzle geometry with easily machineable injectors and produce a boundary condition that would represent a free stream representative of a true flight condition. This free stream was simulated to be at 10000 meters and Mach 3. Figure 32 illustrates the changes in the box parameters as well as the “Injector 3” family. The same boundary conditions as per Table 5 were used in this simulation and the values can be found in Appendix C. Two separate simulations were run with roughly five percent total mass flow rate through the two Injectors. The first utilized similar pressure and velocities across both Injectors 1 and 2. The second simulation increased these parameters in Injector 1 and decreased them in Injector 2 but maintained a total five percent mass flow rate. Time constraints limited the number of simulations performed for this case.

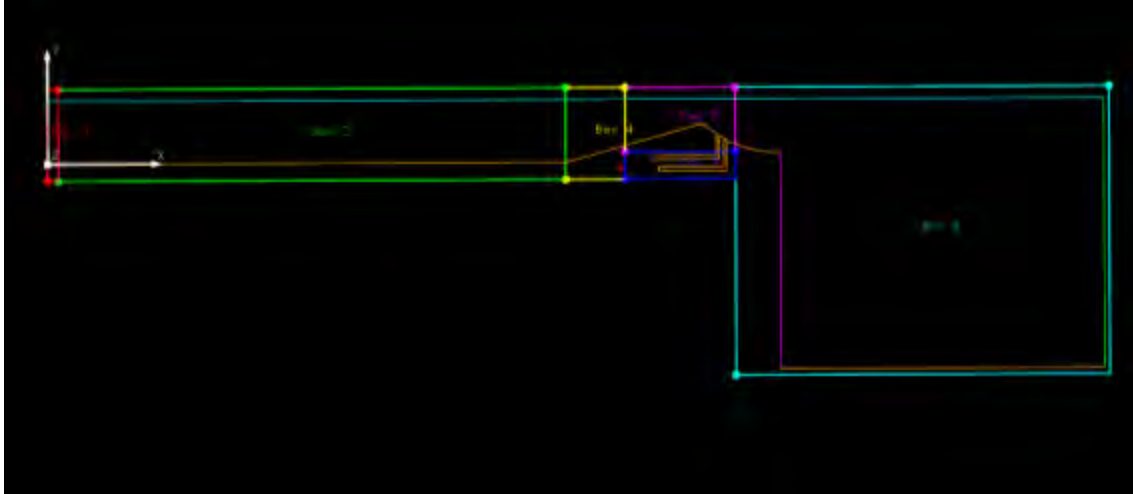


Figure 32. CFD++ Snapshot of Initial Condition Boxes on Model of 2 Injectors at a 0° and 90°, With a Free Stream Boundary Condition

5. Tecplot 360 2010

Tecplot 360 2010 is post processing software program designed by Tecplot, Inc. This software was preferred over the CFD++ post processing package due to its ability to represent the results conveniently for comparison to the shadowgraph results. Tecplot 360 also produced a better, more user friendly method of collecting flow data and visualizing the streamlines. This allowed for a much easier method of comparing the actual test with the computer simulations.

B. SIMULATION RESULTS

1 Steady State/Refresh Condition

a. *Three Secondary Injectors/All Models*

The steady state, or refresh, simulations utilized the parameters found in Table 7. The initial runs were initiated based on previous work, Case 1 (see [2]), and were based off of a constant mass flow rate in the combustion section of 1.94 kg/sec. Then, the injector parameters were varied until a suitable result was realized. Other cases were preliminarily analyzed but did not produce positive results. These included cases that set Injector 1 at 45°, Injector 2 at 52.5°, and Injector 3 at 60°, the reverse of those angles, and a single Injector at a 0° angle (purely vertical).

Simulation	Injector Pressure (Pa)	Injector Velocity (m/s)	Percent Total Mass Flow Rate (per Injector)
Case 1: Run 1	151987	33.75	1.00
Run 2	151987	37.50	1.50
Case 2: Increasing	121590 (Injector 1)	30.00	0.50
	136789 (Injector 2)	33.75	1.00
	151987 (Injector 3)	37.50	1.50
Case 3: Decreasing	151987 (Injector 1)	37.50	1.50
	136789 (Injector 2)	33.75	1.00
	121590 (Injector 3)	30.00	0.50
Case 4: Run 1	131722	34.90	1.00
Run 2	131722	69.20	2.00
Case 5: Run 1	111457	61.89	1.50

Table 7. CFD++ Injector Boundary Conditions, Initial Conditions
(3 Injectors at a 45° Angle, Without an External Free Stream)

Case 2 varied the injector flow rate to begin at a lower setting for Injector 1 (0.50% total mass flow) and increase up to Injector 3 (1.50% total mass flow). Case 3 reversed these parameters, beginning with a higher flow rate in Injector 1 (1.50% total mass flow) and decrease to Injector 3 (0.50% total mass flow). Case 4 maintained a one percent and two percent mass flow rate per Injector, but decreased the pressure resulting in an increased velocity. Case 4, Run 2 showed an improvement to previous cases and illustrated the importance of velocity (momentum) for the injector parameters. Therefore, Case 5 was run with an even lower pressure, 1.1 atmospheres, and a resulting increase in velocity. Figures 34-40 illustrate the various conditions of these runs as well as the subsonic “pillow” that is formed. Figure 33 is a CFD++ analysis with no pressure as a baseline for comparison. Each figure was taken at a time step of 700 microseconds. It was determined that at this time step, the flow simulation was fully developed and steady.

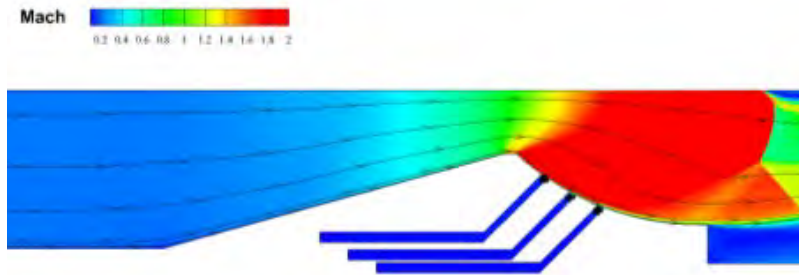


Figure 33. Steady State Simulation, 3 Injector Nozzle at 45° Angle, No Injector Flow, Baseline

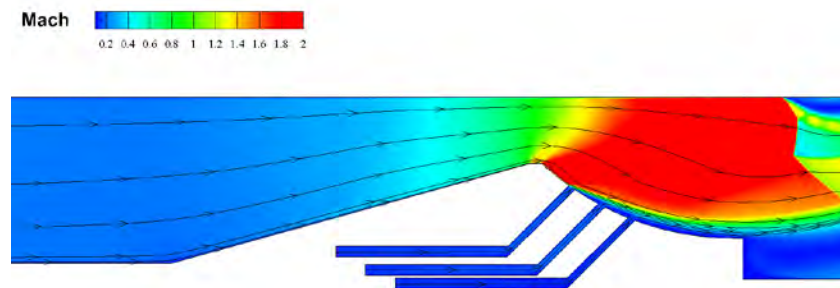


Figure 34. Steady State Simulation, 3 Injector Nozzle at 45° Angle, Case 1, Run 1

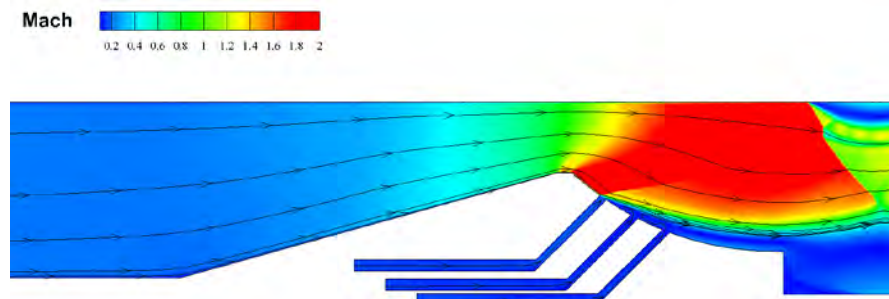


Figure 35. Steady State Simulation, 3 Injector Nozzle at 45° Angle, Case 1, Run2

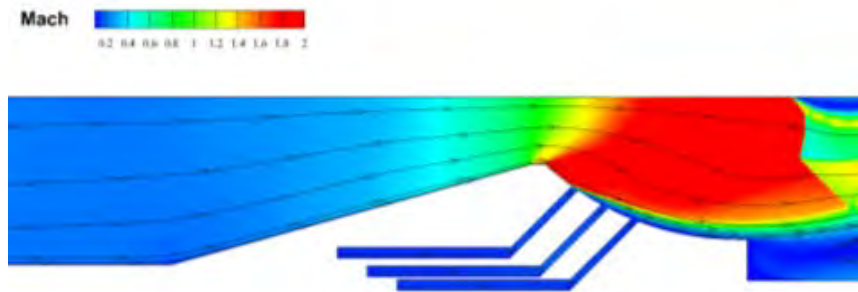


Figure 36. Steady State Simulation, 3 Injector Nozzle at 45° Angle, Case 2

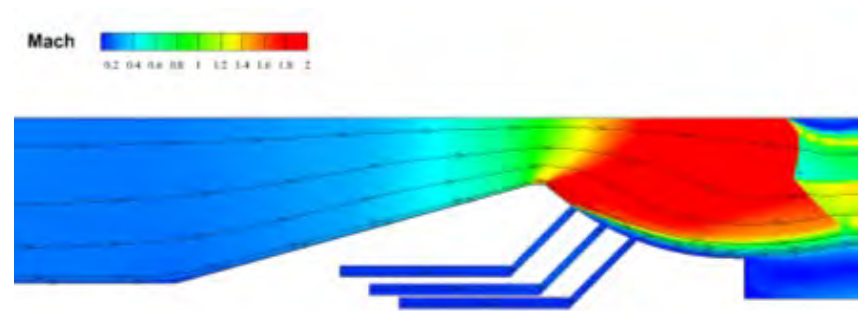


Figure 37. Steady State Simulation, 3 Injector Nozzle at 45° Angle, Case 3

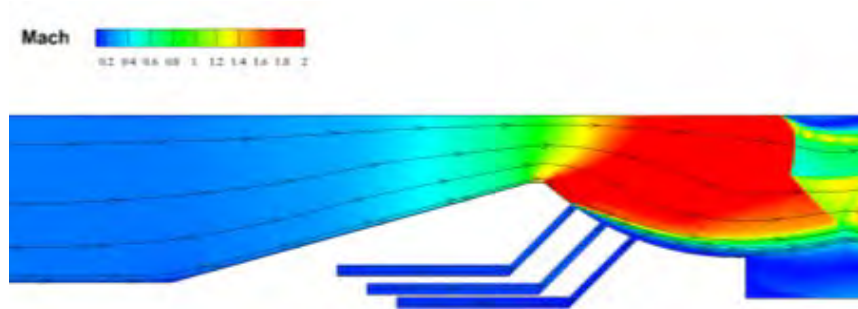


Figure 38. Steady State Simulation, 3 Injector Nozzle at 45° Angle, Case 4, Run 1

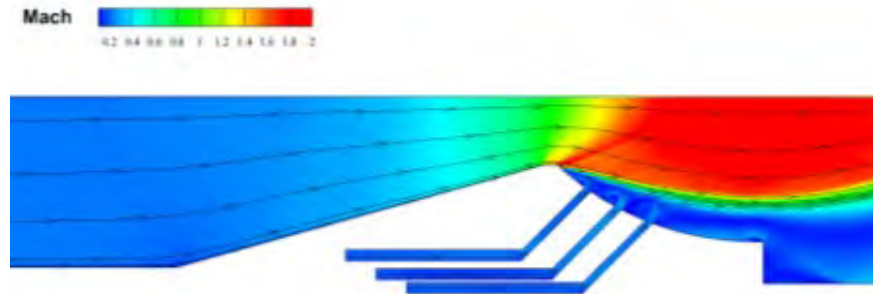


Figure 39. Steady State Simulation, 3 Injector Nozzle at 45° Angle, Case 4, Run 2

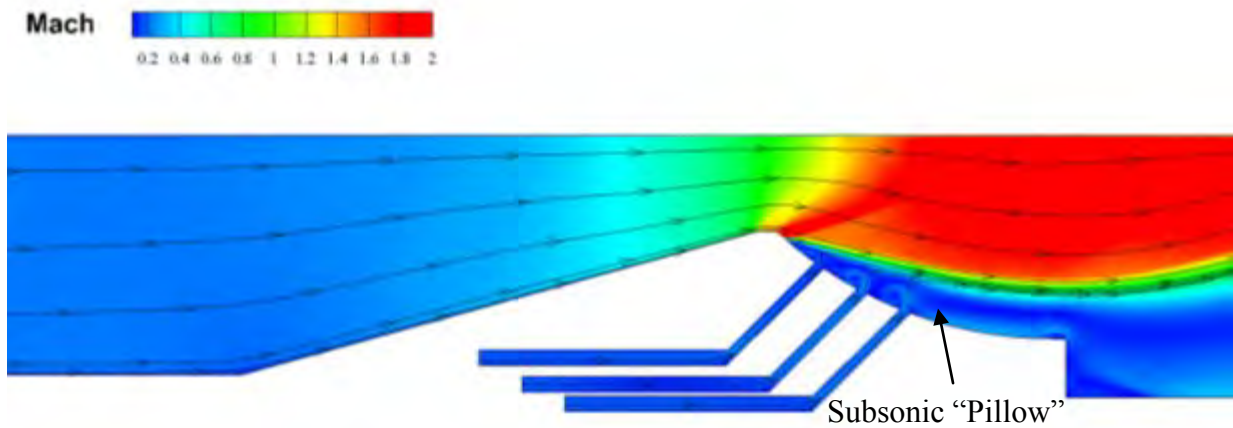


Figure 40. Steady State Simulation, 3 Injector Nozzle at 45° Angle, Case 5, Run 1

Case 5 showed the best “pillow” and results of all the analysis completed. Therefore, further CFD++ analysis was conducted using this pressure and varied mass flow rate through changes in velocity at the initial input. Table 8 shows the varying parameters and Figures 41–45 illustrate the results.

Simulation	Injector Pressure (Pa)	Injector Velocity (m/s)	Percent Mass Flow Rate (per Injector)
Case 6: Run 1	111457	61.89	1.50
Run 2	111457	68.08	1.65
Case 7: Max	111457	137.5	3.30
Case 8: Dual	111457	103.1	2.50
Case 9: Single	111457	206.3	5.00

Table 8. CFD++ Injector Boundary Conditions, Same Pressure, Varying Mass Flow Rate (3 Injectors at a 45° Angle, Without an External Free Stream)

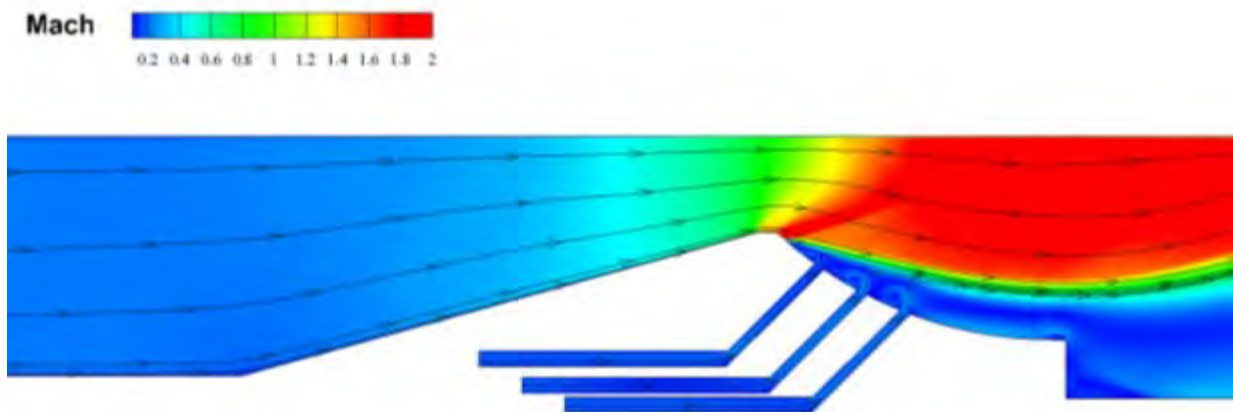


Figure 41. Steady State Simulation, 3 Injector Nozzle at 45° Angle, Case 6, Run 1

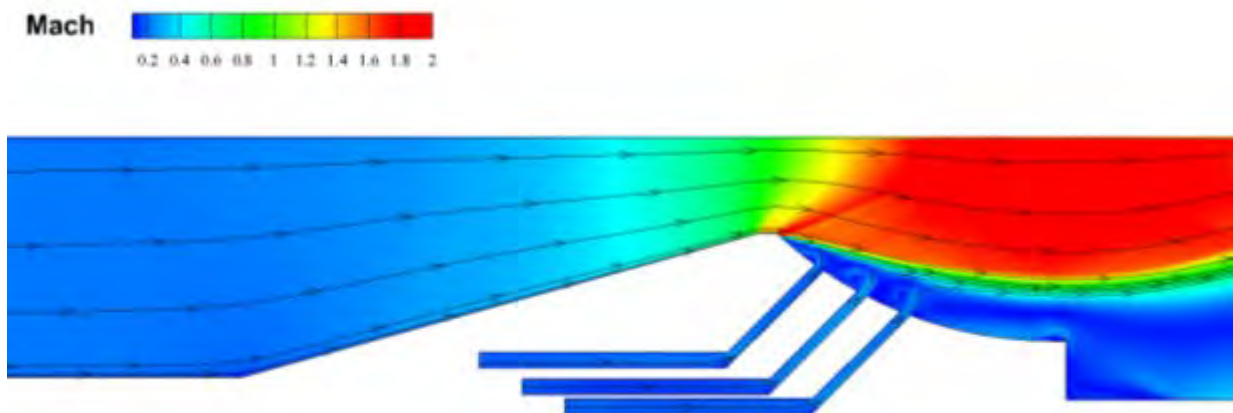


Figure 42. Steady State Simulation, 3 Injector Nozzle at 45° Angle, Case 6, Run 2

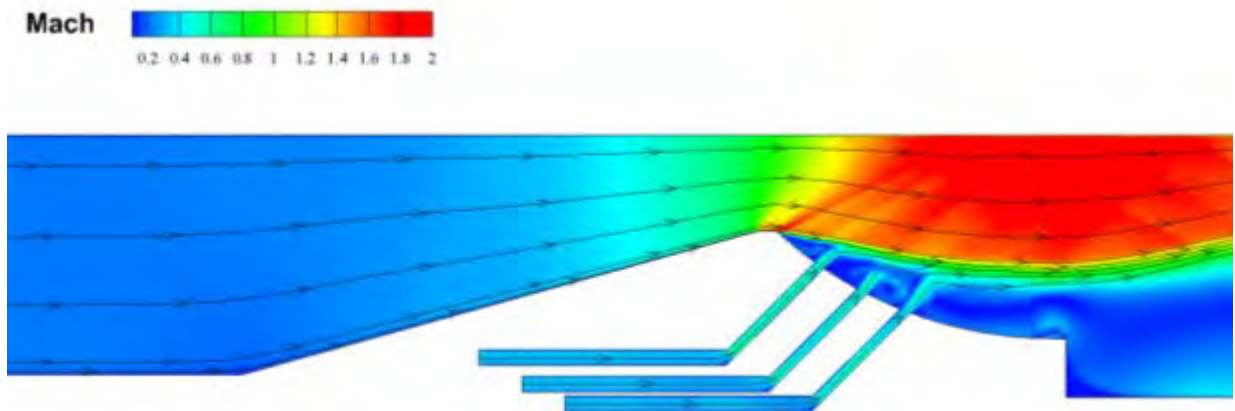


Figure 43. Steady State Simulation, 3 Injector Nozzle at 45° Angle,
Case 7, Max \dot{m}

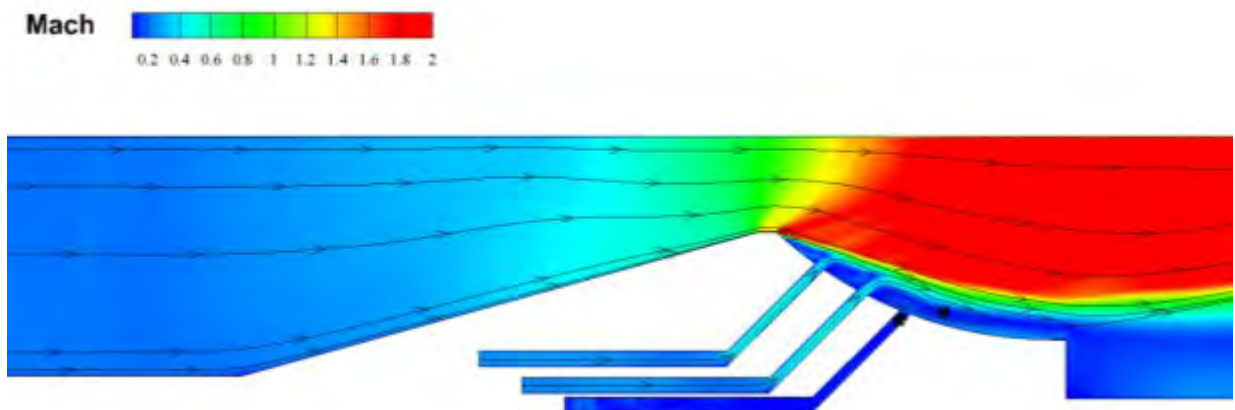


Figure 44. Steady State Simulation, 3 Injector Nozzle at 45° Angle,
Case 8, 2 Injectors Used

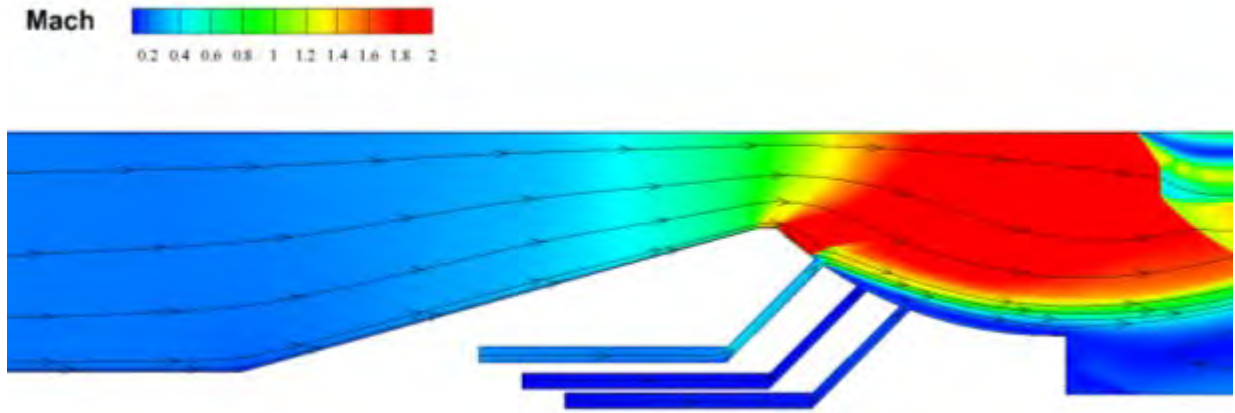


Figure 45. Steady State Simulation, 3 Injector Nozzle at 45° Angle,
Case 9, Single Injector Used

Initial analysis indicates that utilizing all three injectors produced more favorable flow field and thrust characteristics over the dual or single injector. Therefore, a thrust analysis was conducted to compare the results from the cases that were 3.0, 4.5, 5.0, 6.0, and 10 percent total mass flow rate through the three injectors. Tecplot was used to extract pressure and momentum data at the exit plane for each of these runs. This data was used to calculate the thrust at the exit plane based on Equation 2 and then plotted. This plot can be seen in Figure 46.

Equation 2 [6]:

$$F = v_e \dot{m} + (p_e - p_3)A_e$$

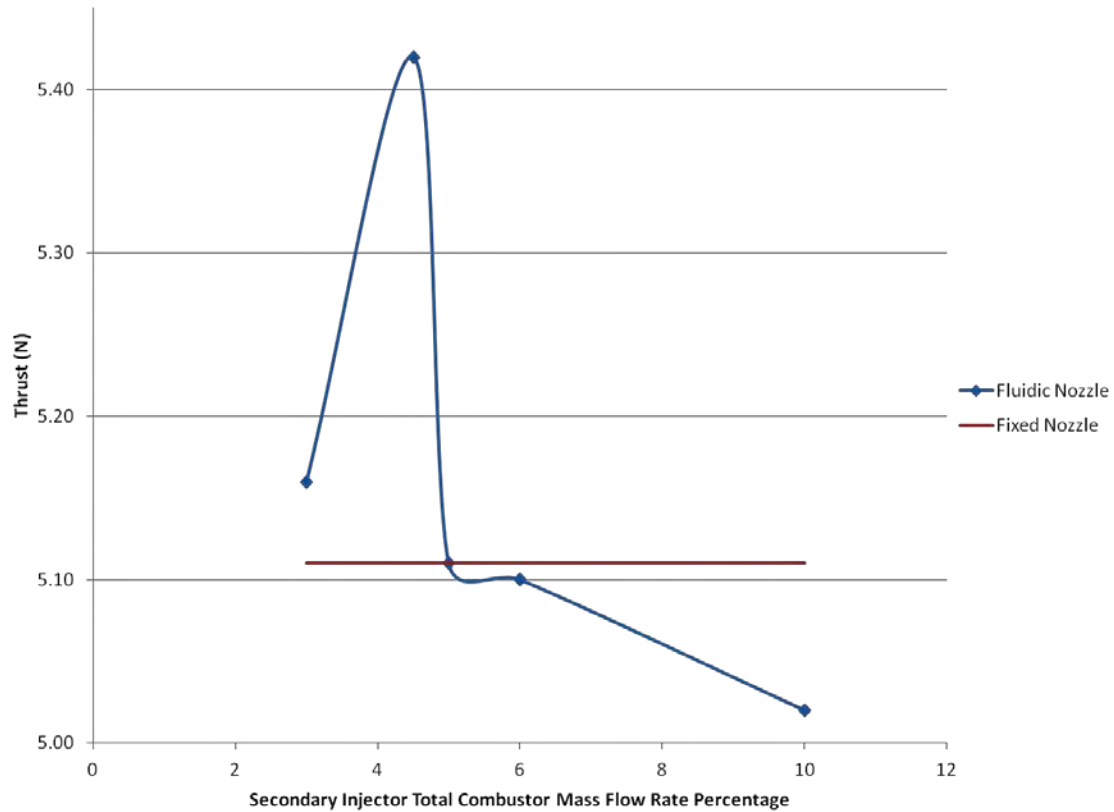


Figure 46. Thrust vs. Secondary Injector Total Combustor Mass Flow Rate Percentage (3 Injectors at a 45° Angle, Without an External Free Stream)

Figure 46 shows that as the total combustion section mass flow rate percentage through the injectors was increased, there existed a maximum value of thrust improvement. It also shows that when plotted against a fixed nozzle, there is also a point of mass flow rate percentage where the thrust is actual decreased. This is caused by the back flow from the low atmospheric pressure outside the nozzle flowing into the nozzle, thereby contributing a negative momentum component to the thrust equation. This is most clearly illustrated in Figure 43, maximum mass flow rate. The large “pillow” at the bottom plane of the nozzle up to the exit plane is fully developed using flow from the ambient pressure outside the nozzle. While this flow is present in all the runs, the amount of back flow eventually overcomes the increase in the expansion efficiency and thrust produced from the combustion products. Additional simulations between three percent

and five percent total combustion mass flow rate could possibly produce further improvement into the observed thrust value.

The result of the CFD++ analysis for the three injectors at a 45° angle is that a total mass flow rate of 4.5% of the combustion section produced the greatest increase in thrust for the steady state condition. Therefore, the detonation simulation was conducted utilizing this mass flow rate to visualize the nozzles response to detonation-driven flow across the Injectors.

b. Two Secondary Injectors Operating at a Flight Condition

Although the three injector models produced better results, two CFD++ simulation were run for a two injector case with a supersonic free stream external to the nozzle. Since the two injector run, shown in Figure 44, indicated the expected “pillow” was produced, the flight simulation run used two injectors at simple 0° and 90° angles. In the place of Injector 3, a free flow boundary condition was created at the exit plane. This plane was set at the flight condition of 10000 meters and Mach 3.0 for Case 10 and 11 and set at sea level, Mach 3.0 for Case 12. These conditions can be found in Appendix C. Table 9 shows the base initial conditions for the two runs.

Simulation	Injector Pressure (Pa)	Injector Velocity (m/s)	Percent Mass Flow Rate (per Injector)
Case 10: Same Flow	111457	103.2	2.50
Case 11: Mixed Flow 10000m, M=3	131722 (Injector 1)	103.2 (Injector 1)	3.00
	131722 (Injector 2)	69.20 (Injector 2)	2.00
Case 12: Mixed Flow Sea Level, M=3	131722 (Injector 1)	103.2 (Injector 1)	3.00
	131722 (Injector 2)	69.20 (Injector 2)	2.00

Table 9. CFD++ Injector Boundary Conditions, Initial Research (2 Injectors at 0° and 90°, With an External Free Stream Flight Condition)

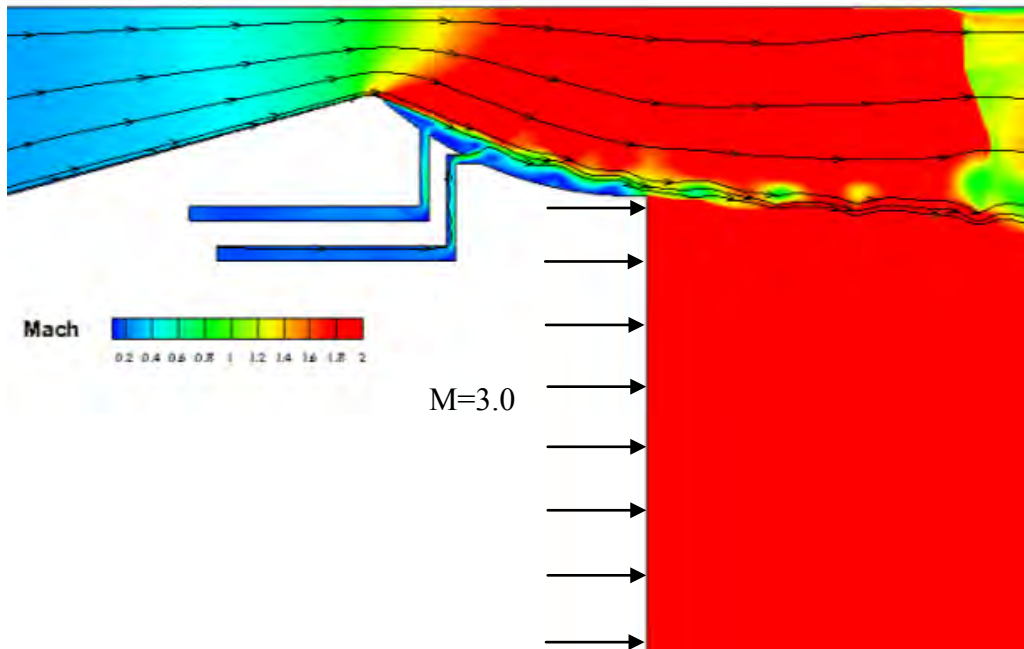


Figure 47. Steady State Simulation, 2 Injectors , M=3.0 Free Stream at 10,000 meters, Case 10

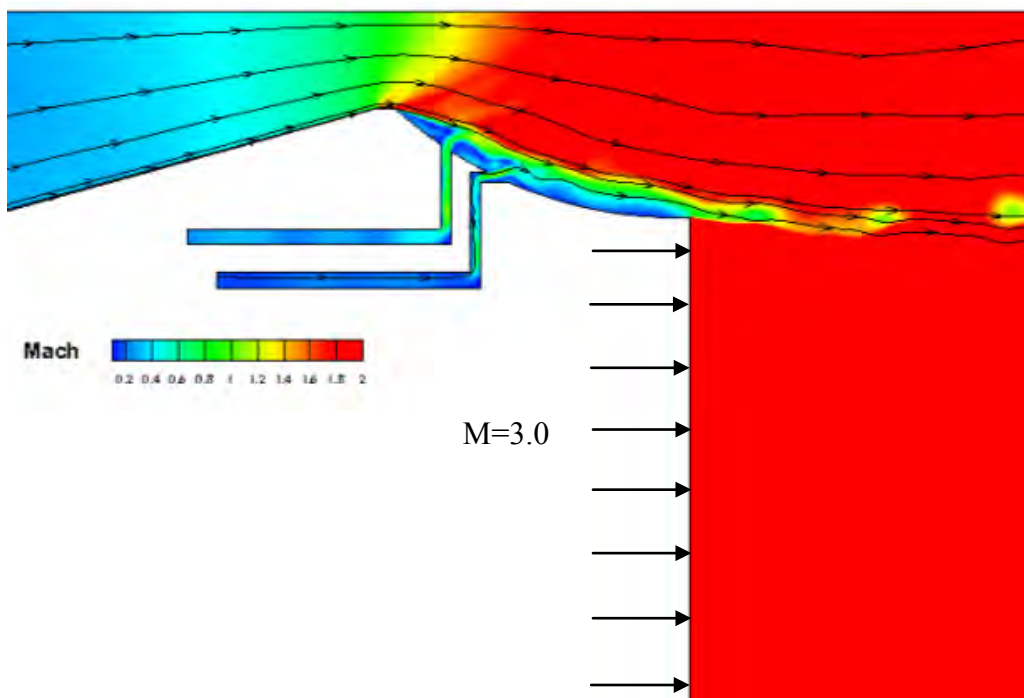


Figure 48. Steady State Simulation, 2 Injectors , M=3.0 Free Stream at 10,000 meters, Case 11

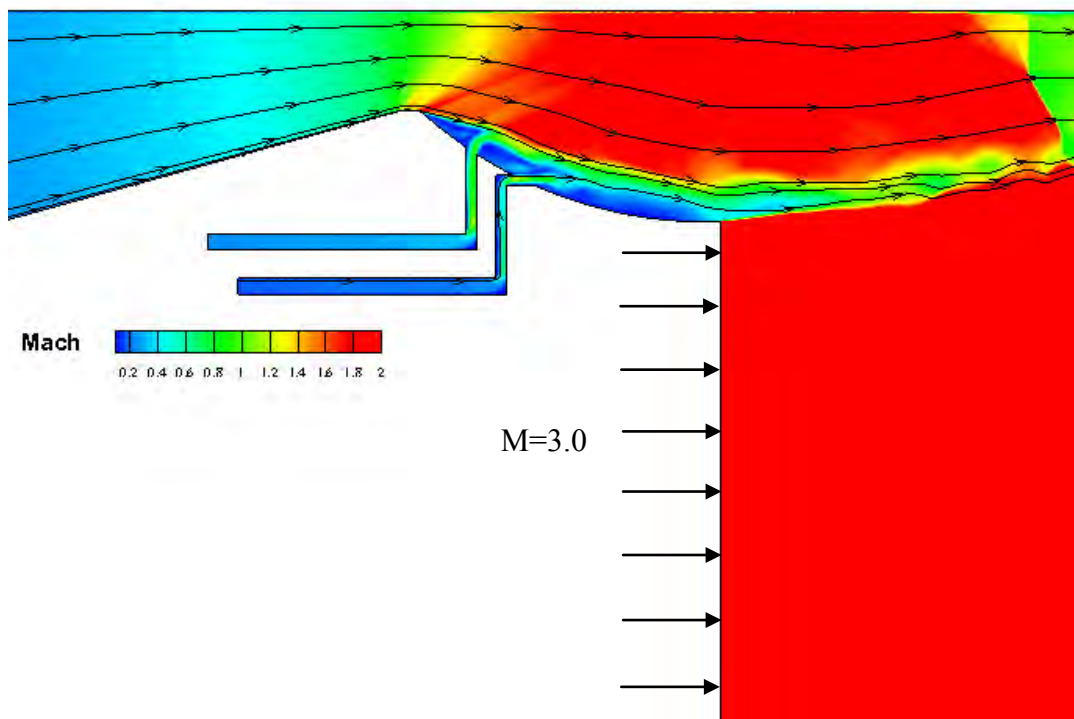


Figure 49. Steady State Simulation, 2 Injectors, Free Stream at Sea Level, Case 12

Although more time was needed to explore this free stream condition, the beginning of the development of a subsonic “pillow” can be seen near the throat in Figures 47 through 49. This shows the first injector redirected the combustor flow as desired. However, the second injector does not appear to directly continue the development, but does contribute to the mass flow constrained near the nozzle wall. This was less prevalent in Case 12 using a free stream at sea level. The higher pressures limited the effect of the second injector. However, the nozzle being simulated was designed for operation at sea level so a better “pillow” was expected. Figure 49 shows that a “pillow” can be formed but the angles may not be optimal. Additional time to explore this trend could have determined an effective mass flow rate, or perhaps a better injector angle set-up to pursue. Most importantly, it shows that a “pillow” can be developed with two injectors at standard angles, easily constructed for a 3-dimensional nozzle.

2 Detonation Case

Based on the results found above for the simulated test condition of three injectors at a 45° angle and 4.5% mass flow rate, a full detonation case event condition was simulated. The CFD++ parameters can be found in Appendix C and Table 6. The output file for the best case run, Case 6 from Table 8, was placed as the starting parameters for the simulation. The initial detonation flow is illustrated in Figures 50"53.

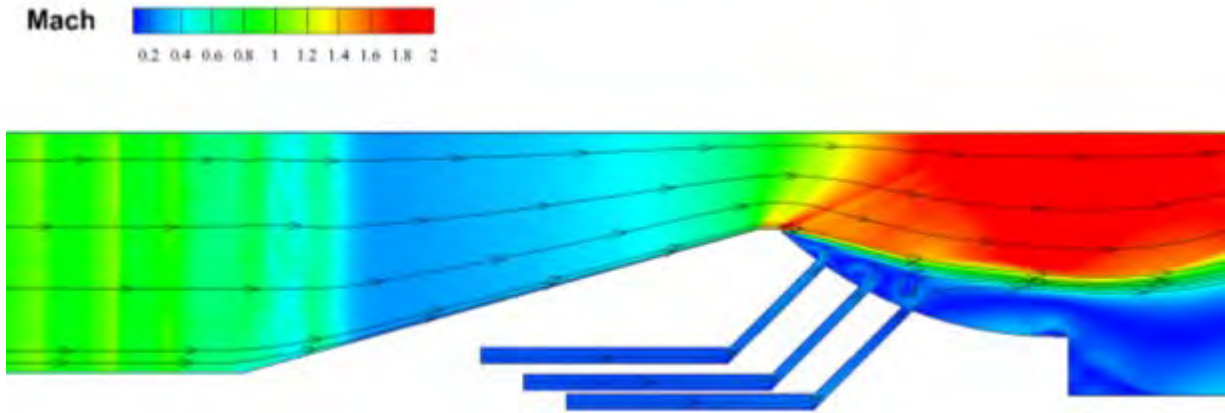


Figure 50. Detonation Simulation, 3 Injector Nozzle at 45° Angle,
 $t_{\text{ign}} + 30$ microseconds

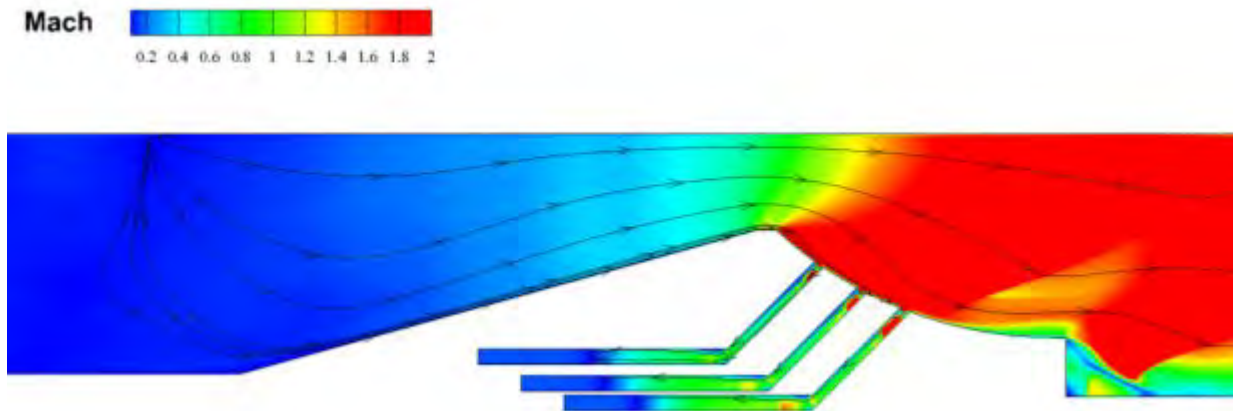


Figure 51. Detonation Simulation, 3 Injector Nozzle at 45° Angle,
 $t_{\text{ign}} + 50$ microseconds

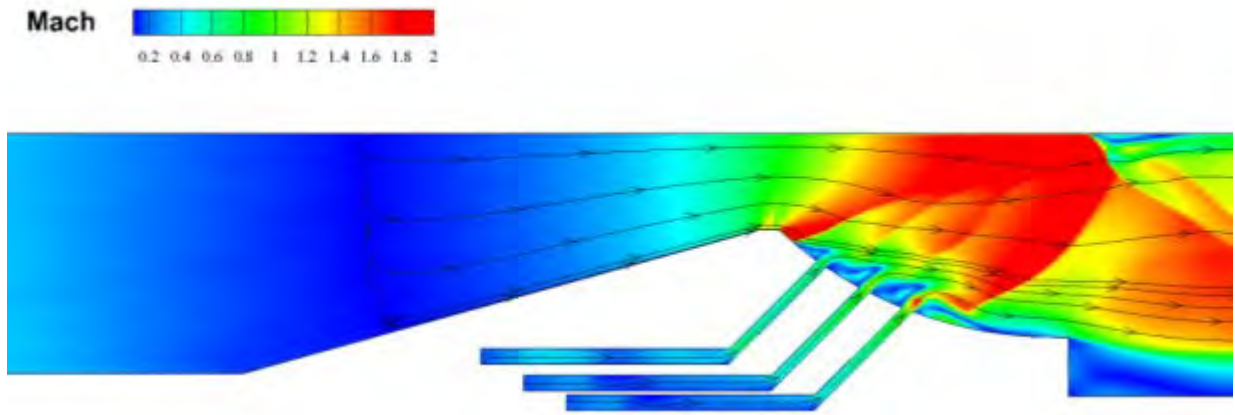


Figure 52. Detonation Simulation, 3 Injector Nozzle at 45° Angle,
 $t_{\text{ign}} + 80$ microseconds

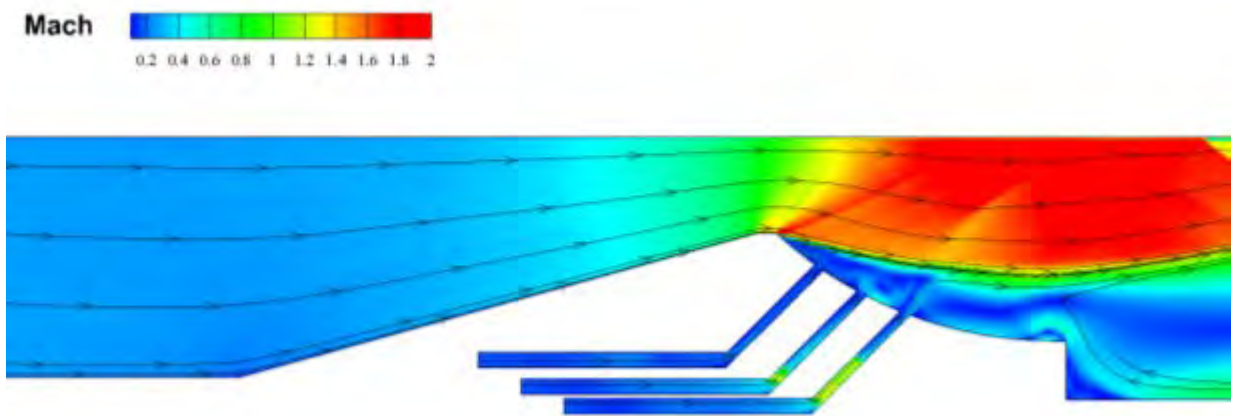


Figure 53. Detonation Simulation, 3 Injector Nozzle at 45° Angle,
 $t_{\text{ign}} + 130$ microseconds

After the initial detonation wave travels through the nozzle, the nozzle injectors begin to rebuild the “pillow” by 130 microseconds after ignition. Following this initial rebuild, one of many shock reflections off the back wall of the combustion section, or ringdown, travels through the nozzle. These ringdowns can occur up to three times before a new refresh condition is achieved. One such case of ringdown and nozzle recovery is shown in Figure s54 and 55.

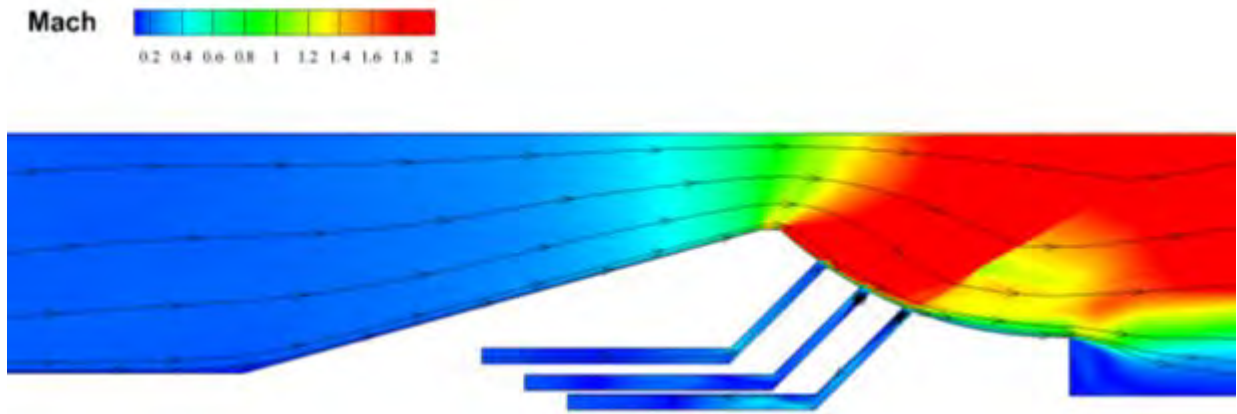


Figure 54. Detonation Simulation, 3 Injector Nozzle at 45° Angle,
 $t_{\text{ign}} + 190$ microseconds

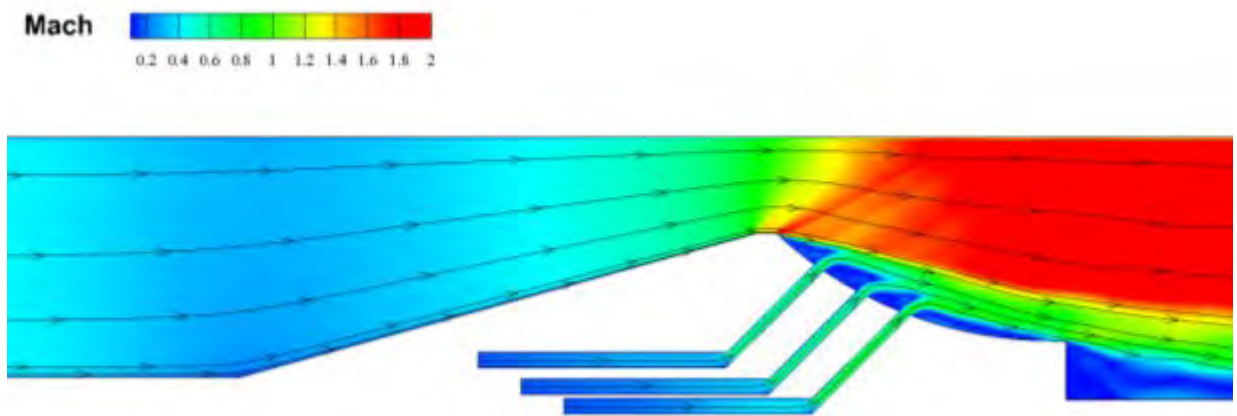


Figure 55. Detonation Simulation, 3 Injector Nozzle at 45° Angle,
 $t_{\text{ign}} + 300$ microseconds

After a few combustor oscillations, the nozzle “pillow” is rebuilt and returned to a refresh condition awaiting the next detonation in the PDE cycle. Figures 56 through 58 show this rebuild.

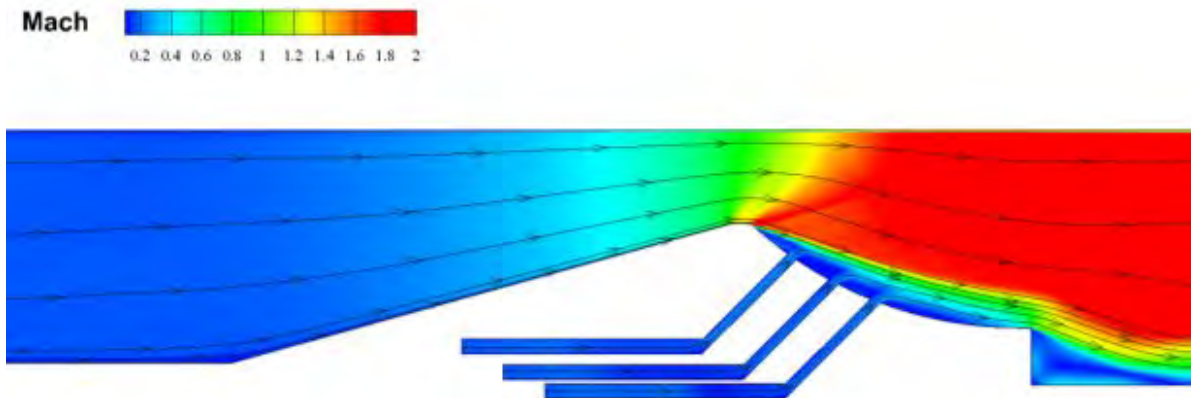


Figure 56. Detonation Simulation, 3 Injector Nozzle at 45° Angle,
 $t_{\text{ign}} + 500$ microseconds

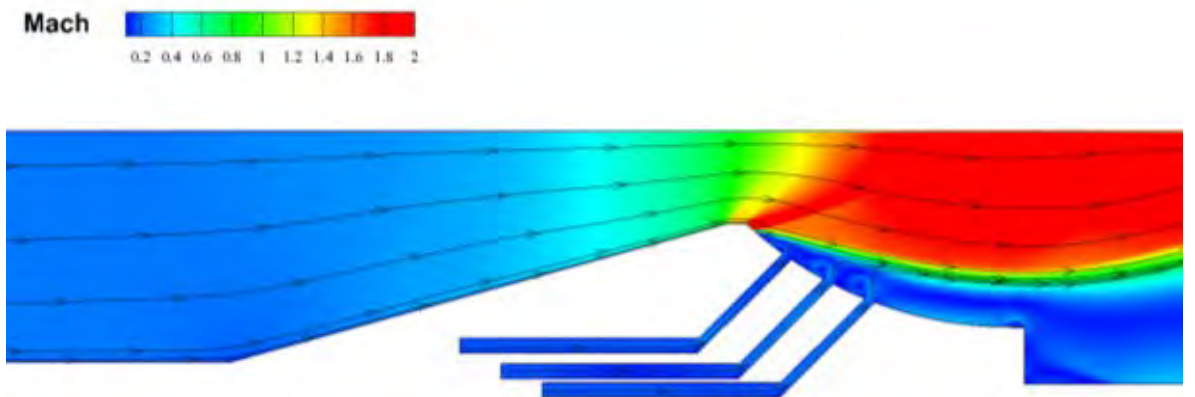


Figure 57. Detonation Simulation, 3 Injector Nozzle at 45° Angle,
 $t_{\text{ign}} + 700$ microseconds

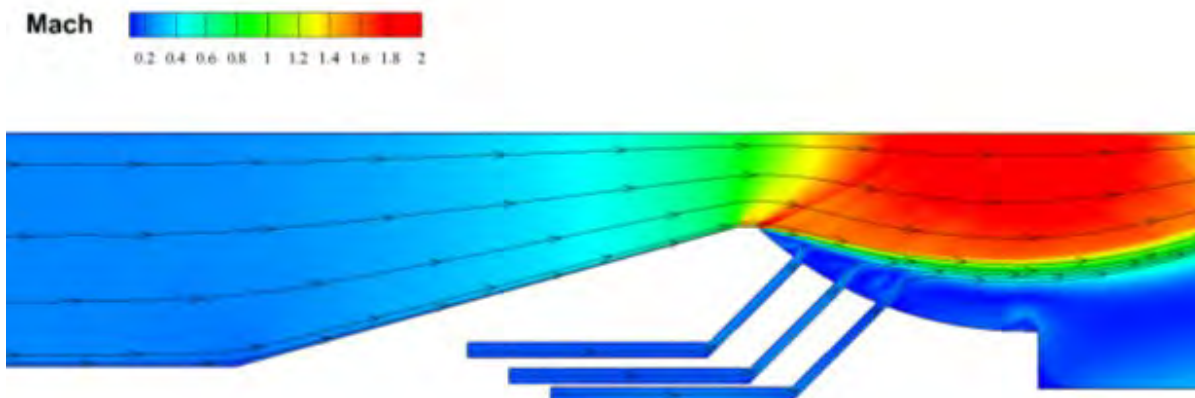


Figure 58. Detonation Simulation, 3 Injector Nozzle at 45° Angle,
 $t_{\text{ign}} + 1$ millisecond

Data was taken from the output files for the detonation simulation every 10 microseconds using Tecplot. Tecplot allowed the height of the “pillow” to be determined based on the streamlines within the combustor flow. From here, an effective nozzle exit area could be calculated and compared throughout the entire detonation cycle. This produced a time varying effective nozzle area ratio, ϵ . The average pressure inside the combustor, p_1 , just prior to the nozzle’s converging section was recorded for each time step. Using the known ambient pressure, p_3 , a pressure ratio was determined. Utilizing these two ratios, data points were placed on the Thrust Coefficient versus Area Ratio curve. This data was then fitted with a best-fit curve to represent the expected nozzle efficiency curve. Figure 59 illustrates these data points and curve.

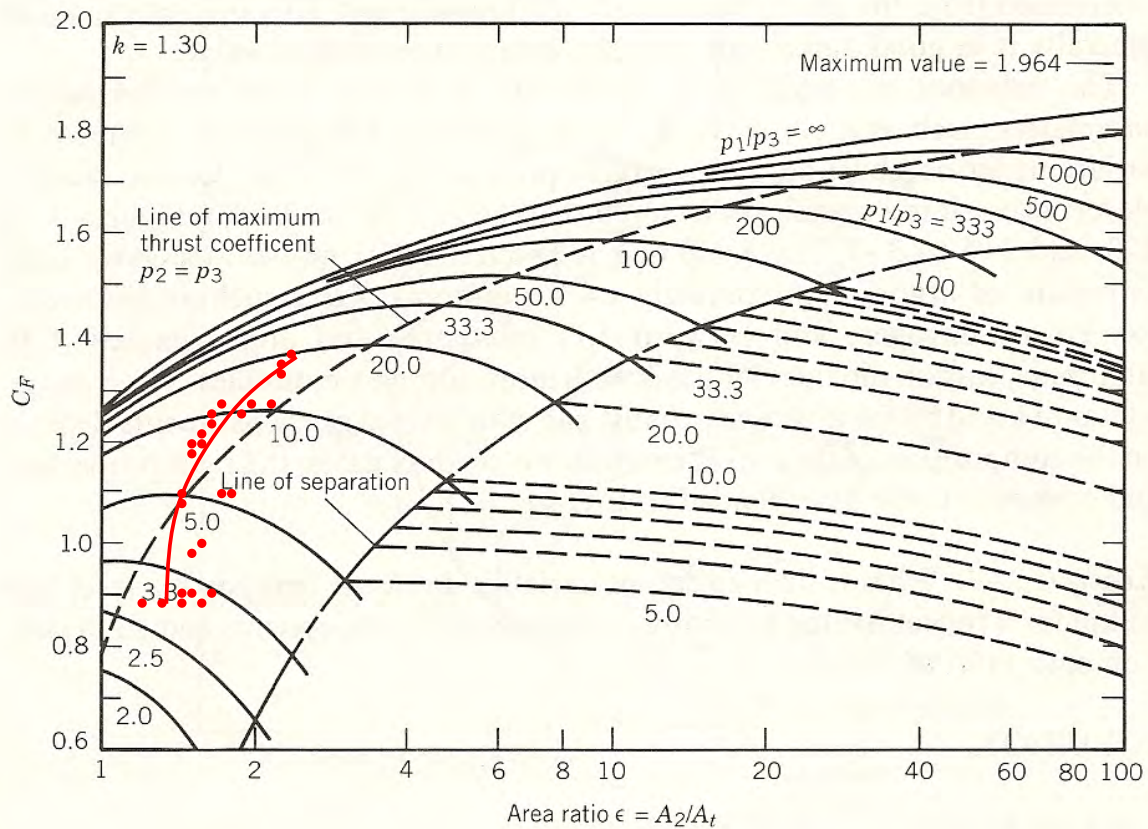


Figure 59. Detonation Results Overlaid on Coefficient of Thrust versus Area Ratio Curve (From [6])

Although the curve does not exactly track on the line of maximum thrust coefficient, it does show the nozzle exit area under the detonation simulation change. The resulting plot illustrates that the nozzle does produce a fluidically augmented nozzle while not allowing the refresh condition to drop into the flow separation region.

THIS PAGE INTENTIONALLY LEFT BLANK

VI. CONCLUSION AND FUTURE WORK

A. CONCLUSION

This research investigated the use of a fluidically augmented nozzle to effectively adjust the nozzle area ratio in order to produce near-ideal expanded flow conditions for each segment of a PDE cycle. An experimental combustor with optical access was created using a previously designed nozzle. The test section was evaluated under both non-detonation and detonation conditions and a shadowgraph imaging technique was used to capture the flow field features. Computer aided modeling was used in conjunction with CFD++ to computationally determine the fluid mechanics of the nozzle under various conditions. The results for similar conditions for both the experimental evaluation and the simulations were compared to determine the simulation accuracy. The results indicate that the CFD++ models appear to have accurately captured the governing flow features and, if properly initiated with appropriate initial conditions, can be used for further evaluations without the need for experimental testing.

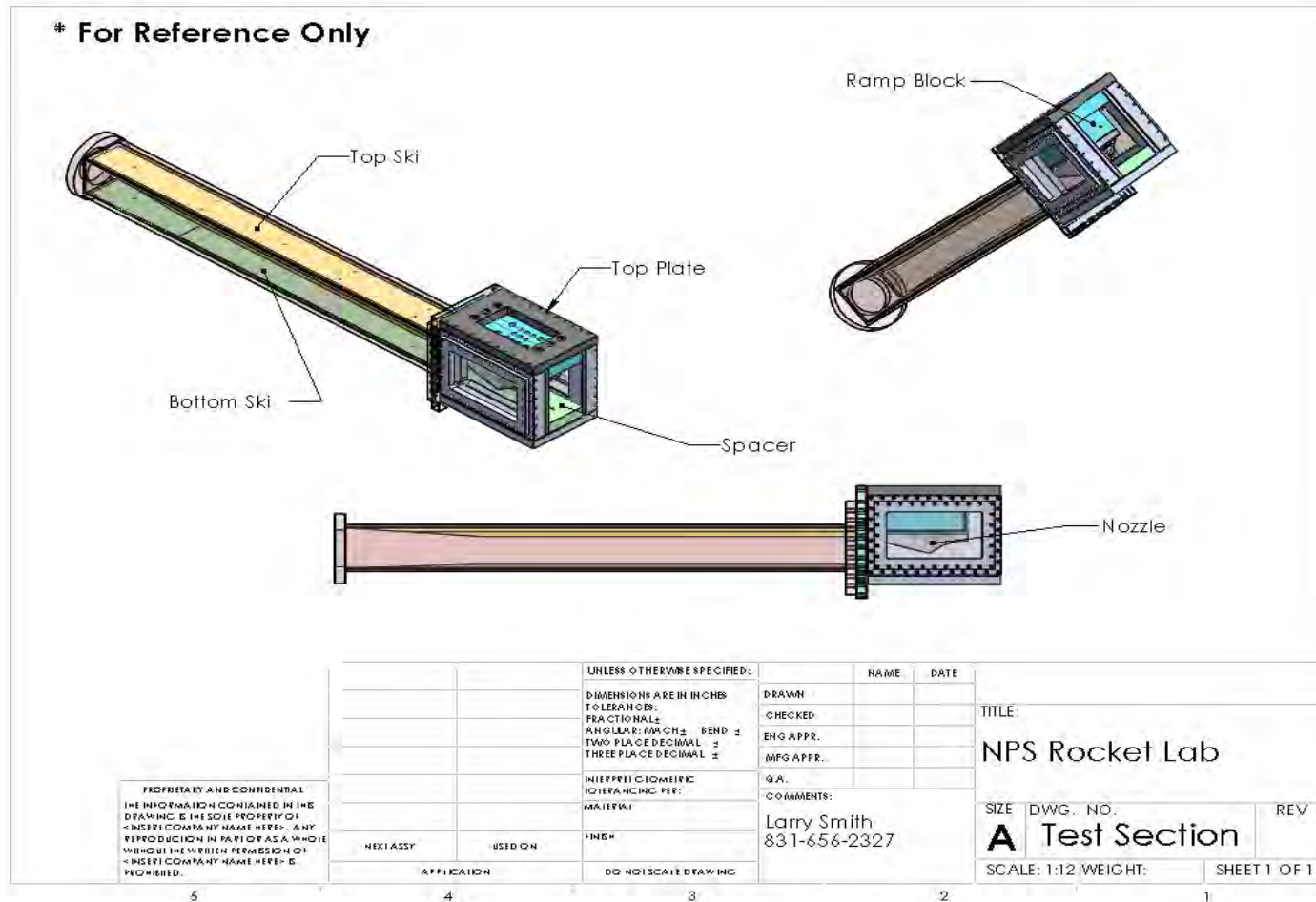
B. FUTURE WORK

This research has found the most efficient mass flow rate percentage needed for a very specific model. It, however, does not broaden the scope to apply the results to any given nozzle shape. Therefore, more research in both a 3-dimensional nozzle test set up as well as a multiple cycle PDE could possibly produce more appropriate results for real world systems and a broader range of applications. Future research could also possible create a mathematical model that can simply calculate the needed secondary injector pressure based on the given parameters of combustor pressure and area ratio. Finally, an accurate thrust measurement evaluation could conclude more precisely the benefit of a fluidically augmented nozzle.

THIS PAGE INTENTIONALLY LEFT BLANK

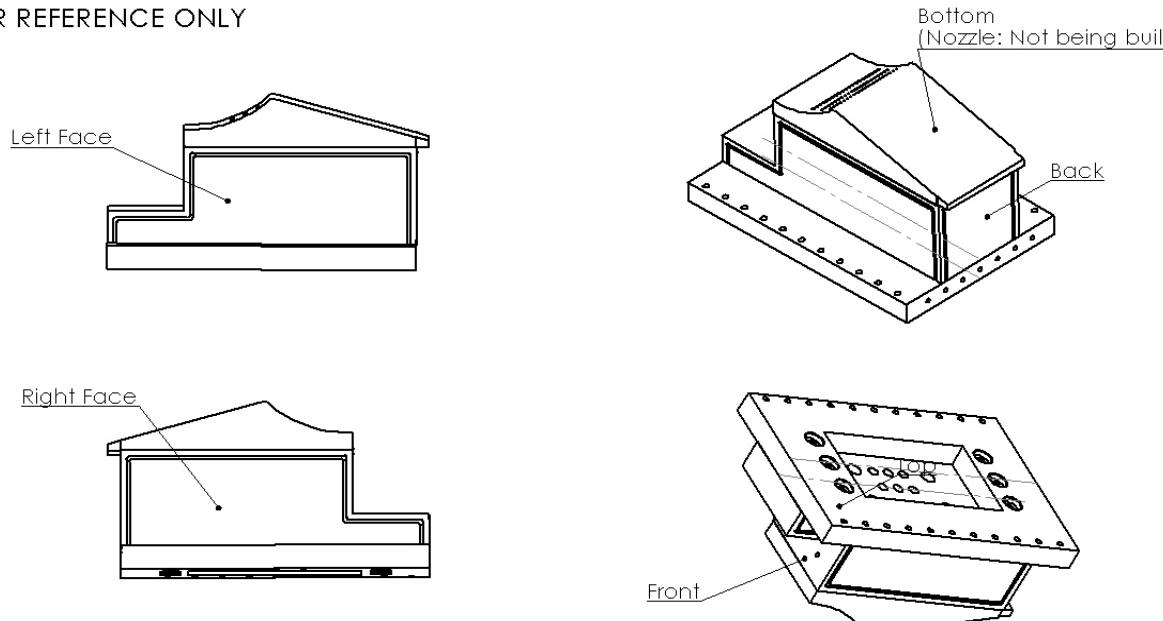
APPENDIX A: MANUFACTURED DRAWINGS

A. TEST SECTION OVERVIEW



B. NOZZLE WITH BLOCK AND TOP PLATE

*FOR REFERENCE ONLY



Left Face

Right Face

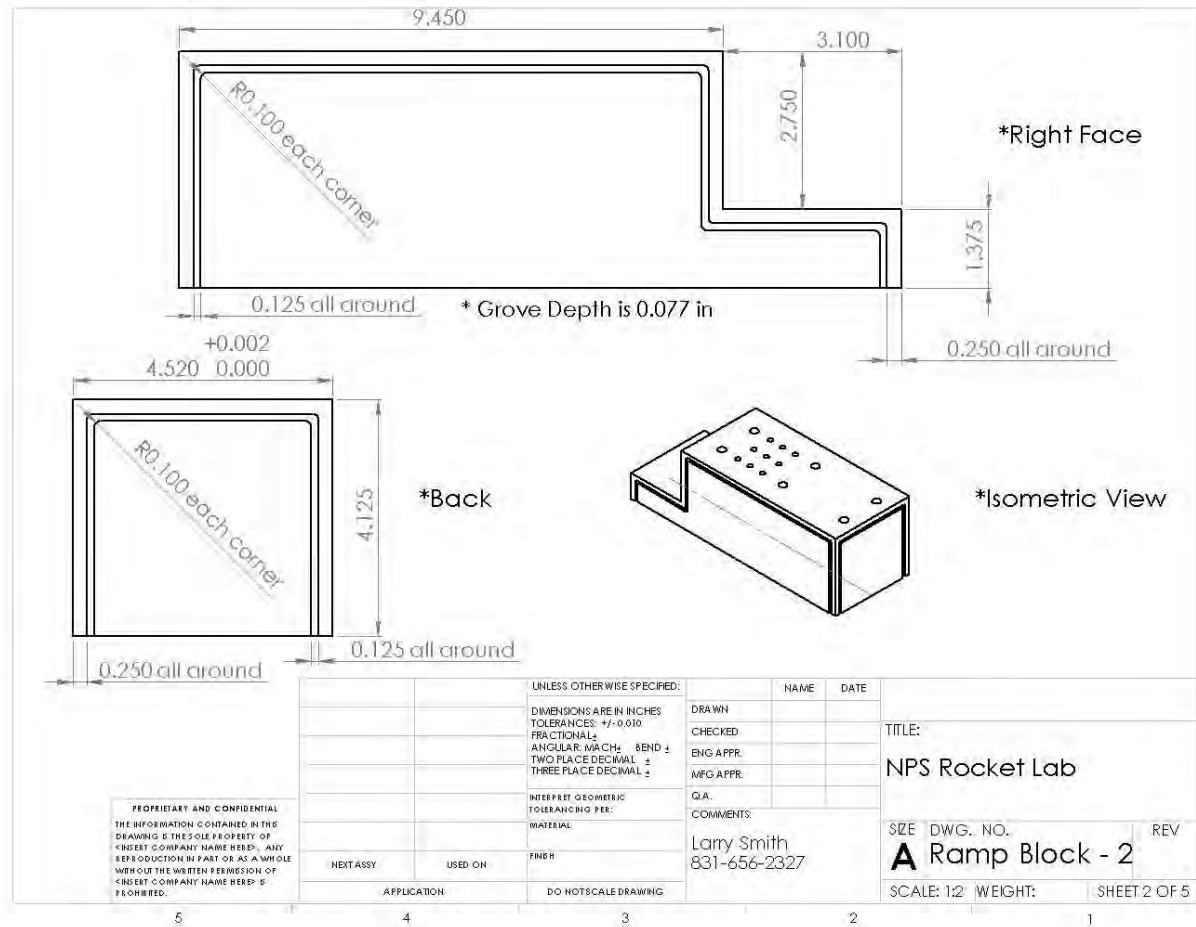
Back

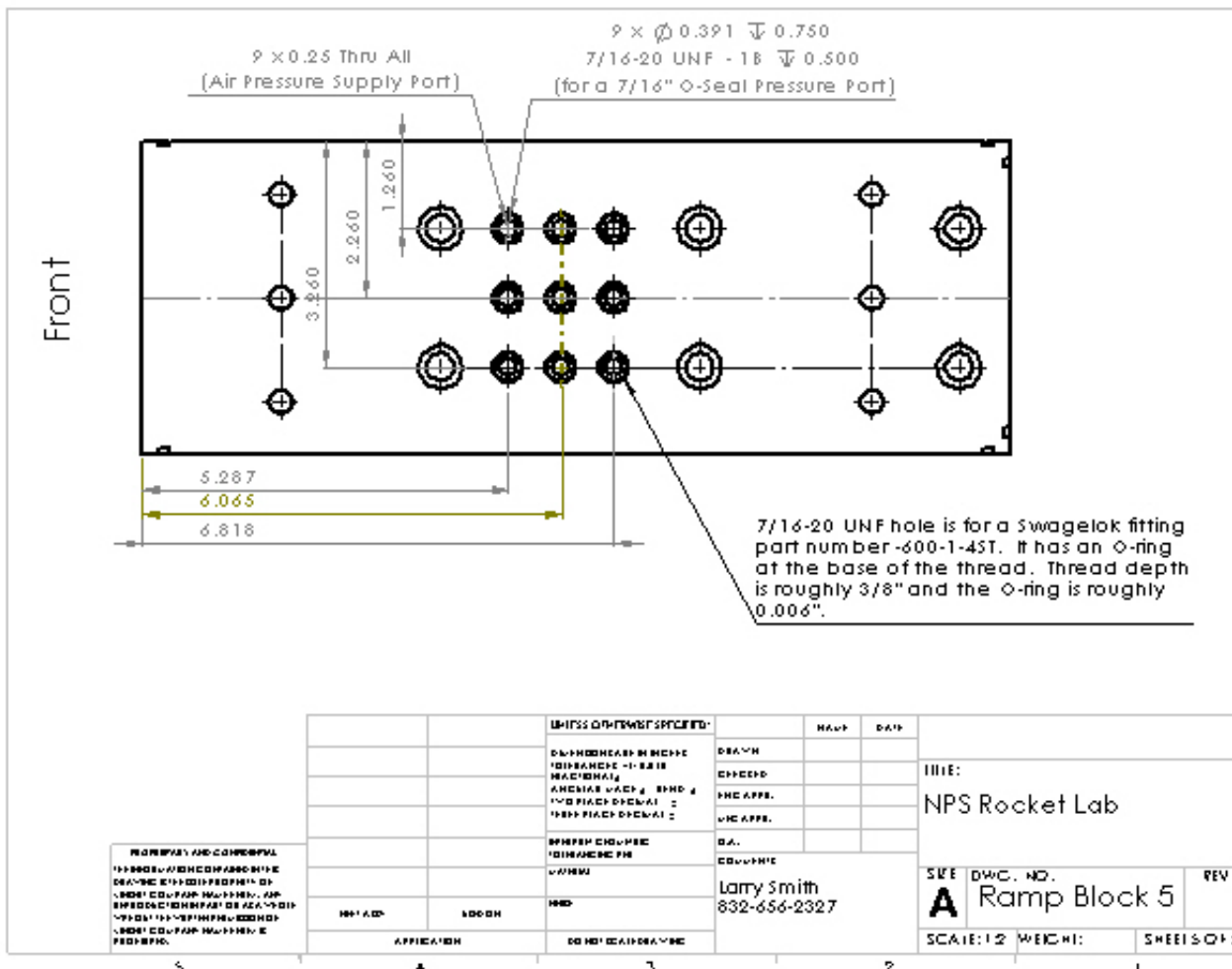
Front

Bottom
(Nozzle: Not being built)

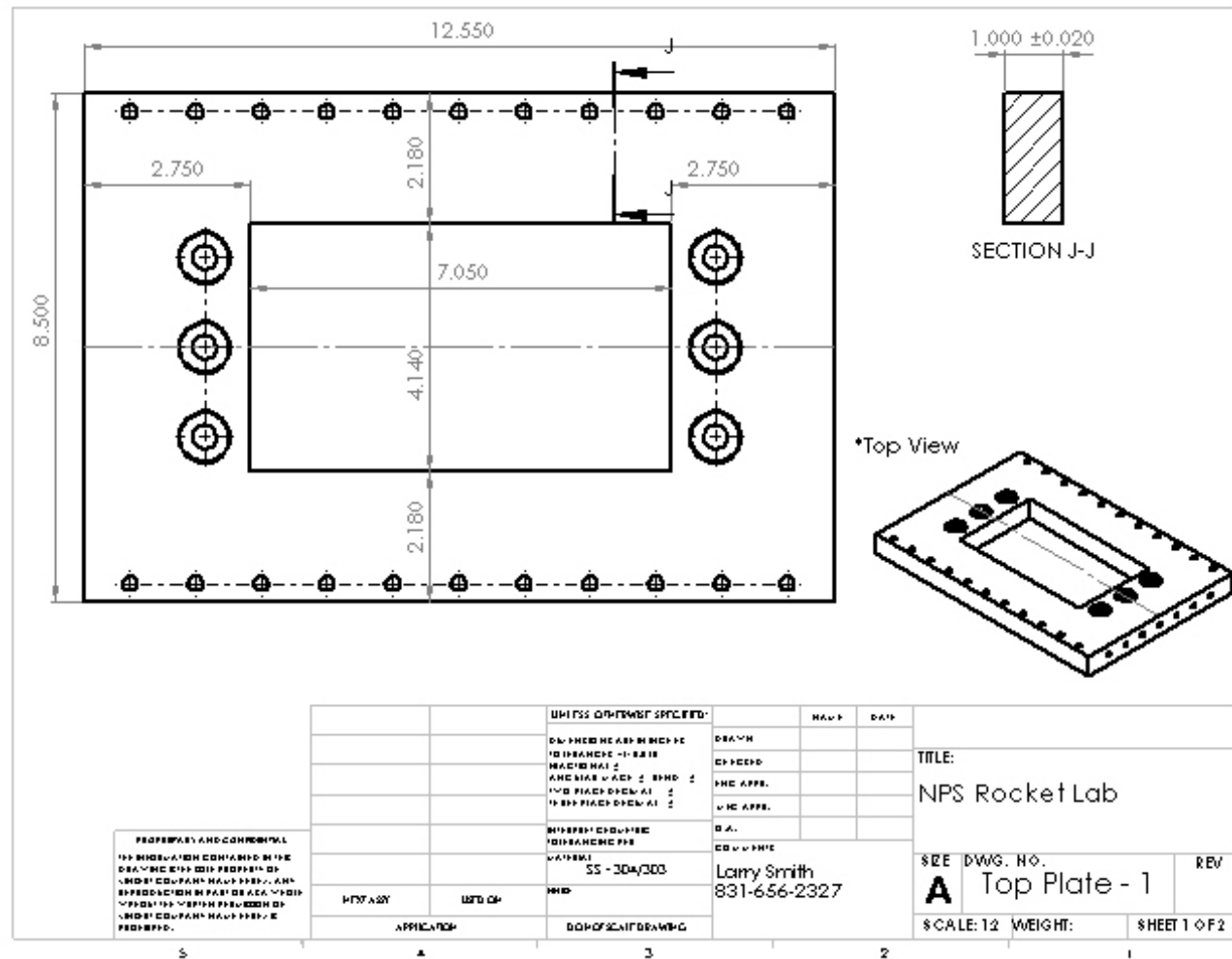
PROPRIETARY AND CONFIDENTIAL THE INFORMATION CONTAINED IN THIS DRAWING IS THE SOLE PROPERTY OF <INSERT COMPANY NAME HERE>. ANY REPRODUCTION IN PART OR AS A WHOLE WITHOUT THE WRITTEN PERMISSION OF <INSERT COMPANY NAME HERE> IS PROHIBITED.		UNLESS OTHERWISE SPECIFIED:		NAME	DATE	TITLE: NPS Rocket Lab SIZE DWG. NO. REV A Whole Assembly SCALE: 1:5 WEIGHT: SHEET 1 OF 1
		DIMENSIONS ARE IN INCHES		DRAWN		
		TOLERANCES:		CHECKED		
		FRACTIONALS		ENG APPR.		
		ANGULAR: \pm BEND \pm		MFG APPR.		
		INTERPRET GEOMETRIC TOLERANCING PER:	Q.A.			
		MATERIAL	COMMENTS:			
		FINISH	Larry Smith 831-656-2327			
NEXT ASSY	USED ON					
APPLICATION		DO NOT SCALE DRAWING				

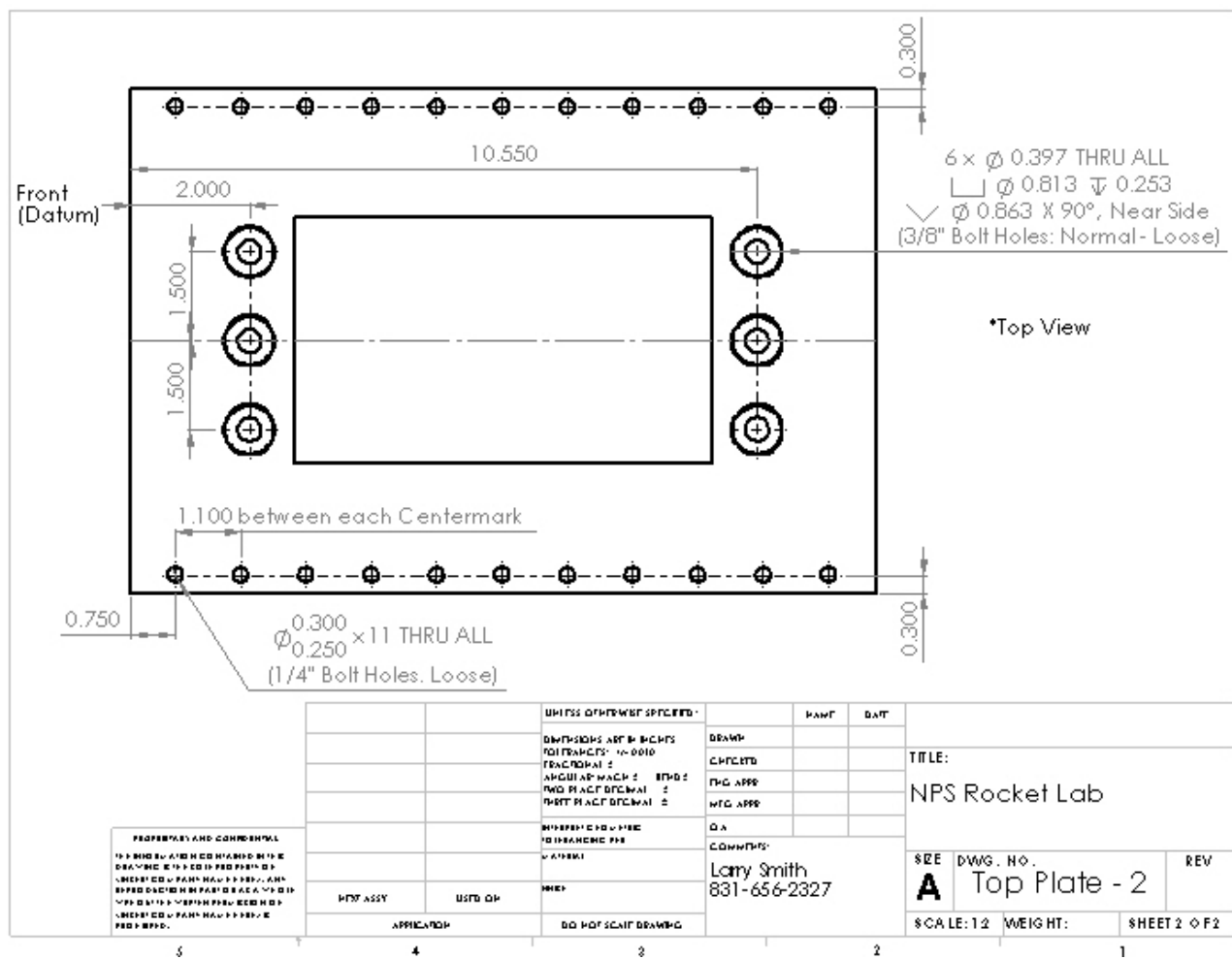
C. RAMP BLOCK



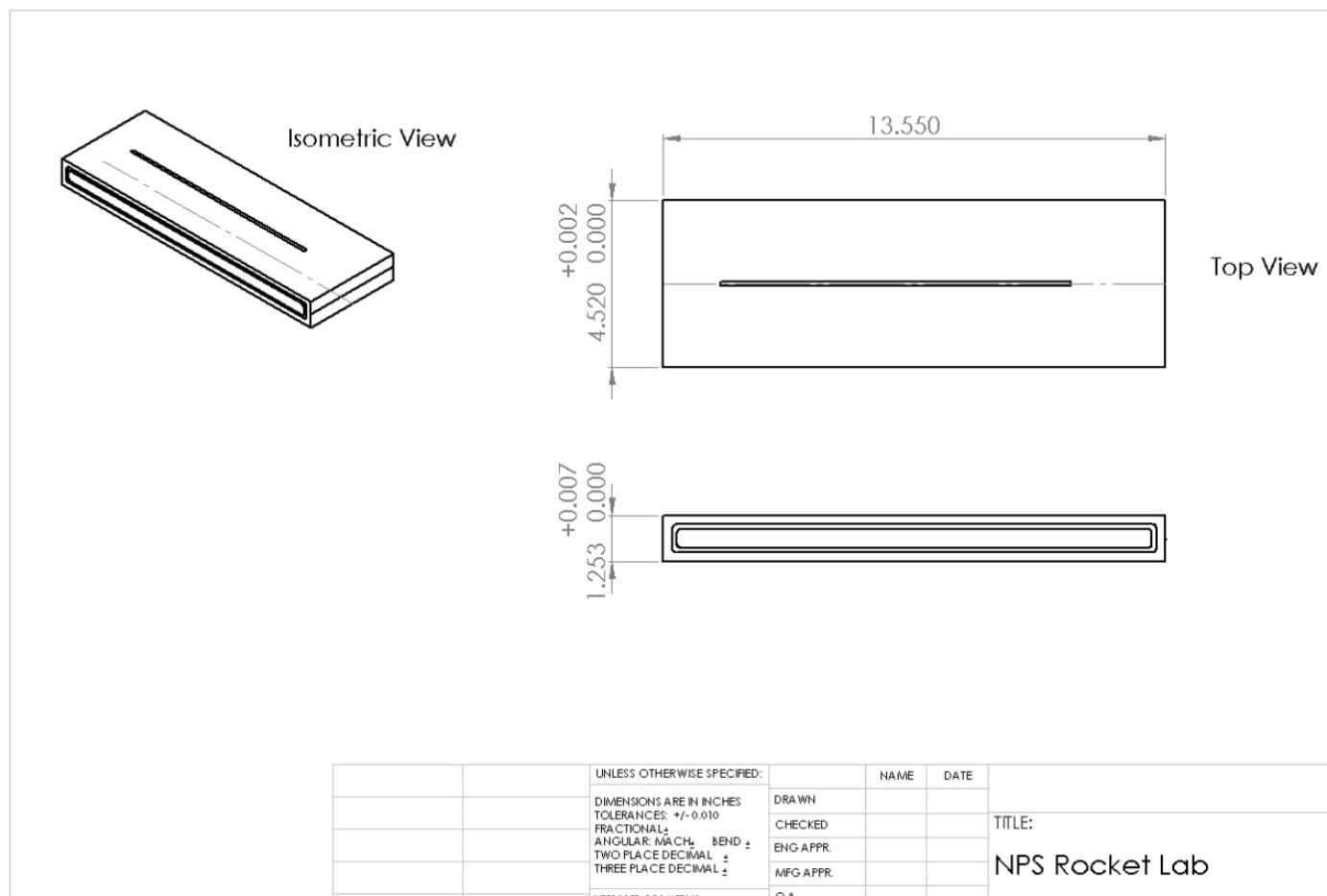


D. TOP PLATE

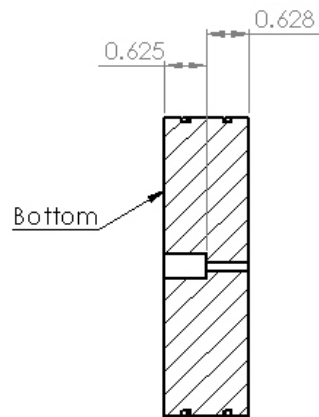




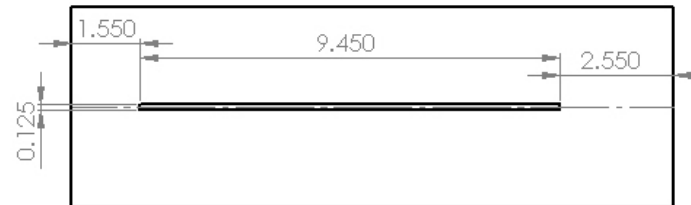
E. SPACER



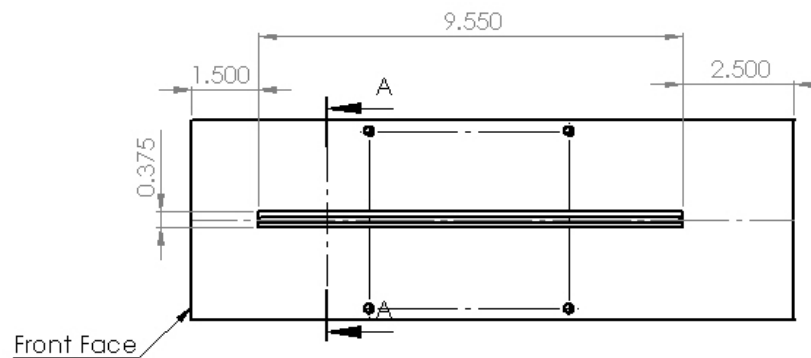
These are slits cut through the center of the block. One is wider and longer, leading to the narrow one. Depth of each slit is very flexible as long as the narrow slit is final on the top portion of the block.



SECTION A-A
SCALE 1 : 2



Top View



Bottom View

Front Face

PROPRIETARY AND CONFIDENTIAL
THE INFORMATION CONTAINED IN THIS
DRAWING IS THE SOLE PROPERTY OF
<INSERT COMPANY NAME HERE>. ANY
REPRODUCTION IN PART OR AS A WHOLE
WITHOUT THE WRITTEN PERMISSION OF
<INSERT COMPANY NAME HERE> IS
PROHIBITED.

		UNLESS OTHERWISE SPECIFIED:		NAME		DATE	
		DIMENSIONS ARE IN INCHES		DRAWN			
		TOLERANCES: ±.001		CHECKED			
		FRACTIONS: 1/16		ENG APPR.			
		ANGULAR: MATCH BEND ±		MTC APPR.			
		TWO PLACE DECIMAL ±		Q.A.			
		THREE PLACE DECIMAL ±		COMMENTS:			
		INTERPRET GEOMETRIC TOLERANCING PER:		Larry Smith			
		MATERIAL:		831-656-2327			
		FINISH:					
NEXT ASSY		USED ON					
APPLICATION		DO NOT SCALE DRAWING					
				TITLE:			
				NPS Rocket Lab			
SIZE		DWG. NO.		REV			
A		Ski Block - 2					
SCALE: 1:5		WEIGHT:		SHEET 1 OF 1			

5

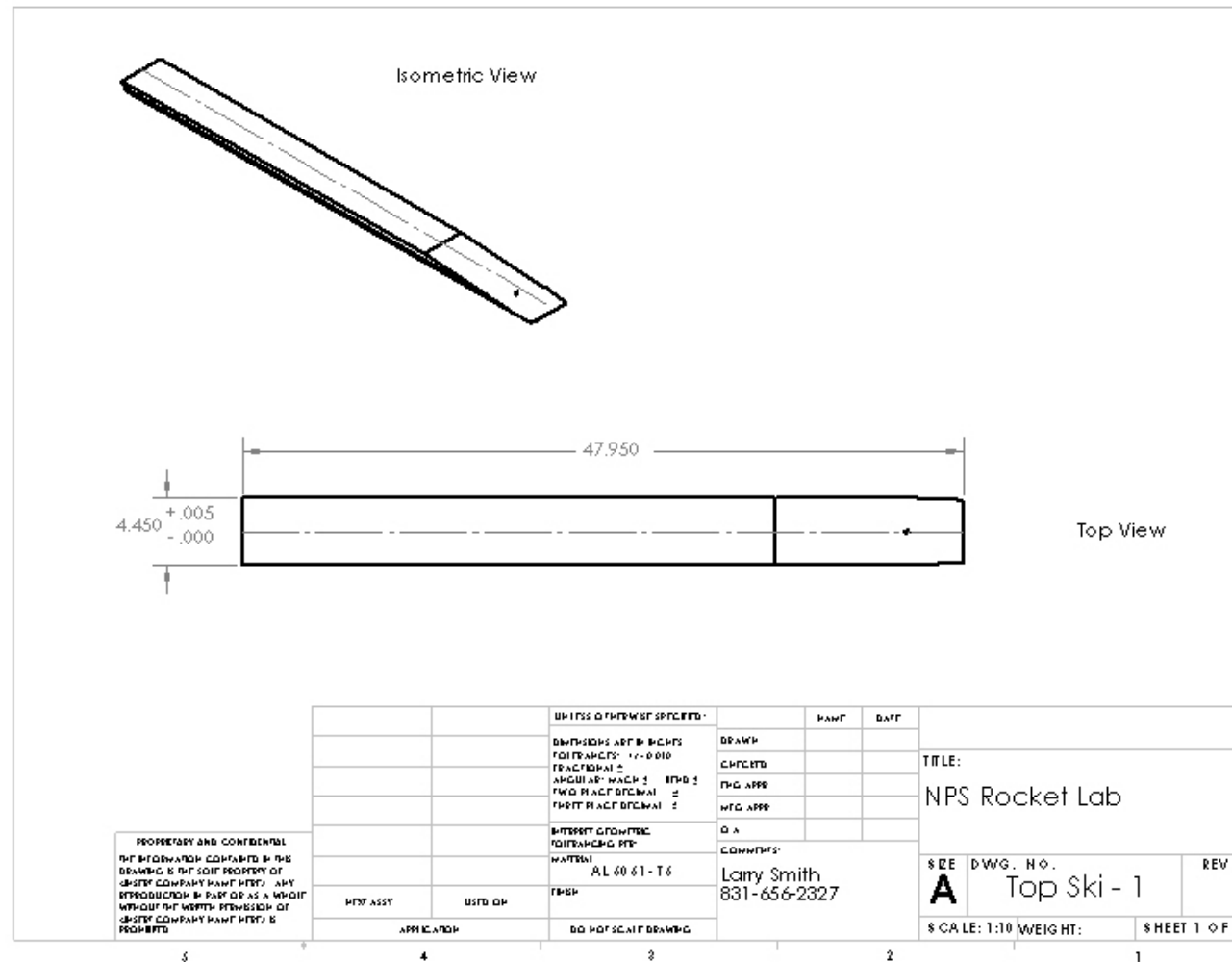
4

3

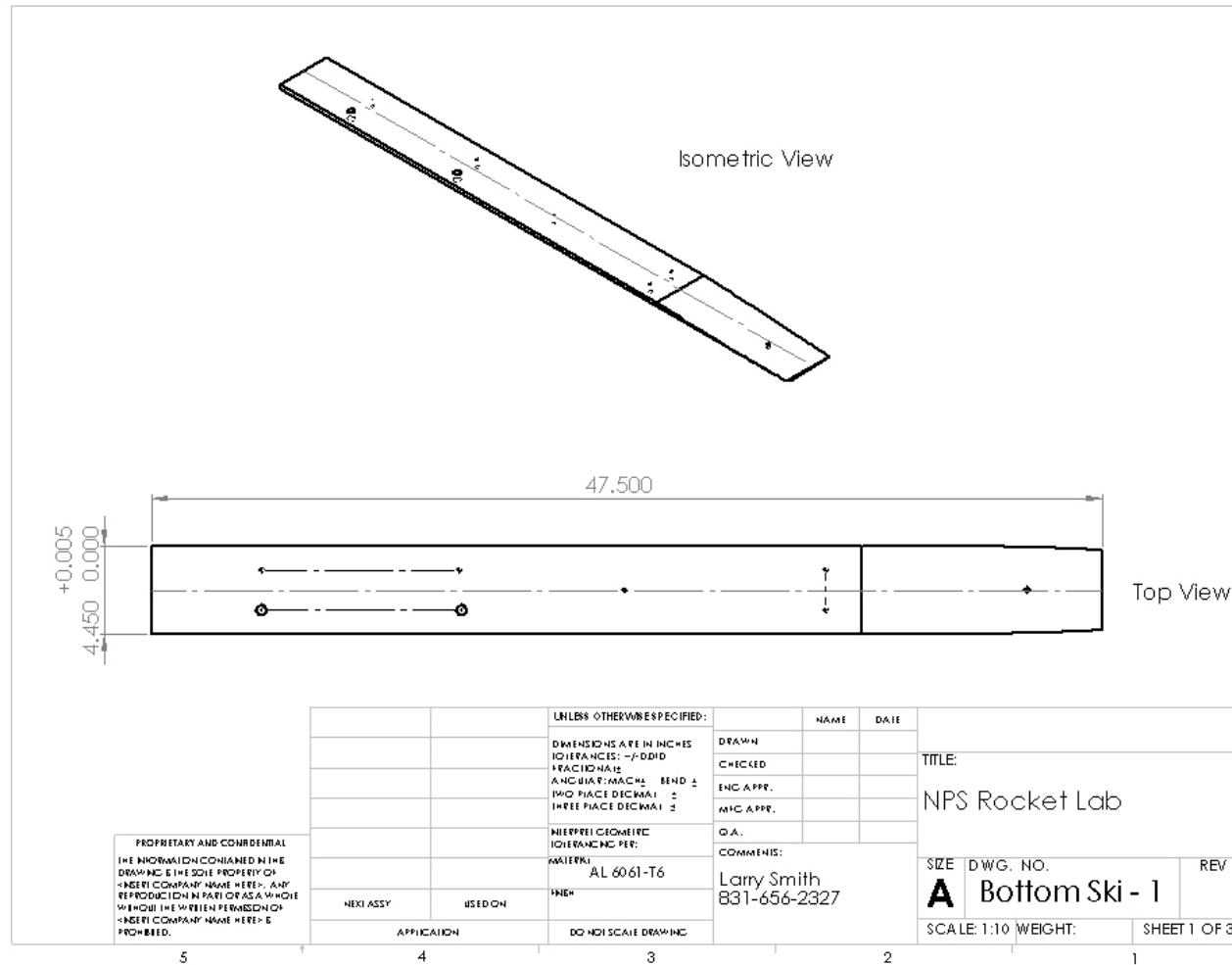
2

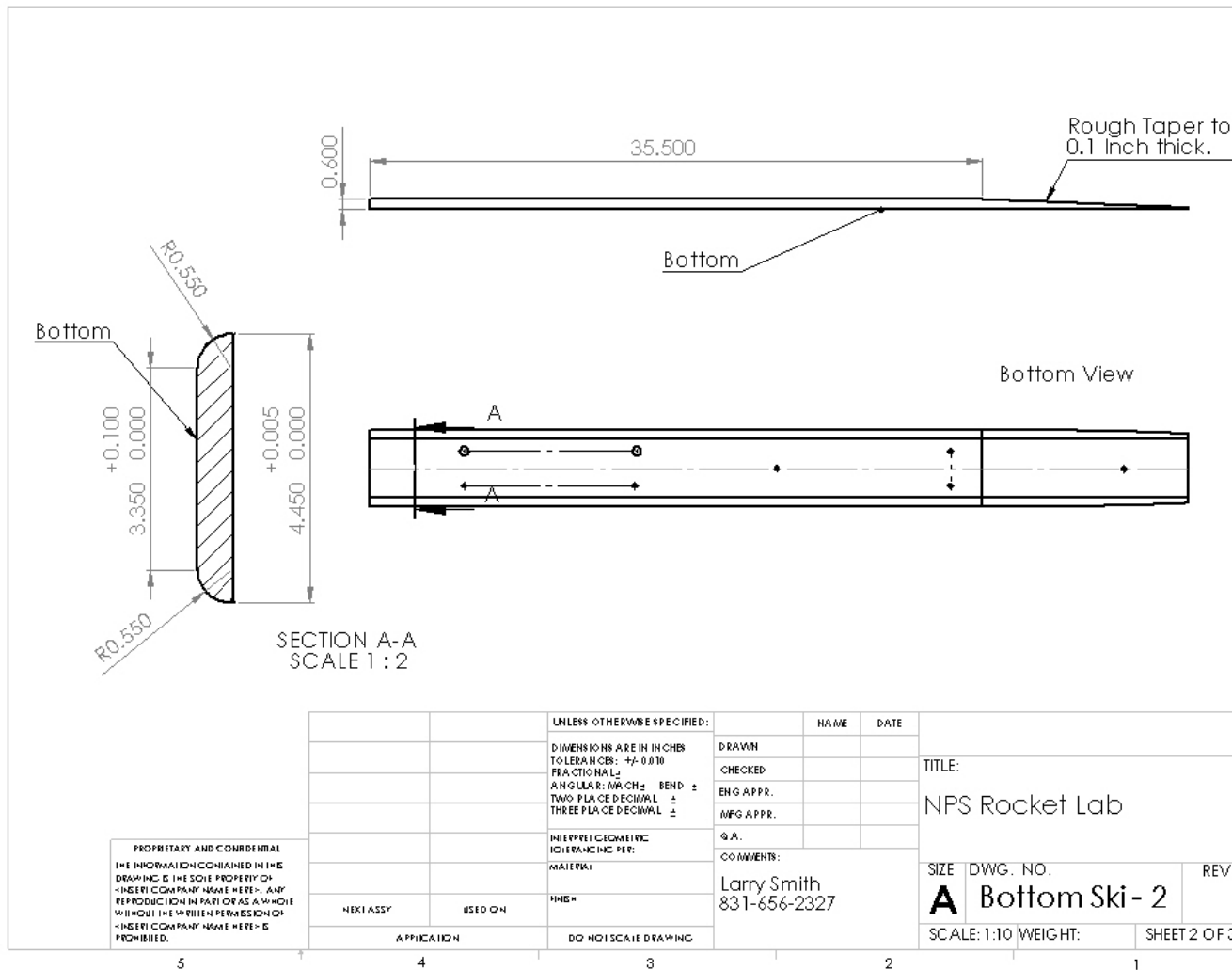
1

F. TOP SKI



G. BOTTOM SKI





THIS PAGE INTENTIONALLY LEFT BLANK

APPENDIX B: NASA CEA GUI

NASA-GLENN CHEMICAL EQUILIBRIUM PROGRAM CEA2, FEBRUARY 5, 2004
 BY BONNIE MCBRIDE AND SANFORD GORDON
 REFS: NASA RP-1311, PART I, 1994 AND NASA RP-1311, PART II, 1996

```
output massf
prob case=22225560 det
phi 1
t,k= 450
```

```
p(atm)=3
output trace=1e-5
reac
oxid Air wt%= 100.
fuel H2 wt%= 100.
end
```

```
OPTIONS: TP=F HP=F SP=F TV=F UV=F SV=F DETN=T SHOCK=F REFL=F INCD=F
RKT=F FROZ=F EQL=F IONS=F SIUNIT=T DEBUG=F SHKDBG=F DETDBG=F TRNSPT=F
```

T,K = 450.0000

TRACE= 1.00E-05 S/R= 0.000000E+00 H/R= 0.000000E+00 U/R= 0.000000E+00

P,BAR = 3.039750

REACTANT	WT.FRAC	(ENERGY/R),K	TEMP,K	DENSITY
EXPLODED FORMULA				
O: Air	1.000000	0.000000E+00	0.00	0.0000
N	1.56168	0.41959 AR 0.00937	C	0.00032
F: H2	1.000000	0.000000E+00	0.00	0.0000
H	2.00000			

SPECIES BEING CONSIDERED IN THIS SYSTEM
 (CONDENSED PHASE MAY HAVE NAME LISTED SEVERAL TIMES)
 LAST thermo.inp UPDATE: 9/09/04

g 3/98 *Ar	g 7/97 *C	tpis79 *CH
g 4/02 CH2	g 4/02 CH3	g11/00 CH2OH
g 7/00 CH3O	g 8/99 CH4	g 7/00 CH3OH
srd 01 CH3OOH	g 8/99 *CN	g12/99 CNN
tpis79 *CO	g 9/99 *CO2	tpis91 COOH
tpis91 *C2	g 6/01 C2H	g 1/91 C2H2,acetylene
g 5/01 C2H2,vinylidene	g 4/02 CH2CO,ketene	g 3/02 O(CH)2O
srd 01 HO(CO)2OH	g 7/01 C2H3,vinyl	g 9/00 CH3CN
g 6/96 CH3CO,acetyl	g 1/00 C2H4	g 8/88 C2H4O,ethylen-o
g 8/88 CH3CHO,ethanal	g 6/00 CH3COOH	srd 01 OHCH2COOH
g 7/00 C2H5	g 7/00 C2H6	g 8/88 CH3N2CH3
g 8/88 C2H5OH	g 7/00 CH3OCH3	srd 01 CH3O2CH3
g 7/00 CCN	tpis91 CNC	srd 01 OCCN
tpis79 C2N2	g 8/00 C2O	tpis79 *C3
n 4/98 C3H3,1-propynl	n 4/98 C3H3,2-propynl	g 2/00 C3H4,allene
g 1/00 C3H4,propyne	g 5/90 C3H4,cyclo-	g 3/01 C3H5,allyl
g 2/00 C3H6,propylene	g 1/00 C3H6,cyclo-	g 6/01 C3H6O,propylox
g 6/97 C3H6O,acetone	g 1/02 C3H6O,propanal	g 7/01 C3H7,n-propyl
g 9/85 C3H7,i-propyl	g 2/00 C3H8	g 2/00 C3H8O,1propanol
g 2/00 C3H8O,2propanol	srd 01 CNCOCN	g 7/88 C3O2
g tpis *C4	g 7/01 C4H2,butadiyne	g 8/00 C4H4,1,3-cyclo-
n10/92 C4H6,butadiene	n10/93 C4H6,1butyne	n10/93 C4H6,2butyne
g 8/00 C4H6,cyclo-	n 4/88 C4H8,1-butene	n 4/88 C4H8,cis2-buten
n 4/88 C4H8,tr2-butene	n 4/88 C4H8,isobutene	g 8/00 C4H8,cyclo-
g10/00 (CH3COOH)2	n10/84 C4H9,n-butyl	n10/84 C4H9,i-butyl
g 1/93 C4H9,s-butyl	g 1/93 C4H9,t-butyl	g12/00 C4H10,n-butane
g 8/00 C4H10,isobutane	g 6/01 C4N2	g 8/00 *C5

g 5/90	C5H6,1,3cyclo-	g 1/93	C5H8,cyclo-	n 4/87	C5H10,1-pentene
g 2/01	C5H10,cyclo-	n10/84	C5H11,pentyl	g 1/93	C5H11,t-pentyl
n10/85	C5H12,n-pentane	n10/85	C5H12,i-pentane	n10/85	CH3C(CH3)2CH3
g 2/93	C6H2	g11/00	C6H5,phenyl	g 8/00	C6H5O,phenoxy
g 8/00	C6H6	g 8/00	C6H5OH,phenol	g 1/93	C6H10,cyclo-
n 4/87	C6H12,1-hexene	g 6/90	C6H12,cyclo-	n10/83	C6H13,n-hexyl
g 6/01	C6H14,n-hexane	g 7/01	C7H7,benzyl	g 1/93	C7H8
g12/00	C7H8O,cresol-mx	n 4/87	C7H14,1-heptene	n10/83	C7H15,n-heptyl
n10/85	C7H16,n-heptane	n10/85	C7H16,2-methylh	n 4/89	C8H8,styrene
n10/86	C8H10,ethylbenz	n 4/87	C8H16,1-octene	n10/83	C8H17,n-octyl
n 4/85	C8H18,n-octane	n 4/85	C8H18,isoctane	n10/83	C9H19,n-nonyl
g 3/01	C10H8,naphthale	n10/83	C10H21,n-decyl	g 8/00	C12H9,o-bipheny
g 8/00	C12H10,biphenyl	g 6/97	*H	g 6/01	HCN
g 1/01	HCO	tpis89	HCCN	g 6/01	HCCO
g 6/01	HNC	g 7/00	HNCO	g10/01	HNO
tpis89	HNO2	g 5/99	HNO3	g 4/02	HO2
tpis78	*H2	g 5/01	HCHO,formaldehy	g 6/01	HCOOH
g 8/89	H2O	g 6/99	H2O2	g 6/01	(HCOOH)2
g 5/97	*N	g 6/01	NCO	g 4/99	*NH
g 3/01	NH2	tpis89	NH3	tpis89	NH2OH
tpis89	*NO	g 4/99	NO2	j12/64	NO3
tpis78	*N2	J12/64	N2O	g 6/01	NCN
g 5/99	N2H2	tpis89	NH2NO2	g 4/99	N2H4
g 4/99	N2O	g 4/99	N2O3	tpis89	N2O4
g 4/99	N2O5	tpis89	N3	g 4/99	N3H
g 5/97	*O	g 4/02	*OH	tpis89	*O2
g 8/01	O3	g 12/0	THDCPD,endo	g 12/0	THDCPD,exo
g11/99	N2H4(L)	n 4/83	C(gr)	n 4/83	C(gr)
n 4/83	C(gr)	n12/84	CH3OH(L)	n12/84	C2H5OH(L)
n 4/85	C6H14(L),n-hexa	n12/88	C6H5NH2(L)	n10/86	C6H6(L)
g11/99	H2O(cr)	g 8/01	H2O(L)	g 8/01	H2O(L)

O/F = 34.296226

ENTHALPY	EFFECTIVE FUEL	EFFECTIVE OXIDANT	MIXTURE
(KG-MOL)(K)/KG	h(2)/R	h(1)/R	h0/R
	0.00000000E+00	0.00000000E+00	0.00000000E+00
KG-FORM.WT./KG	bi(2)	bi(1)	b0i
*N	0.00000000E+00	0.53915890E-01	0.52388364E-01
*O	0.00000000E+00	0.14486046E-01	0.14075632E-01
*Ar	0.00000000E+00	0.32331996E-03	0.31415977E-03
*C	0.00000000E+00	0.11013248E-04	0.10701224E-04
*H	0.99212255E+00	0.00000000E+00	0.28108460E-01

POINT ITN	T	N	O	AR	C
	H				
POINT ITN	T	N	O	AR	C
	H				
POINT ITN	T	N	O	AR	C
	H				
POINT ITN	T	N	O	AR	C
	H				

DETONATION PROPERTIES OF AN IDEAL REACTING GAS

CASE = 22225560

OXIDANT	REACTANT	WT FRACTION	ENERGY	TEMP
		(SEE NOTE)	KJ/KG-MOL	K
Air		1.0000000	0.000	0.000
H2		1.0000000	0.000	0.000

O/F= 34.29623 %FUEL= 2.833164 R,EQ.RATIO= 1.000000 PHI,EQ.RATIO= 1.000000

UNBURNED GAS

P1, BAR	3.0397
T1, K	450.00
H1, KJ/KG	207.12
M1, (1/n)	21.008
GAMMA1	1.3931
SON VEL1,M/SEC	498.1

BURNED GAS

P, BAR	32.019
T, K	3049.22
RHO, KG/CU M	3.0308 0
H, KJ/KG	1534.12
U, KJ/KG	477.68
G, KJ/KG	-30209.3
S, KJ/(KG)(K)	10.4103

M, (1/n)	23.998
(dLV/dLP)t	-1.00960
(dLV/dLT)p	1.2011
Cp, KJ/(KG)(K)	3.2775
GAMMA5	1.1667
SON VEL,M/SEC	1110.2

DETONATION PARAMETERS

P/P1	10.533
T/T1	6.776
M/M1	1.1423
RHO/RHO1	1.7757
DET MACH NUMBER	3.9579
DET VEL,M/SEC	1971.5

MASS FRACTIONS

*Ar	1.2550-2
*CO	1.3488-4
*CO2	2.5903-4
*H	2.4332-4
HO2	2.1331-5
*H2	2.6804-3
H2O	2.1962-1
*NO	1.0496-2
*N2	7.2887-1
*O	1.3433-3
*OH	1.4039-2
*O2	9.7109-3

* THERMODYNAMIC PROPERTIES FITTED TO 20000.K

PRODUCTS WHICH WERE CONSIDERED BUT WHOSE MASS FRACTIONS
WERE LESS THAN 1.000000E-05 FOR ALL ASSIGNED CONDITIONS

*C	*CH	CH2	CH3	CH2OH
CH3O	CH4	CH3OH	CH3OOH	*CN
CNN	COOH	*C2	C2H	C2H2,acetylene
C2H2,vinylidene	CH2CO,ketene	O(CH)2O	HO(CO)2OH	C2H3,vinyl
CH3CN	CH3CO,acetyl	C2H4	C2H4O,ethylen-o	CH3CHO,ethanal
CH3COOH	OHCH2COOH	C2H5	C2H6	CH3N2CH3
C2H5OH	CH3OCH3	CH3O2CH3	CCN	CNC
OCCN	C2N2	C2O	*C3	C3H3,1-propynl
C3H3,2-propynl	C3H4,allene	C3H4,propyne	C3H4,cyclo-	C3H5,allyl
C3H6,propylene	C3H6,cyclo-	C3H6O,propylox	C3H6O,acetone	C3H6O,propanal
C3H7,n-propyl	C3H7,i-propyl	C3H8	C3H8O,1propanol	C3H8O,2propanol
CNCOCN	C3O2	*C4	C4H2,butadiyne	C4H4,1,3-cyclo-
C4H6,butadiene	C4H6,1butyne	C4H6,2butyne	C4H6,cyclo-	C4H8,1-butene
C4H8,cis2-buten	C4H8,tr2-butene	C4H8,isobutene	C4H8,cyclo-	(CH3COOH)2
C4H9,n-butyl	C4H9,i-butyl	C4H9,s-butyl	C4H9,t-butyl	C4H10,n-butane
C4H10,isobutane	C4N2	*C5	C5H6,1,3cyclo-	C5H8,cyclo-

C5H10,1-pentene	C5H10,cyclo-	C5H11,pentyl	C5H11,t-pentyl	C5H12,n-pentane
C5H12,i-pentane	CH3C(CH3)2CH3	C6H2	C6H5,phenyl	C6H5O,phenoxy
C6H6	C6H5OH,phenol	C6H10,cyclo-	C6H12,1-hexene	C6H12,cyclo-
C6H13,n-hexyl	C6H14,n-hexane	C7H7,benzyl	C7H8	C7H8O,cresol-mx
C7H14,1-heptene	C7H15,n-heptyl	C7H16,n-heptane	C7H16,2-methylh	C8H8,styrene
C8H10,ethylbenz	C8H16,1-octene	C8H17,n-octyl	C8H18,n-octane	C8H18,isoctane
C9H19,n-nonyl	C10H8,naphthale	C10H21,n-decyl	C12H9,o-bipheny	C12H10,biphenyl
HCN	HCO	HCCN	HCCO	HNC
HNCO	HNO	HNO2	HNO3	HCHO,formaldehy
HCOOH	H2O2	(HCOOH)2	*N	NCO
*NH	NH2	NH3	NH2OH	NO2
NO3	N2O	NCN	N2H2	NH2NO2
N2H4	N2O	N2O3	N2O4	N2O5
N3	N3H	O3	THDCPD,endo	THDCPD,exo
N2H4(L)	C(gr)	CH3OH(L)	C2H5OH(L)	C6H14(L),n-hexa
C6H5NH2(L)	C6H6(L)	H2O(cr)	H2O(L)	

NOTE. WEIGHT FRACTION OF FUEL IN TOTAL FUELS AND OF OXIDANT IN TOTAL OXIDANTS

APPENDIX C: CFD++ DATA FILES

1. Steady State (Refresh) Simulation for 3 Injectors at 45° Angle

45 Degree Injection Angle, 1.5% Injector Mass Flow Rate			
Mesh Size	968401		
Boundary Conditions			
Inlet	Multi-species PV Based Inflow/Outflow		
	Pressure	303975	Pa
	Temperature	450	K
	x-velocity	98.2	m/s
	y-velocity	0.0	m/s
	z-velocity	0.0	m/s
	q	1.224745	m/s
	L	.0006482519	m
	H ₂	0.02833164	Mass Fraction
	H	0.0	
	O	0.0	
	O ₂	0.2265	
	H ₂ O	0.0	
	H ₂ O ₂	0.0	
	HO ₂	0.0	
	OH	0.0	
Outlet	Simple Back Pressure		

	Pressure	101325	Pa
Injector 1, Injector 2, and Injector 3	Pressure Temperature and Normal Velocity Inflow		
	Pressure	111457	Pa
	Temperature	450	K
	Normal Velocity	61.89	m/s
	q	0.7579946	m/s
	L	0.0212248	M
	H ₂	0.0	Mass Fraction
	H	0.0	
	O	0.0	
	O ₂	0.2265	
	H ₂ O	0.0	
	H ₂ O ₂	0.0	
	HO ₂	0.0	
	OH	0.0	
Symmetry	Multi-species Adiabatic Wall		
Walls	Multi-species Adiabatic Wall		
Initial Conditions			
Box 1	x _{min}	-0.00005	m
	x _{max}	0.0125	m
	y _{min}	-0.002	m
	y _{max}	0.0875	m
	z _{min}	0.0	m

	z_{\max}	0.0	m
	Pressure	303975	Pa
	Temperature	450	K
	x-velocity	98.2	m/s
	y-velocity	0.0	m/s
	z-velocity	0.0	m/s
	q	1.224745	m/s
	L	0.006482519	m
	H ₂	0.02833164	Mass Fraction
	H	0.0	
	O	0.0	
	O ₂	0.2265	
	H ₂ O	0.0	
	H ₂ O ₂	0.0	
	HO ₂	0.0	
	OH	0.0	
Box 2	x_{\min}	0.0125	m
	x_{\max}	0.61	m
	y_{\min}	-0.002	m
	y_{\max}	0.0875	m
	z_{\min}	0.0	m
	z_{\max}	0.0	m
	Pressure	303975	Pa

	Temperature	450	K
	x-velocity	100	m/s
	y-velocity	0.0	m/s
	z-velocity	0.0	m/s
	q	1.224745	m/s
	L	0.004785153	m
	H ₂	0.0	Mass Fraction
	H	0.0	
	O	0.0	
	O ₂	0.2265	
	H ₂ O	0.0	
	H ₂ O ₂	0.0	
	HO ₂	0.0	
	OH	0.0	
Box 3	x _{min}	0.6815	m
	x _{max}	0.755	m
	y _{min}	-0.015	m
	y _{max}	0.012	m
	z _{min}	0.0	m
	z _{max}	0.0	m
	Pressure	167558	Pa
	Temperature	450	K
	x-velocity	37.5	m/s

	y-velocity	0.0	m/s
	z-velocity	0.0	m/s
	q	0.4592793	m/s
	L	0.02314926	m
	H ₂	0.0	Mass Fraction
	H	0.0	
	O	0.0	
	O ₂	0.2265	
	H ₂ O	0.0	
	H ₂ O ₂	0.0	
	HO ₂	0.0	
	OH	0.0	
Box 4	x _{min}	0.61	m
	x _{max}	0.6815	m
	y _{min}	-0.002	m
	y _{max}	0.0875	m
	z _{min}	0.0	m
	z _{max}	0.0	m
	Pressure	303975	Pa
	Temperature	450	K
	x-velocity	100	m/s
	y-velocity	0.0	m/s
	z-velocity	0.0	m/s

	q	1.224745	m/s
	L	0.004785153	m
	H ₂	0.0	Mass Fraction
	H	0.0	
	O	0.0	
	O ₂	0.2265	
	H ₂ O	0.0	
	H ₂ O ₂	0.0	
	HO ₂	0.0	
	OH	0.0	
Box 5	x _{min}	0.6815	m
	x _{max}	0.755	m
	y _{min}	0.012	m
	y _{max}	0.0875	m
	z _{min}	0.0	m
	z _{max}	0.0	m
	Pressure	200000	Pa
	Temperature	400	K
	x-velocity	100	m/s
	y-velocity	0.0	m/s
	z-velocity	0.0	m/s
	q	1.224745	m/s
	L	0.005950135	m

	H ₂	0.0	Mass Fraction
	H	0.0	
	O	0.0	
	O ₂	0.2265	
	H ₂ O	0.0	
	H ₂ O ₂	0.0	
	HO ₂	0.0	
	OH	0.0	
Box 6	x _{min}	0.755	m
	x _{max}	1.25	m
	y _{min}	-0.12	m
	y _{max}	0.0875	m
	z _{min}	0.0	m
	z _{max}	0.0	m
	Pressure	101325	Pa
	Temperature	298	K
	x-velocity	0.0	m/s
	y-velocity	0.0	m/s
	z-velocity	0.0	m/s
	q	0.001224745	m/s
	L	7.036989	m
	H ₂	0.0	Mass Fraction
	H	0.0	

	O	0.0	
	O ₂	0.2265	
	H ₂ O	0.0	
	H ₂ O ₂	0.0	
	HO ₂	0.0	
	OH	0.0	
Time Integration			
Is this a restart:		No	
Simulation Strategy:		Transient	
Integration Type:		Implicit	
Number of global time steps for this run:		1000	
Max. cumulative # of global time steps:		0	
Turn on dual time-stepping:		Yes	
Stop run at a given global time value:		No	
Implicit scheme type:		Point-Implicit	
Global time step based on Courant #:		No	
Spatially varying local time step:		Yes	
At restart, use Courant # for local time step from:		Values Below	
Courant # for local time step ramped from:		1 to 100	
Local Courant # ramped from global step number:		1 to 100	
Local Max. Courant # adjustment factor:		0.95	

Terminate run if adjusted local Courant # is <:	1.00E-04
Global time step size:	1.00E-05 s
Max. # of internal (local) iter. per global step:	50
Global step internal iter. Termination criterion:	0.1
Order of global time stepping:	2nd
Extrapolate using old dq/dt (1st iteration):	No
Local iteration convergence acceler.:	Multigrid (old)
Turn on temporal-smoothing:	Yes
Smoothing factor:	0.75
Turn on time-step spatial-smoothing:	Yes
Number of smoothing passes:	4
Maximum time-step growth factor:	1.5

2. Detonation Simulation with 3 Injectors at a 45° Angle

45 Degree Injection Angle, 1.5% Injector Mass Flow Rate			
Mesh Size	968401		
Boundary Conditions			
Inlet	Multi-species Adiabatic Wall		
Outlet	Simple Back Pressure		
	Pressure	101325	Pa
Injector 1, Injector 2, and Injector 3	Pressure Temperature and Normal Velocity		
	Pressure	111457	Pa
	Temperature	450	K
	Normal Velocity	61.89	m/s
	q	0.7579946	m/s
	L	0.0212248	M
	H ₂	0.0	Mass Fraction
	H	0.0	
	O	0.0	
	O ₂	0.2265	
	H ₂ O	0.0	
	H ₂ O ₂	0.0	
	HO ₂	0.0	
	OH	0.0	
Symmetry	Multi-species Adiabatic Wall		
Walls	Multi-species Adiabatic Wall		

Initial Conditions			
Box 1	x_{\min}	-0.00005	m
	x_{\max}	0.0125	m
	y_{\min}	-0.002	m
	y_{\max}	0.0875	m
	z_{\min}	0.0	m
	z_{\max}	0.0	m
	Pressure	303975	Pa
	Temperature	450	K
	x-velocity	98.2	m/s
	y-velocity	0.0	m/s
	z-velocity	0.0	m/s
	q	1.224745	m/s
	L	0.006482519	m
	H ₂	0.02833164	Mass Fraction
	H	0.0	
	O	0.0	
	O ₂	0.2265	
	H ₂ O	0.0	
	H ₂ O ₂	0.0	
	HO ₂	0.0	
	OH	0.0	
Box 2	x_{\min}	0.0125	m

	x_{\max}	0.61	m
	y_{\min}	-0.002	m
	y_{\max}	0.0875	m
	z_{\min}	0.0	m
	z_{\max}	0.0	m
	Pressure	303975	Pa
	Temperature	450	K
	x-velocity	100	m/s
	y-velocity	0.0	m/s
	z-velocity	0.0	m/s
	q	1.224745	m/s
	L	0.004785153	m
	H ₂	0.0	Mass Fraction
	H	0.0	
	O	0.0	
	O ₂	0.2265	
	H ₂ O	0.0	
	H ₂ O ₂	0.0	
	HO ₂	0.0	
	OH	0.0	
Box 3	x_{\min}	0.6815	m
	x_{\max}	0.755	m
	y_{\min}	-0.015	m

	y _{max}	0.012	m
	z _{min}	0.0	m
	z _{max}	0.0	m
	Pressure	167558	Pa
	Temperature	450	K
	x-velocity	37.5	m/s
	y-velocity	0.0	m/s
	z-velocity	0.0	m/s
	q	0.4592793	m/s
	L	0.02314926	m
	H ₂	0.0	Mass Fraction
	H	0.0	
	O	0.0	
	O ₂	0.2265	
	H ₂ O	0.0	
	H ₂ O ₂	0.0	
	HO ₂	0.0	
	OH	0.0	
Box 4	x _{min}	0.61	m
	x _{max}	0.7	m
	y _{min}	-0.00005	m
	y _{max}	0.0875	m
	z _{min}	0.0	m

	z_{\max}	0.0	m
	Pressure	303975	Pa
	Temperature	450	K
	x-velocity	100	m/s
	y-velocity	0.0	m/s
	z-velocity	0.0	m/s
	q	1.224745	m/s
	L	0.004785153	m
	H ₂	0.0	Mass Fraction
	H	0.0	
	O	0.0	
	O ₂	0.2265	
	H ₂ O	0.0	
	H ₂ O ₂	0.0	
	HO ₂	0.0	
	OH	0.0	
Box 5	x_{\min}	0.6815	m
	x_{\max}	0.755	m
	y_{\min}	0.012	m
	y_{\max}	0.0875	m
	z_{\min}	0.0	m
	z_{\max}	0.0	m
	Pressure	200000	Pa

	Temperature	400	K
	x-velocity	100	m/s
	y-velocity	0.0	m/s
	z-velocity	0.0	m/s
	q	1.224745	m/s
	L	0.005950135	m
	H ₂	0.0	Mass Fraction
	H	0.0	
	O	0.0	
	O ₂	0.2265	
	H ₂ O	0.0	
	H ₂ O ₂	0.0	
	HO ₂	0.0	
	OH	0.0	
Box 6	x _{min}	0.755	m
	x _{max}	1.25	m
	y _{min}	-0.12	m
	y _{max}	0.0875	m
	z _{min}	0.0	m
	z _{max}	0.0	m
	Pressure	101325	Pa
	Temperature	298	K
	x-velocity	0.0	m/s

	y-velocity	0.0	m/s
	z-velocity	0.0	m/s
	q	0.001224745	m/s
	L	7.036989	m
	H ₂	0.0	Mass Fraction
	H	0.0	
	O	0.0	
	O ₂	0.2265	
	H ₂ O	0.0	
	H ₂ O ₂	0.0	
	HO ₂	0.0	
	OH	0.0	
	Time Integration		
Is this a restart:		Yes	
Simulation Strategy:		Transient	
Integration Type:		Implicit	
Number of global time steps for this run:		6000	
Max. cumulative # of global time steps:		0	
Turn on dual time-stepping:		Yes	
Stop run at a given global time value:		No	
Implicit scheme type:		Point-Implicit	
Global time step based on Courant #:		No	
Spatially varying local time step:		Yes	

At restart, use Courant # for local time step from:	Values Below
Courant # for local time step ramped from:	1 to 100
Local Courant # ramped from global step number:	1 to 100
Local Max. Courant # adjustment factor:	0.95
Terminate run if adjusted local Courant # is <:	1.00E-04
Global time step size:	1.00E-05 s
Max. # of internal (local) iter. per global step:	50
Global step internal iter. Termination criterion:	0.1
Order of global time stepping:	2nd
Extrapolate using old dq/dt (1st iteration):	No
Local iteration convergence acceler.:	Multigrid (old)
Turn on temporal-smoothing:	Yes
Smoothing factor:	0.75
Turn on time-step spatial-smoothing:	Yes
Solution File Modification By Box	
Copy cdepsout.bin to cdepsin.bin before tool runs:	No
Copy cdepsout.bin to cdepsin.bin after tool runs:	No

x_{\min}	-0.00005
x_{\max}	0.0125
y_{\min}	-0.02
y_{\max}	0.0875
z_{\min}	0.0
z_{\max}	0.0
Number of variables for this box:	15
Variable 1:	9727200
Variable 2:	3050
Variable 3:	100
Variable 4:	0.0
Variable 5:	0.0
Variable 6:	1.224745
Variable 7:	0.003815446
Variable 8:	0.0026804
Variable 9:	0.00024332
Variable 10:	0.0013433
Variable 11:	0.0097109
Variable 12:	0.21962
Variable 13:	0.0
Variable 14:	0.000021331
Variable 15:	0.014039

3. Steady State (Refresh) Simulation for 2 Injectors and Free Stream

45 Degree Injection Angle, 1.5% Injector Mass Flow Rate			
Mesh Size	968401		
Boundary Conditions			
Inlet	Multi-species PV Based Inflow/Outflow		
	Pressure	303975	Pa
	Temperature	450	K
	x-velocity	98.2	m/s
	y-velocity	0.0	m/s
	z-velocity	0.0	m/s
	q	1.224745	m/s
	L	.0006482519	m
	H ₂	0.02833164	Mass Fraction
	H	0.0	
	O	0.0	
	O ₂	0.2265	
	H ₂ O	0.0	
	H ₂ O ₂	0.0	
	HO ₂	0.0	
	OH	0.0	
Outlet	Simple Back Pressure		
	Pressure	101325	Pa
Injector 1	Pressure Temperature and Normal Velocity Inflow		

	Pressure	131722	Pa
	Temperature	450	K
	Normal Velocity	103.155	m/s
	q	1.263386	m/s
	L	0.0127342	M
	H ₂	0.0	Mass Fraction
	H	0.0	
	O	0.0	
	O ₂	0.2265	
	H ₂ O	0.0	
	H ₂ O ₂	0.0	
	HO ₂	0.0	
	OH	0.0	
Injector 2	Pressure Temperature and Normal Velocity Inflow		
	Pressure	131722	Pa
	Temperature	450	K
	Normal Velocity	69.2	m/s
	q	0.875235	m/s
	L	0.01595271	M
	H ₂	0.0	Mass Fraction
	H	0.0	
	O	0.0	
	O ₂	0.2265	

	H ₂ O	0.0		
	H ₂ O ₂	0.0		
	HO ₂	0.0		
	OH	0.0		
Injector 3 (Free Stream)	Pressure Temperature and Normal Velocity Inflow			
	Pressure	26497.5	Pa	
	Temperature	223.25	K	
	Normal Velocity	898.51	m/s	
	q	11.00445	m/s	
	L	0.00179092	M	
	H ₂	0.0	Mass Fraction	
	H	0.0		
	O	0.0		
	O ₂	0.2265		
	H ₂ O	0.0		
	H ₂ O ₂	0.0		
	HO ₂	0.0		
	OH	0.0		
	Symmetry	Multi-species Adiabatic Wall		
Walls	Multi-species Adiabatic Wall			
Initial Conditions				
Box 1	x _{min}	-0.00005	m	

	x _{max}	0.0125	m
	y _{min}	-0.002	m
	y _{max}	0.0875	m
	z _{min}	0.0	m
	z _{max}	0.0	m
	Pressure	303975	Pa
	Temperature	450	K
	x-velocity	98.2	m/s
	y-velocity	0.0	m/s
	z-velocity	0.0	m/s
	q	1.224745	m/s
	L	0.006482519	m
	H ₂	0.02833164	Mass Fraction
	H	0.0	
	O	0.0	
	O ₂	0.2265	
	H ₂ O	0.0	
	H ₂ O ₂	0.0	
	HO ₂	0.0	
	OH	0.0	
Box 2	x _{min}	0.0125	m
	x _{max}	0.61	m
	y _{min}	-0.002	m

	y _{max}	0.0875	m
	z _{min}	0.0	m
	z _{max}	0.0	m
	Pressure	303975	Pa
	Temperature	450	K
	x-velocity	100	m/s
	y-velocity	0.0	m/s
	z-velocity	0.0	m/s
	q	1.224745	m/s
	L	0.004785153	m
	H ₂	0.0	Mass Fraction
	H	0.0	
	O	0.0	
	O ₂	0.2265	
	H ₂ O	0.0	
	H ₂ O ₂	0.0	
	HO ₂	0.0	
	OH	0.0	
Box 3	x _{min}	0.6815	m
	x _{max}	0.755	m
	y _{min}	-0.015	m
	y _{max}	0.012	m
	z _{min}	0.0	m

	z_{\max}	0.0	m
	Pressure	167558	Pa
	Temperature	450	K
	x-velocity	37.5	m/s
	y-velocity	0.0	m/s
	z-velocity	0.0	m/s
	q	0.4592793	m/s
	L	0.02314926	m
	H ₂	0.0	Mass Fraction
	H	0.0	
	O	0.0	
	O ₂	0.2265	
	H ₂ O	0.0	
	H ₂ O ₂	0.0	
	HO ₂	0.0	
	OH	0.0	
Box 4	x_{\min}	0.61	m
	x_{\max}	0.6815	m
	y_{\min}	-0.002	m
	y_{\max}	0.0875	m
	z_{\min}	0.0	m
	z_{\max}	0.0	m
	Pressure	303975	Pa

	Temperature	450	K
	x-velocity	100	m/s
	y-velocity	0.0	m/s
	z-velocity	0.0	m/s
	q	1.224745	m/s
	L	0.004785153	m
	H ₂	0.0	Mass Fraction
	H	0.0	
	O	0.0	
	O ₂	0.2265	
	H ₂ O	0.0	
	H ₂ O ₂	0.0	
	HO ₂	0.0	
	OH	0.0	
Box 5	x _{min}	0.6815	m
	x _{max}	0.755	m
	y _{min}	0.012	m
	y _{max}	0.0875	m
	z _{min}	0.0	m
	z _{max}	0.0	m
	Pressure	200000	Pa
	Temperature	400	K
	x-velocity	100	m/s

	y-velocity	0.0	m/s
	z-velocity	0.0	m/s
	q	1.224745	m/s
	L	0.005950135	m
	H ₂	0.0	Mass Fraction
	H	0.0	
	O	0.0	
	O ₂	0.2265	
	H ₂ O	0.0	
	H ₂ O ₂	0.0	
	HO ₂	0.0	
	OH	0.0	
Box 6	x _{min}	0.755	m
	x _{max}	1.25	m
	y _{min}	-0.12	m
	y _{max}	0.0875	m
	z _{min}	0.0	m
	z _{max}	0.0	m
	Pressure	101325	Pa
	Temperature	298	K
	x-velocity	0.0	m/s
	y-velocity	0.0	m/s
	z-velocity	0.0	m/s

	q	0.001224745	m/s
	L	7.036989	m
	H ₂	0.0	Mass Fraction
	H	0.0	
	O	0.0	
	O ₂	0.2265	
	H ₂ O	0.0	
	H ₂ O ₂	0.0	
	HO ₂	0.0	
	OH	0.0	
Time Integration			
Is this a restart:		No	
Simulation Strategy:		Transient	
Integration Type:		Implicit	
Number of global time steps for this run:		1000	
Max. cumulative # of global time steps:		0	
Turn on dual time-stepping:		Yes	
Stop run at a given global time value:		No	
Implicit scheme type:		Point-Implicit	
Global time step based on Courant #:		No	
Spatially varying local time step:		Yes	
At restart, use Courant # for local time step from:		Values Below	

Courant # for local time step ramped from:	1 to 100
Local Courant # ramped from global step number:	1 to 100
Local Max. Courant # adjustment factor:	0.95
Terminate run if adjusted local Courant # is <:	1.00E-04
Global time step size:	1.00E-05 s
Max. # of internal (local) iter. per global step:	50
Global step internal iter. Termination criterion:	0.1
Order of global time stepping:	2nd
Extrapolate using old dq/dt (1st iteration):	No
Local iteration convergence acceler.:	Multigrid (old)
Turn on temporal-smoothing:	Yes
Smoothing factor:	0.75
Turn on time-step spatial-smoothing:	Yes
Number of smoothing passes:	4
Maximum time-step growth factor:	1.5

4. Steady State (Refresh) Simulation for 2 Injectors and Free Stream, Sea Level

45 Degree Injection Angle	
Mesh Size	968401
Boundary Conditions	
Inlet	Multi-species PV Based Inflow/Outflow

	Pressure	303975	Pa
	Temperature	450	K
	x-velocity	98.2	m/s
	y-velocity	0.0	m/s
	z-velocity	0.0	m/s
	q	1.224745	m/s
	L	.0006482519	m
	H ₂	0.02833164	Mass Fraction
	H	0.0	
	O	0.0	
	O ₂	0.2265	
	H ₂ O	0.0	
	H ₂ O ₂	0.0	
	HO ₂	0.0	
	OH	0.0	
Outlet	Simple Back Pressure		
	Pressure	101325	Pa
Injector 1	Pressure Temperature and Normal Velocity Inflow		
	Pressure	131722	Pa
	Temperature	450	K
	Normal Velocity	103.155	m/s
	q	1.263386	m/s
	L	0.0127342	M

	H ₂	0.0	Mass Fraction
	H	0.0	
	O	0.0	
	O ₂	0.2265	
	H ₂ O	0.0	
	H ₂ O ₂	0.0	
	HO ₂	0.0	
	OH	0.0	
Injector 2	Pressure Temperature and Normal Velocity Inflow		
	Pressure	131722	Pa
	Temperature	450	K
	Normal Velocity	69.2	m/s
	q	0.875235	m/s
	L	0.01595271	M
	H ₂	0.0	Mass Fraction
	H	0.0	
	O	0.0	
	O ₂	0.2265	
	H ₂ O	0.0	
	H ₂ O ₂	0.0	
	HO ₂	0.0	
	OH	0.0	
Injector 3	Pressure Temperature and Normal Velocity Inflow		

(Free Stream)	Pressure	101325	Pa
	Temperature	289.15	K
	Normal Velocity	1020.9	m/s
	q	12.50342	m/s
	L	0.0006916	M
	H ₂	0.0	Mass Fraction
	H	0.0	
	O	0.0	
	O ₂	0.2265	
	H ₂ O	0.0	
	H ₂ O ₂	0.0	
	HO ₂	0.0	
	OH	0.0	
Symmetry	Multi-species Adiabatic Wall		
Walls	Multi-species Adiabatic Wall		
Initial Conditions			
Box 1	x _{min}	-0.00005	m
	x _{max}	0.0125	m
	y _{min}	-0.002	m
	y _{max}	0.0875	m
	z _{min}	0.0	m
	z _{max}	0.0	m

	Pressure	303975	Pa
	Temperature	450	K
	x-velocity	98.2	m/s
	y-velocity	0.0	m/s
	z-velocity	0.0	m/s
	q	1.224745	m/s
	L	0.006482519	m
	H ₂	0.02833164	Mass Fraction
	H	0.0	
	O	0.0	
	O ₂	0.2265	
	H ₂ O	0.0	
	H ₂ O ₂	0.0	
	HO ₂	0.0	
	OH	0.0	
Box 2	x _{min}	0.0125	m
	x _{max}	0.61	m
	y _{min}	-0.002	m
	y _{max}	0.0875	m
	z _{min}	0.0	m
	z _{max}	0.0	m
	Pressure	303975	Pa
	Temperature	450	K

	x-velocity	100	m/s
	y-velocity	0.0	m/s
	z-velocity	0.0	m/s
	q	1.224745	m/s
	L	0.004785153	m
	H ₂	0.0	Mass Fraction
	H	0.0	
	O	0.0	
	O ₂	0.2265	
	H ₂ O	0.0	
	H ₂ O ₂	0.0	
	HO ₂	0.0	
	OH	0.0	
Box 3	x _{min}	0.6815	m
	x _{max}	0.755	m
	y _{min}	-0.015	m
	y _{max}	0.012	m
	z _{min}	0.0	m
	z _{max}	0.0	m
	Pressure	167558	Pa
	Temperature	450	K
	x-velocity	37.5	m/s
	y-velocity	0.0	m/s

	z-velocity	0.0	m/s
	q	0.4592793	m/s
	L	0.02314926	m
	H ₂	0.0	Mass Fraction
	H	0.0	
	O	0.0	
	O ₂	0.2265	
	H ₂ O	0.0	
	H ₂ O ₂	0.0	
	HO ₂	0.0	
	OH	0.0	
Box 4	x _{min}	0.61	m
	x _{max}	0.6815	m
	y _{min}	-0.002	m
	y _{max}	0.0875	m
	z _{min}	0.0	m
	z _{max}	0.0	m
	Pressure	303975	Pa
	Temperature	450	K
	x-velocity	100	m/s
	y-velocity	0.0	m/s
	z-velocity	0.0	m/s
	q	1.224745	m/s

	L	0.004785153	m
	H ₂	0.0	Mass Fraction
	H	0.0	
	O	0.0	
	O ₂	0.2265	
	H ₂ O	0.0	
	H ₂ O ₂	0.0	
	HO ₂	0.0	
	OH	0.0	
Box 5	x _{min}	0.6815	m
	x _{max}	0.755	m
	y _{min}	0.012	m
	y _{max}	0.0875	m
	z _{min}	0.0	m
	z _{max}	0.0	m
	Pressure	200000	Pa
	Temperature	400	K
	x-velocity	100	m/s
	y-velocity	0.0	m/s
	z-velocity	0.0	m/s
	q	1.224745	m/s
	L	0.005950135	m
	H ₂	0.0	Mass Fraction

	H	0.0	
	O	0.0	
	O ₂	0.2265	
	H ₂ O	0.0	
	H ₂ O ₂	0.0	
	HO ₂	0.0	
	OH	0.0	
Box 6	x _{min}	0.755	m
	x _{max}	1.25	m
	y _{min}	-0.12	m
	y _{max}	0.0875	m
	z _{min}	0.0	m
	z _{max}	0.0	m
	Pressure	101325	Pa
	Temperature	298	K
	x-velocity	0.0	m/s
	y-velocity	0.0	m/s
	z-velocity	0.0	m/s
	q	0.001224745	m/s
	L	7.036989	m
	H ₂	0.0	Mass Fraction
	H	0.0	
	O	0.0	

	O ₂	0.2265	
	H ₂ O	0.0	
	H ₂ O ₂	0.0	
	HO ₂	0.0	
	OH	0.0	
Time Integration			
Is this a restart:		No	
Simulation Strategy:		Transient	
Integration Type:		Implicit	
Number of global time steps for this run:		1000	
Max. cumulative # of global time steps:		0	
Turn on dual time-stepping:		Yes	
Stop run at a given global time value:		No	
Implicit scheme type:		Point-Implicit	
Global time step based on Courant #:		No	
Spatially varying local time step:		Yes	
At restart, use Courant # for local time step from:		Values Below	
Courant # for local time step ramped from:		1 to 100	
Local Courant # ramped from global step number:		1 to 100	
Local Max. Courant # adjustment factor:		0.95	
Terminate run if adjusted local Courant # is <:		1.00E-04	

Global time step size:	1.00E-05 s
Max. # of internal (local) iter. per global step:	50
Global step internal iter. Termination criterion:	0.1
Order of global time stepping:	2nd
Extrapolate using old dq/dt (1st iteration):	No
Local iteration convergence acceler.:	Multigrid (old)
Turn on temporal-smoothing:	Yes
Smoothing factor:	0.75
Turn on time-step spatial-smoothing:	Yes
Number of smoothing passes:	4
Maximum time-step growth factor:	1.5

LIST OF REFERENCES

- [1] R. Friedman, "American Rocket Society," Vol. 24, p. 349, November 1953
- [2] J. R. McClure III, "Dynamic fluidic nozzles for pulse detonation engine applications," M.S. thesis, Naval Postgraduate School, Monterey, CA, 2010.
- [3] D. M. Juillet, "Detonation diffraction in a multi-Step channel," M.S. thesis, Naval Postgraduate School, Monterey, CA, 2010.
- [4] R. D. Flack, *Fundamentals of Jet Propulsion with Applications*. Cambridge: Cambridge University Press, 2005.
- [5] G. D. Roy and S. M. Frolov, *Pulse and Continuous Detonation Propulsion*. Moscow, Russia: Torus Press, 2006.
- [6] G. P. Sutton and O. Biblarz, *Rocket Propulsion Elements*, 7th ed. New York City, NY: John Wiley & Sons, Inc. 2001.
- [7] P. H. Oosthuizen and W. E. Carscalen, *Compressible Fluid Flow*. New York City, NY: McGraw-Hill, 1997.
- [8] J. H. S. Lee, *The Detonation Phenomenon*. Cambridge: Cambridge University Press, 2008.
- [9] K. W. Ragland and K. M. Bryden, *Combustion Engineering*, 2nd ed. Boca Raton, FL: CRC Press, 2011.
- [10] G. S. Settles, *Schlieren and Shadowgraph Technique: Visualizing Phenomena in Transparent Media*, Springer-Verlag Berlin Heidelberg, New York, 2001.
- [11] M. J. Zehe, *Chemical Equilibrium with Applications*, Glenn Research Center, NASA, 20 Jan 2010
<http://www.grc.nasa.gov/WWW/CEAWeb/ceaRequestForm.htm>

THIS PAGE INTENTIONALLY LEFT BLANK

INITIAL DISTRIBUTION LIST

1. Defense Technical Information Center
Ft. Belvoir, Virginia
2. Dudley Knox Library
Naval Postgraduate School
Monterey, California
3. Professor Christopher Brophy
Department of Mechanical and Aerospace Engineering
Monterey, California
4. Professor Anthony Gannon
Department of Mechanical and Aerospace Engineering
Monterey, California
5. Professor Knox Milsaps
Department of Mechanical and Aerospace Engineering
Monterey, California
6. LCDR Larry Smith
Naval Postgraduate School
Monterey, California